Laser Engineering

Kelin Kuhn
University of Washington

Acquisition Editor: Eric Svendsen
Editor-in-Chief: Marcia Horton
Production Manager: Baysni Mendoza de Leon
Editor-in-Chief: Jerome Grant
Director of Production and Manufacturing: David W. Riccardi
Manufacturing Manager: Trudy Pisciotti
Full Service Coordinator: Donna Sullivan
Composition/Production Service: ETP Harrison
Editorial Assistant: Andrea Au
Creative Director: Paula Maylahn
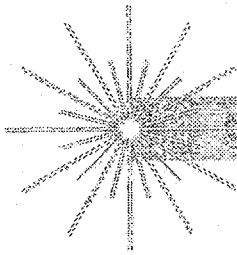Art Director: Jayne Conte
Cover Designer: Bruce Kenselaar

The author and publisher of this book have used their best efforts in preparing this book. These efforts
include the development, research, and testing of the theories and programs to determine their effectiveness.
The author and publisher make no warranty of any kind, expressed or implied, with regard to these programs
or the documentation contained in this book. The author and publisher shall not be liable in any event for
incedental or consequential damages in connection with, or arising out of, the furnishing, performance, or
use of these programs.

Contents

iv

Contents

Contents

11 TRANSITION-METAL SOLID-STATE LASERS   344

12 OTHER MAJOR COMMERCIAL LASERS   384

APPENDIX   *441*

11

Transition-Metal Solid-State Lasers

Objectives

- To summarize the sequence of historical events leading to the development of the transition-metal solid-state laser.
- To summarize commercial applications for transition-metal solid-state lasers.
- To compare and contrast the energy band structure and major laser properties for the primary commercial solid-state laser materials (ruby, alexandrite, Ti:sapphire, Nd:YAG).
- To describe the design of ring laser cavities.
- To compare and contrast ring laser cavities with linear cavities.
- To describe the importance of birefringent filters.
- To compute the intensity transmittance for a birefringent filter.
- To describe the construction of a commercial laser pumped continuous wave Ti:sapphire laser.
- To describe the design principles underlying femtosecond pulse laser design. This would include such issues as group velocity dispersion (GVD), self-phase modulation (SPM), femtosecond pulse temporal measurement, colliding pulse mode-locking (CPM), grating pulse compression, solitons, and Kerr-lens mode-locking (KLM).
- To describe the construction of a commercial ultrashort pulse Ti:sapphire laser.

344
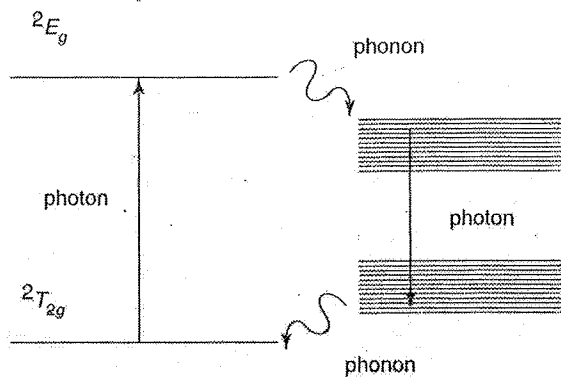
Figure 11.1   The transition-metal solid-state tunable lasers use metals in the fourth row of the periodic table as the active ions. These metals can produce transitions that involve phonons as well as photons (often called vibronic or phonon-terminated transitions). Such transitions can create tunable four-level laser behavior.

11.1 HISTORY

The history of transition-metal solid-state tunable lasers is exceptionally fascinating. For the HeNe, argon-ion and Nd:YAG lasers (even the diode pumped Nd:YAG lasers) the majority of the laser science was in place by the mid-1960s and commercial development proceeded rapidly after that. Transition-metal tunable solid-state lasers are quite different. Transition-metal tunable solid-state lasers are barely mentioned in review papers on tunable laser technology as recently as 1982.[1]

Ti:sapphire lasers (the current stars of the solid-state tunable laser market) were discovered by Moulton in 1982.[2] However, early results with Ti:sapphire were not promising due to difficulties with material growth.[3] It was only after the materials problems were solved that the true potential of the Ti:sapphire laser was realized. As a consequence, much of the laser development (including the remarkable self-mode-locking properties of Ti:sapphire discussed in Section 11.5) has occurred relatively recently.

The transition-metal solid-state tunable lasers use metals in the fourth row of the periodic table as the active ions. The transition-metals have a partially filled 3d shell, and the various observed transitions occur near this shell. 3d electrons interact more strongly with the crystal field than the 4f electrons in conventional solid-state lasers such as Nd:YAG. This can produce transitions that involve phonons as well as photons (often called vibronic or phonon-terminated transitions). Such transitions are rather peculiar, as they can create four-level laser behavior between two level transitions. A schematic of a vibronic transition is illustrated in Figure 11.1.

In a vibronic transition an optical photon is used to make the transition from the ground state to the pump state. Then the electron decays to the upper laser state by releasing a phonon (an acoustical quanta similar to a photon). The laser action occurs between the upper and lower laser states. The lower laser state then decays to the ground state by releasing

---

[1]B. D. Guenther and R. G. Buser, *IEEE J. of Quantum Electron.* QE-18:1179 (1982).

[2]P. F. Moulton, *Solid State Research Report*, DTIC AD-A124305/4 (1982:3) (Lexington: MIT Lincoln Lab., 1982), pp. 15–21.

[3]P. Lacovara and L. Esterowitz, *IEEE J. of Quantum Electron.* QE-21:1614 (1985).

another phonon. Thus, four-state laser behavior is obtained from a system that is effectively two-state. More importantly, since a wide variety of phonon transitions are possible, the upper and lower laser states consist of large manifolds of states. Therefore, highly tunable laser action is possible.

The first vibronic laser was reported by Johnson et al. at Bell Laboratories in 1963.[4] It was a divalent transition-metal laser using Ni^{2+} in MgF_2. It stimulated some early work by McCumber in the theory of vibronic lasers.[5] However, it was cryogenically cooled and did not excite much commercial interest.

Further efforts by Johnson and his colleagues during the mid to late 1960s resulted in several more cryogenically cooled divalent transition-metal lasers. These included Co^{2+} in MgF_2 and V^{2+} in MgF_2.[6]

A major advancement occurred in 1976 when Morris and Cline[7] observed that alexandrite ($BeAl_2O_4{:}Cr^{3+}$ or chromium doped chrysoberyl, tunable from 700 nm to 818 nm) would lase on a vibronic transition. Walling et al. confirmed these results and demonstrated Q-switching behavior.[8] Alexandrite was particularly interesting at the time of its discovery because it lased at room temperature and increased in output power as the temperature increased.[9]

The successful use of Cr^{3+} in a beryl crystal led to several other interesting vibronic lasers. In particular, in 1982 Shand and Walling,[10] and independently Buchert et al.,[11] showed that emerald ($Be_3Al_2(SiO_3){:}Cr^{3+}$, another type of chromium-doped chrysoberyl and tunable from roughly 700 nm to 800 nm) would lase as a vibronic laser at room temperature. Chromium was also found to generate vibronic laser performance in gadolinium scandium gallium garnet (GSGG).[12]

These encouraging results in chromium-doped materials led to a rebirth in tunable solid-state laser research. Ti:sapphire (the crown jewel of modern tunable solid-state lasers)

---

[4] L. F. Johnson, R. E. Dietz, and H. J. Guggenheim, *Phys. Rev. Lett.* 11:318 (1963).

[5] D. E. McCumber, *Phys. Rev.* 134:A299 (1964); D. E. McCumber, *J. Math. Phys.* 5:508 (1964); and D. E. McCumber, *Phys. Rev.* 136:A954 (1964).

[6] L. F. Johnson, R. E. Dietz, and H. J. Guggenheim, *Appl. Phys. Lett.* 5:21 (1964); L. F. Johnson and H. J. Guggenheim, *J. Appl. Phys.* 38:4837 (1967); L. F. Johnson and H. J. Guggenheim, *J. Appl. Phys.* 38:4837 (1967); and L. F. Johnson, H. J. Guggenheim and R. A. Thomas, *Phys. Rev.* 149:179 (1966).

[7] R. C. Morris and C. F. Cline, "Chromium-Doped Beryllium Aluminate Lasers," U.S. Patent #3,997,853, Dec. 14, 1976.

[8] J. C. Walling, H. P. Jenssen, R. C. Morris, E. W. O'Dell, and O. G. Peterson, Annual meeting Opt. Sci. Amer., San Francisco, CA, 1978; J. C. Walling, H. P. Benson, R. C. Morris, E. W. O'Dell, and G. Peterson, *Opt. Lett.* 4:182 (1979); J. C. Walling, O. G. Peterson, H. P. Jenssen, R. C. Morris, and E. W. O'Dell, *IEEE J. Quantum Electron.* QE-16:1302 (1980); and C. L. Sam, J. C. Walling, H. P. Jenssen, R. C. Morris, and E. W. O'Dell, *Proc. Soc. Photo-Opt. Inst. Eng. (SPIE)* 247:130 (1980).

[9] M. L. Shand and H. Jenssen, *IEEE J. of Quantum Electron.* QE-19:480 (1983).

[10] M. Shand and J. Walling, *IEEE J. of Quantum Electron.* QE-18:1829 (1982).

[11] J. Buchert, A. Katz, and R. R. Alfano, *IEEE J. of Quantum Electron.* QE-19:1477 (1983).

[12] E. V. Zharikov, N. N. Il'ichev, S. P. Kaltin, V. V. Laptev, A. A. Malyutin, V. V. Osiko, V. G. Ostroumov, P. P. Pashinin, A. M. Prokhorov, V. A. Smirnov, A. F. Umyskov, and I. A. Shcherbakov, *Sov. J. Quantum Electron.* 13:1274 (1983).

was discovered in 1982 by Moulton at MIT Lincoln Labs.[13] Although sapphire is the oldest laser material (ruby is Cr^{3+} in sapphire) the discovery of the broadly tunable nature of Ti^{3+} in sapphire was quite unexpected. A review report on tunable solid-state lasers published in 1982[14] and a review paper on alexandrite lasers in 1985[15] do not even mention Ti:sapphire.

Part of the delay in Ti:sapphire emerging as a viable commercial tunable solid-state laser was materials-based. Early Ti:sapphire crystals showed an absorption at the lasing wavelengths that was approximately an order of magnitude higher than the absorption in high-quality sapphire. A number of possible defects were proposed[16] and after much investigation the residual absorption in vertical-gradient-freeze (VGF) crystals was shown to be due to quadruply ionized titanium (Ti^{4+}) substituting for the aluminum in the sapphire.[17,18] Growth and annealing methods have significantly reduced this problem in modern commercial Ti:sapphire material.

In spite of its many advantages, Ti:sapphire does suffer from a few disadvantages. In particular, its short upper state lifetime (3.2 μs) makes it quite difficult to pump with a lamp. Although lamp-pumped Ti:sapphire lasers have been built,[19] most commercial Ti:sapphire lasers are pumped with argon-ion or doubled Nd:YAG lasers.

Several other materials have seen some commercial interest as possible lamp pumped laser materials. In particular $LiCaAlF_6:Cr^{3+}$ and $LiSrAlF_6:Cr^{3+}$ have seen some interest as possible tunable commercial laser sources.[20] A number of other chromium-doped materials including Cr:forsterite and Cr:YAG are also showing strong potential.[21]

Transition-metal solid-state tunable lasers are still being actively developed. Barnes[22] and Budgor et al.[23] provide good overview treatments of this developing field. In addition, there are three special issues in IEEE journals on tunable lasers.[24]

[13]P. F. Moulton, *Solid State Research Report.* DTIC AD-A124305/4 (1982:3) (MIT Lincoln Lab., Lexington, 1982), pp. 15–21, reported by P. F. Moulton, "Recent Advances in Solid-State Lasers," *Proc. Con. Lasers Electro-opt.,* Anaheim, CA, 1984, paper WA2.

[14]B. D. Guenther and R. G. Buser, *IEEE J. of Quantum Electron.* QE-18:1179 (1982).

[15]J. C. Walling, D. F. Heller, H. Samelson, D. J. Harter, J. A. Pete, and R. C. Morris, *IEEE J. of Quantum Electron.* QE-21:1568 (1985).

[16]P. Lacovara and L. Esterowitz, *IEEE J. of Quantum Electron.* QE-21:1614 (1985).

[17]A. Sanchez, A. J. Strauss, R. L. Aggarwal, and R. E. Fahey, *IEEE J. of Quantum Electron.* 24:995 (1988).

[18]R. Aggarwal, A. Sanchez, M. Stuppi, R. Fahey, A. Strauss, W. Rapoport, and C. Khattak, *IEEE J. of Quantum Electron.* 24:1003 (1988).

[19]P. Lacovara, L. Esterowitz and R. Allen, *Opt. Lett.* 10:273 (1985).

[20]S. A. Payne, L. L. Chase, H. W. Newkirk, L. K. Smith, and W. F. Krupke, *IEEE J. of Quantum Electron.* 24:2243 (1988); and S. A. Payne, L. L. Chase, L. K. Smith, W. L. Kway, and H. W. Newkirk, *J. Appl. Phys.* 66:1051 (1989).

[21]C. Pollock, D. Barber, J. Mass, and S. Markgraf, *IEEE J. of Sel. Topics in Quantum Electron.* 1:62 (1995).

[22]Norman P. Barnes, "Transition Metal Solid State Lasers," in *Tunable Lasers Handbook,* ed F. J. Duarte (San Diego: Academic Press, 1995).

[23]A. Budgor, L. Esterowtiz, and L. G. DeShazer, eds, *Tunable Solid State Lasers II* (Berlin: Springer Verlag, 1986).

[24]*IEEE J. of Quantum Electron.* QE-18 (1982); QE-21 (1985); and *IEEE J. of Sel. Topics in Quantum Electron.* (1995).

11.2 APPLICATIONS

Transition-metal solid-state tunable lasers provide two major features. First, they are tunable over a broad range of visible and near IR wavelengths. Second, they can be used to produce extremely short pulses.

The tunability feature means that these lasers are ideal for spectroscopic applications. This not only includes traditional scientific spectroscopy, but also medical diagnostic spectroscopy. For example, Ti:sapphire lasers have been used to perform an optical version of conventional mammography.[25] There are also potential applications for absorption, Raman, and fluorescence spectroscopy in medical imaging.[26]

Solid-state lasers compete with dye lasers for medical applications requiring both tunability and intensity. Primary among these are cosmetic surgery for port wine birthmarks, telangiectasia, warts, stretch marks, acne scars, removing tattoos, and psoriasis.[27] Tunable solid-state lasers also compete with dye lasers for medical applications such as shattering kidney stones.[28]

In addition, the extremely short pulses possible with tunable solid-state lasers are finding application in micromachining. Femtosecond-pulsed Ti:sapphire lasers can be used for micromachining holes in metal and polymer substrates as well as for ablating photoresist films and cutting traces on semiconductor materials.[29] Ti:sapphire lasers compete with Nd:YAG, diode-pumped Nd:YAG, and excimer lasers for this extremely important market.

11.3 LASER MATERIALS

Ruby, alexandrite, and Ti:sapphire are the major transition-metal solid-state laser materials. Although ruby is not used commercially as a tunable laser, it does have a tunable vibronic transition. Interestingly enough, the band structure of alexandrite is quite similar to ruby; except in alexandrite the vibronic transition is the important one and the narrow line transition is not used. In contrast, Ti:sapphire has crystalline and mechanical properties virtually identical to ruby, but a dramatically different band structure.

A number of publications can provide additional information for the interested reader. Overview treatments are given by Weber,[30] Koechner,[31] and Duarte,[32] while more specific

---

[25]*Laser Focus World*, Feb.: 38 (1996).

[26]*Laser Focus World*, Feb.: 72 (1996).

[27]*Laser Focus World*, May: 66-7 (1996).

[28]*Laser Focus World*, May: 66-7 (1996).

[29]*Laser Focus World*, January: 22 (1996).

[30]Marvin J. Weber, ed, *Handbook of Laser Science and Technology, Vol. 1, Lasers and Masers* (Boca Raton, FL: CRC Press, Inc., 1982); and more recently, Marvin J. Weber, ed, *Handbook of Laser Science and Technology, Supplement 1, Lasers* (Boca Raton, FL: CRC Press, Inc., 1991).

[31]Walter Koechner, *Solid State Laser Engineering*, 4th ed. (Berlin: Springer-Verlag, 1996).
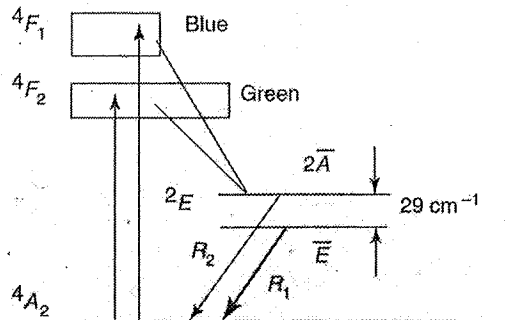
Figure 11.2   The energy band diagram for ruby.

information can be obtained from the wide variety of review papers on alexandrite[33] and Ti:sapphire.[34,35] Manufacturer data sheets and application notes are also very useful.[36]

11.3.1 Ruby—Primary Line at 694.3 nm

Ruby (chromium-doped Al_2O_3) is a red or pink hexagonal crystal whose most familiar application is jewelry. Ruby is an optically uniaxial crystal[37] that is hard (Moh's hardness of 9), of good optical quality, and extremely thermally conductive (0.42 W/cm-K at 300K). Ruby is nonhygroscopic, refractory, and is generally considered the most durable of the common laser crystals (with the possible exception of Ti:sapphire). Ruby crystals are typically grown by the Czochralski method (the same method as used for the growth of silicon). Ruby can be grown at 0, 60, or 90 degrees to the optic axis, and laser material is usually grown at 60 degrees.

Sapphire is doped with Cr^{3+} to obtain ruby. The Cr^{3+} substitutes for the Al^{3+} in the crystal. Typical dopings are 0.05 weight percent of Cr_2O_3. However, excess chromium can distort the crystal structure and concentrations are sometimes reduced to 0.03 weight percent to enhance the optical beam quality.

The energy diagram for ruby is given in Figure 11.2. Ruby is three-state and is the only commercially viable three-state laser system. The laser pump bands are principally the $^4F_1$ and the $^4F_2$ bands. The ground state is the $^4A_2$ band. The two pump bands form manifolds centered around the blue (400 nm) and green (555 nm). The pump bands are

---

[32]F. J. Duarte ed, *Tunable Lasers Handbook* (San Diego: Academic Press 1995).

[33]J. C. Walling, D. F. Heller, H. Samelson, D. J. Harter, J. A. Pete, and R. C. Morris, *IEEE J. of Quantum Electron.* QE-21:1568 (1985).

[34]A. Sanchez, A. J. Strauss, R. L. Aggarwal, and R. E. Fahey, *IEEE J. of Quantum Electron.* 24:995 (1988).

[35]R. Aggarwal, A. Sanchez, M. Stuppi, R. Fahey, A. Strauss, W. Rapoport, and C. Khattak, *IEEE J. of Quantum Electron.* 24:1003 (1988).

[36]Major crystal suppliers are Union Carbide (ruby, alexandrite and Ti:sapphire) and Litton Airtron (alexandrite).

[37]A uniaxial crystal is one where two of the Cartesian directions have one index of refraction n_o and the third has a different index of refraction n_e. See Section 8.3 for a discussion of uniaxial and biaxial crystals.

each quite wide, with the blue band about 0.05 microns wide and the green band about 0.07 microns wide.

The lifetime in the pump bands is extremely short, with the ions cascading almost immediately to the metastable ^2E states. The upper ^2E state is termed the $2\overline{A}$ state and the lower is termed the $\overline{E}$ state. The $2\overline{A}$ and $\overline{E}$ states are separated by 29 cm^{-1}, which gives a population ratio at thermal equilibrium of 87%. Thus, while fluorescence in ruby occurs from both the $2\overline{A}$ state to the $^4A_2$ (termed the R_2 transition at 692.9 nm) and from the $\overline{E}$ state to the $^4A_2$ (termed the R_1 transition at 694.3 nm), laser action first occurs on the R_1 transition. Once laser action has begun, the rapid relaxation time from the $2\overline{A}$ to the $\overline{E}$ transition prohibits laser action starting on the R_2 line. The only way to start laser action on the R_2 line is to suppress the R_1 line by special dielectric coated mirrors or internal cavity absorbers. (Interesting enough, even though lasing occurs primarily on the R_1 and R_2 lines, sidebands have been observed on the long wavelength side, in particular at 767 nm, attributed to vibronic lasing.)

Since ruby is uniaxial, its absorption coefficient is a very strong function of the polarization direction of the light (see Figure 11.3). This property strongly affects the beam quality. The best optical quality ruby is grown with the crystal axis at 60 degrees to the boule axis. When such a ruby rod is pumped in a diffuse reflecting pump cavity, pump light parallel to the c-axis will be absorbed differently than pump light perpendicular to the c-axis. This will cause the pump distribution (and thus the laser output beam) to be elliptical.
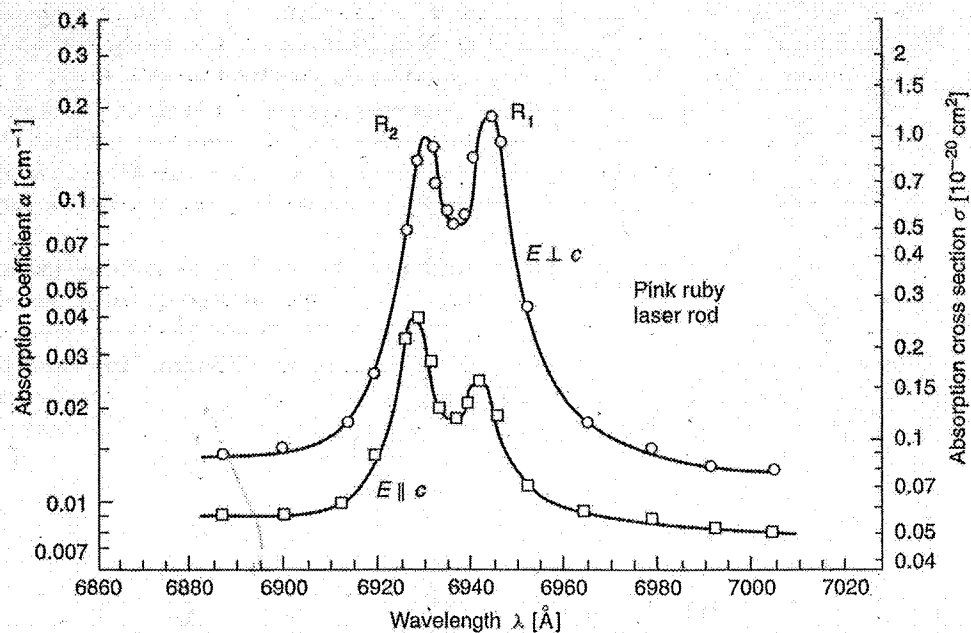
Figure 11.3 Since ruby is uniaxial, its absorption coefficient is a very strong function of the polarization direction of the light. (From D. C. Cronemeyer, *J. Opt. Soc. Am.* 56:1703 (1966). Reprinted with the permission of the Optical Society of America.)
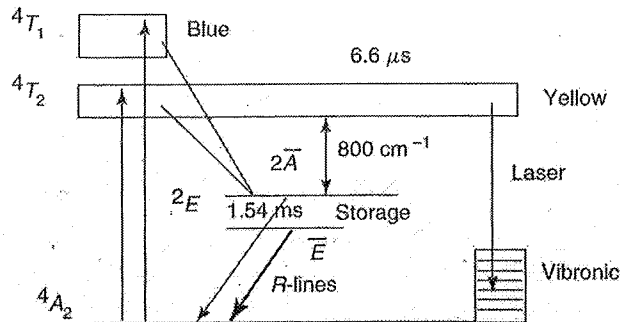
Figure 11.4   The energy band diagram for alexandrite.

11.3.2 Alexandrite—Tunable from 700 nm to 818 nm

Alexandrite ($BeAl_2O_4$:Cr^{3+} or chromium-doped chrysoberyl) is a hard orthorhombic material. Chrysoberyl itself is considered a semiprecious jewelry material and is commonly called oriental topaz. It ranges in color from yellow through green to brown. When chrysoberyl is doped with chromium, the material turns emerald green and displays a secondary red color when viewed in artificial light. (As an aside, one variety of chrysoberyl occurs in a crystal form consisting of parallel arrangements of fibers. When cut as a cabochon, it is called cat's-eye or tiger's-eye.)

Alexandrite is biaxial,[38] hard, of good optical quality, and quite thermally conductive (0.23 W/cm-K as compared with 0.14 W/cm-K for YAG and 0.42 W/cm-K for ruby). Alexandrite is nonhygroscopic, melts at 1870°C, and has a Moh's hardness of 8.5 (which makes it harder and more durable than YAG, but somewhat less than ruby). Additionally, alexandrite has a very high thermal fracture limit (60% of ruby and five times that of YAG).

Doping the yellowish chrysoberyl with chromium results in an emerald green alexandrite crystal. Alexandrite is biaxial and the crystal appears green, red, or blue, depending on the angle and lighting conditions. The principle axes of the indicatrix are aligned with the crystallographic axes.[39] Lasers are usually operated with light parallel to the b-axis because the gain for polarization in this direction is roughly ten times that of any other direction.

As with ruby, the Cr^{3+} occupies the aluminum sites in the crystal. However, there are two different aluminum sites in alexandrite. One site has mirror symmetry, the other has inversion symmetry. Most of the chromium substitutes for aluminum in the larger mirror site (about 78%), which (luckily!) is the dominant site for laser action. The doping in alexandrite can be a great deal higher than with ruby. Doping concentrations as high as 0.4 weight percent still yield crystals of good optical quality (although 0.2 to 0.3 weight percent is somewhat more common).

The energy diagram for alexandrite is given in Figure 11.4. Alexandrite can be operated as either a three-state system or as vibronic four-state system (note the similarity to ruby!). The laser pump bands are principally the $^4T_1$(higher) and the $^4T_2$ (lower) bands. The ground state is the $^4A_2$ band. The two pump bands form manifolds centered around

---

[38]A biaxial crystal is one where all three of the Cartesian directions have different indices of refraction. See Section 8.3 for a discussion of uniaxial and biaxial crystals.

[39]See Section 8.3 for more discussion on the indicatrix.

the blue (410 nm) and yellow (590 nm). The pump bands are each quite wide, with widths approximately 1000 angstroms.

In a fashion similar to ruby, there is a metastable ^2E state. As with ruby, laser action can occur on the R lines of the ^2E state and can generate three-state laser behavior at similar wavelengths (680.4 nm). The major difference between the R-state lasing in alexandrite and ruby is that alexandrite possesses a higher threshold and lower efficiency. Thus, alexandrite is not used as a ruby replacement.

The major value of alexandrite is in its four-state tunable laser energetics. When operated as a four-state laser, alexandrite is a vibronic laser. Lasing action occurs between vibronic rather than purely atomic states. Thus, the emission of a photon is also accompanied by the emission of phonons as the state returns to equilibrium. This is what provides the tunability. The laser wavelength is determined by which of the vibronic states is the top laser state. Any energy not carried off by the photon will then be emitted by phonons to restore the system to its ground state.

Laser action occurs by emission from the $^4T_2$ state to the excited vibronic states within the $^4A_2$ band. Subsequent phonon emission returns the $^4A_2$ band to equilibrium. The $^4T_2$ state is much shorter lived (6.6 μs) than the metastable ^2E states (1.54 ms) and is quite close in energy (800 cm^{-1}), so the metastable ^2E states serve as a storage state for the $^4T_2$ state.

In any laser with a very broad pumping curve, there is the risk that the laser photons themselves will be reabsorbed. Luckily, in alexandrite, there is a deep minimum in excited-ion absorption across the primary laser tuning range. Therefore, excited-ion absorption is not an issue over much of the range. However, the long wavelength tuning limit in alexandrite is due to excited-ion absorption. At higher wavelengths than 818 nm, the excited-ion absorption cross-section is larger than the laser cross-section, and laser action is suppressed.

Alexandrite has exceptionally fascinating behavior with temperature. As the temperature increases in most four-state lasers, the lower laser state population increases, and laser action is reduced. However, the laser output from alexandrite increases with temperature up to a temperature of around 200°C, and then decreases abruptly. This is because there are two competing temperature effects in alexandrite. Although the lower state population does increase with temperature, there is also the coupling between the metastable ^2E storage states and the $^4T_2$ state. As the temperature increases, the population in the upper laser state increases, partly counteracting the increase in population in the lower state. Thus, alexandrite possesses an improvement in performance with temperature at wavelengths greater than 730 nm.

Unfortunately, the lifetimes of the upper and storage states somewhat reduce the advantages of higher temperatures. When the temperature is increased, the population in the $^4T_2$ state increases. However, this state has a shorter lifetime. Thus the effective upper state lifetime (the population-ratioed combination of the two upper state states) is reduced. At some temperature, the combined upper state lifetime is shorter than the pump pulse width and energy is lost in fluorescence. This also reduces the advantages of increasing temperature.

One final temperature effect is worth mentioning. At higher temperatures, the peak of the gain curve shifts to longer wavelengths. This is due to increased phonon populations as well as a shift of the R lines and enhancement of the long wavelength vibronic transitions. The net result is a rather dramatic change in laser wavelength with increasing temperature.
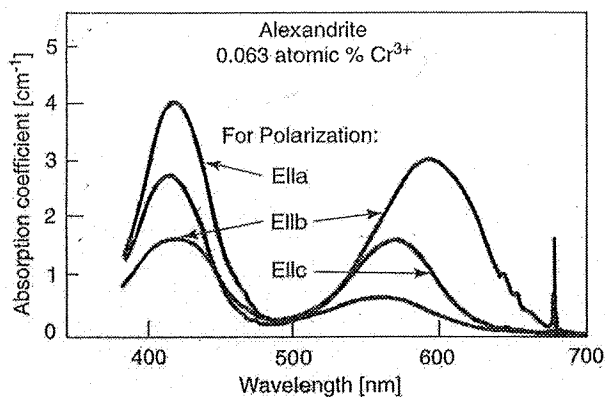
Figure 11.5   Since alexandrite is biaxial, its absorption coefficient is a very strong function of the polarization direction of the light, for all three directions. (Modified from J. C. Walling, H. P. Jenssen, R. C. Morris, E. W. O'Dell, and O. G. Peterson, *Opt. Lett.* 4:182 (1979), Figure 3. Reprinted with the permission of the Optical Society of America).

Since alexandrite is biaxial, its absorption coefficient is a very strong function of the polarization direction of the light, in all three directions! (See Figure 11.5.) This creates some of the same orientation and pumping inhomogeneities observed in ruby.

11.3.3 Ti:sapphire—Tunable from 670 nm to 1090 nm

Ti:sapphire was developed relatively late in laser evolution. However, since the discovery of laser action in Ti:sapphire in 1982, Ti:sapphire has become one of the most widely used solid-state laser materials.

Recall that ruby is chromium-doped Al_2O_3. Ti:sapphire is titanium-doped Al_2O_3. Thus, ruby and Ti:sapphire have many of the same mechanical and optical properties. Ti:sapphire is also an optically uniaxial crystal that is hard (Moh's hardness of 9), of good optical quality, and extremely thermally conductive (0.42 W/cm-K). Ti:sapphire is nonhygroscopic, refractory and is even more durable than ruby due to a slight advantage obtained with the titanium doping.

Sapphire is doped with Ti^{3+} to obtain laser quality Ti:sapphire. The Ti^{3+} substitutes for the Al^{3+} in the crystal. Typical dopings range from 0.03 to 0.15 weight percent of titanium (slightly higher than the chromium in ruby). However, the similarities between ruby and Ti:sapphire do not include the spectroscopy. The energy diagram for Ti:sapphire (Figure 11.6) possesses only two states, but the vibronic nature of the transitions makes it possible to absorb from the bottom of the ground state to the upper vibronic manifold and to lase from the bottom of the upper vibronic manifold down to the vibronic ground states.

This peculiar spectroscopy is driven by the single $(3d)^1$ electron. The $(3d)^1$ state (which would be degenerate in a free transition-metal) is split by the cubic field when the metal is substitutionally doped into the aluminum site in the sapphire. The result is a doubly degenerate excited state ^2E_g and a triply degenerate ground state $^2T_{2g}$. These excited and ground states are further split by the trigonal field and spin orbit coupling. The result is a bottom manifold of states $^2T_{2g}$ and a top manifold ^2E_g. One phonon of energy 172 cm^{-1} couples to the excited state ^2E_g state and two phonons with energies of 220 and 260 cm^{-1} couple to the ground state $^2T_{2g}$. (In comparison, ruby has three d electrons and a rather more conventional energy state diagram!)

^2E_g ^2E $E_{1/2}$

$E_{3/2}$

$^2A_1$

$^2T_{2g}$ $^2E_{1/2}$

^2E

$^1E_{1/2}$

$E_{3/2}$
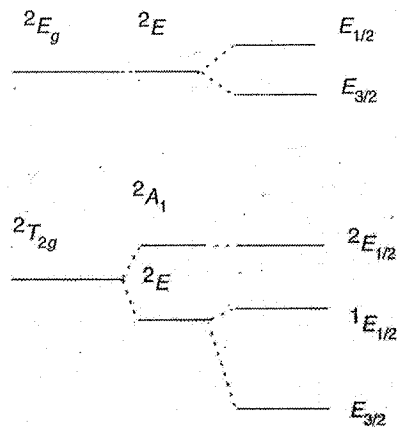
Figure 11.6 The energy band diagram for Ti:sapphire.

π Polarization

Absorbance   Fluorescence

Intensity [arb. units]

Wavelength [nm]
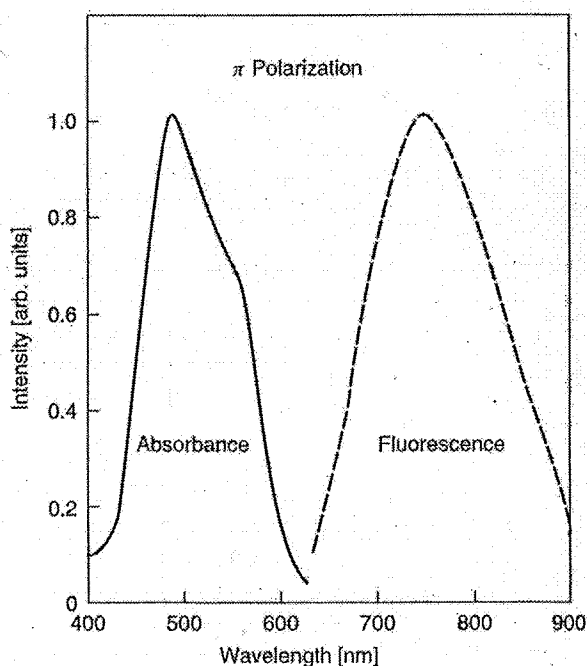
Figure 11.7 Ti:sapphire possesses very large polarization-dependent absorption bands in the blue-green (centered around 490 nm with widths of roughly 150 nm). Similarly, Ti:sapphire possesses very large polarization dependent emission bands in the red/IR (centered around 780 nm with widths of roughly 230 nm). (From P. F. Moulton, *J. Opt. Soc. Am. B* 3:125 (1986). Reprinted with the permission of the Optical Society of America.)

Ti:sapphire possesses very large polarization dependent absorption bands in the blue-green (centered around 490 nm with widths of roughly 150 nm; see Figure 11.7) Absorption of radiation polarized along the optic axis π is nearly twice that of the perpendicular polarization σ. The absorption is generated by vibronic transitions between the ground state $^2T_{2g}$ and the excited state ^2E_g. Similarly, Ti:sapphire possesses very large polarization dependent emission bands in the red/IR (centered around 780 nm with widths of roughly 230 nm). Nearly three times as much light is emitted polarized along the optic axis π as

perpendicular to it σ. The emission is generated by transitions between vibronic transitions from the excited state ^2E_g to vibronic transitions to the ground state $^2T_{2g}$.

It is a delightful property of the vibronic states of Ti:sapphire that the absorption and emission bands barely overlap. Thus, a laser photon generated within the emission band is unlikely to stimulate absorption in the absorption band.

Although Ti:sapphire has a reasonable cross-section ($4.1 \cdot 10^{-19}$ cm^2), it also has a relatively short upper state lifetime (3.2 μs). As a consequence, it is a difficult material to pump with flashlamps. However, flashlamp operation has been achieved, with outputs on the order of 3J/pulse at 2% efficiency. Flashlamps used for Ti:sapphire must typically be altered (for example with a dye) to convert the blue-UV light of the lamp into the blue-green absorption profile of the laser. The usual design strategy for successful operation of a flashlamp pumped Ti:sapphire laser is to create a *very* short flashlamp pulse (less than 10 μs) through clever design of the pulse-forming network.

The blue-green absorption profile of Ti:sapphire is beautifully matched to the output of cw argon lasers, cw internally-doubled Nd:YAG lasers (particularly diode-pumped cw YAGs) and pulsed doubled Nd:YAG lasers. Using a Q-switched doubled Nd:YAG laser as the pump gives the additional advantage of permitting gain-switched operation. (Gain switching is similar to Q-switching, except in gain-switching, the laser gain is turned on very quickly, rather than the laser loss being turned off very quickly.)

The phenomenal bandwidth of Ti:sapphire is ideal for mode-locking. Ti:sapphire lasers have been mode-locked with acousto-optic mode-locking, passive mode-locking, injection-seeding, and coupled-cavity mode-locking. In 1991 it was discovered that Ti:sapphire lasers will self-mode-lock. A flurry of advances occurred in this technology, resulting in elegant methods for self-mode-locking Ti:sapphire lasers with temporal pulse lengths of less than 10 fs. This advancement was a major change in laser development, as until that time all ultrashort pulse lasers were dye lasers (see Section 11.5).

11.3.4 Comparison between Major Solid-State Laser Hosts

Consider the solid-state hosts as shown in Table 11.1. Notice that ruby and Ti:sapphire are the mechanically more robust and thermally conductive. Nd:YAG and alexandrite are both four-state lasers with long upper state populations (permitting lamp pumping), while

TABLE 11.1   SOLID-STATE LASER HOSTS

	Ruby	Nd:YAG	Alaexandrite	Ti:sapphire
Hardness	9	8.2	8.5	9.1
Thermal conductivity (W/cm-K)	0.42 (300 K)	0.14 (300 K)	0.23 (300 K)	0.42 (300 K)
Upper-state lifetime	3.0 ms (300 K)	230 ηs (300 K)	260 ηs (300 K)	3.2 ηs (300 K)
σ_{21} (cross-section) (cm^2)	$2.5 \cdot 10^{-20}$	$6.5 \cdot 10^{-19}$	$1 \cdot 10^{-20}$	$4.1 \cdot 10^{-19}$
Linewidth (Å)	5.3 (11 cm^{-1}) (300 K)	4.5 (300 K)	1000	2300

Ti:sapphire has a very short upper state population (generally requiring laser pumping). Nd:YAG and Ti:sapphire have relatively large cross-sections while alexandrite and ruby have smaller cross-sections. Ti:sapphire has the widest linewidth and ruby the narrowest.

11.4 TI:SAPPHIRE LASER DESIGN

Ti:sapphire lasers differ from conventional solid-state lasers in two major ways: First, Ti:sapphire lasers are typically pumped by an argon-ion or Nd:YAG laser. As a consequence, the resonant cavity geometry is often a ring or folded-Z cavity to allow the pump beam to interact with the laser material while avoiding pump light in the output beam. (Ring laser cavities are discussed in Section 11.4.1.) Second, Ti:sapphire lasers have very large tuning curves. Tuning elements such as etalons do not possess sufficient range to tune Ti:sapphire lasers. Instead, birefringent filters are usually employed. (Birefringent filters are discussed in Section 11.4.2).

11.4.1 Ring Lasers

The first ring resonator was demonstrated in 1963 by Tang et al. in ruby.[40] Although the primary applications for early ring resonators were in optical gyroscopes,[41] ring lasers did not see much commercial application as resonator structures until the development of the dye laser.[42,43] Not only did the ring ease some of the geometrical constraints in building dye lasers, the counter-propagating nature of the mode permitted the construction of the first femtosecond pulse lasers (see Section 11.5).

Ring laser geometries are often necessary with Ti:sapphire lasers, because of the geometrical requirements imposed by pump lasers. Some especially elegant designs have been implemented, including diode-pumped monolithic ring resonators where the entire ring is inside the gain material[44].

Basics on ring resonators. The prototypical laser resonator consists of two mirrors facing each other (see Figure 11.8). This configuration creates electric and magnetic field standing waves in the resonator with a period of one-half of an optical wavelength. These standing waves interact with only part of the volume of the laser material, thus creating spatial inhomogeneities in the gain. This effect is termed *spatial hole burning*.

If the laser is running on multiple longitudinal modes (creating many overlapping standing wave regions), or if the laser is a gas laser (where the atoms are in constant motion), this effect is not very significant. However, for single-mode solid-state lasers, spatial hole burning can significantly reduce the output power of the operating laser mode.

---

[40]C. L. Tang, H. Statz, and G. deMars, Jr., *J. Appl. Phys.* 34:2289 (1963).

[41]W. Chow et al., *Rev. Mod. Phys.* 57:61 (1985).

[42]F. P. Schafer and H. Muller, *Opt. Commun.* 2:407 (1971).

[43]J. M. Green, J. P. Hohimer, and F. K. Tittel, *Opt. Commun.* 7:349 (1973).

[44]T. J. Kane and R. L. Byer, *Opt. Lett.* 10:65 (1985).
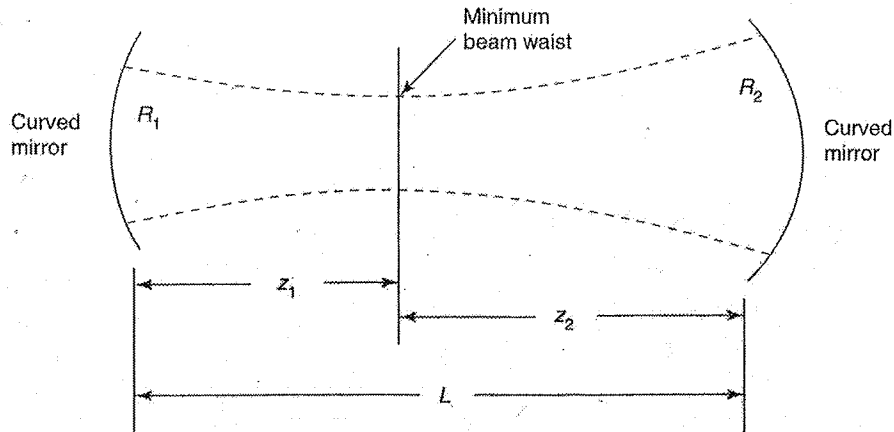
Figure 11.8   The prototypical laser resonator consists of two mirrors facing each other.
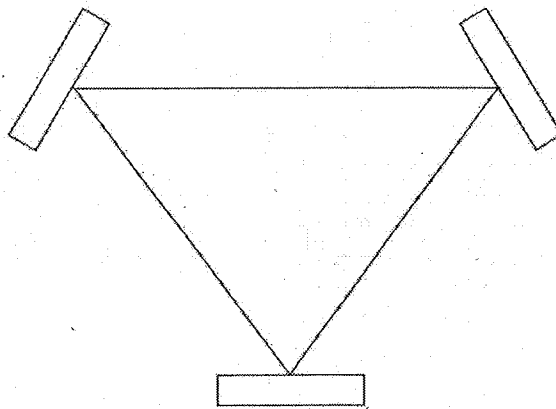
Figure 11.9   A simple ring resonator will have longitudinal modes (the back-and-forth length of a conventional laser is equivalent to the round-trip length of a ring laser) and standing wave patterns (formed by the interaction between the left and right traveling waves in the ring).

Spatial hole burning can be reduced by generating circularly polarized light in the laser material,[45] mechanically moving the material,[46] or by phase modulating the beam entering the material.[47] However, one of the most successful methods for eliminating spatial hole burning is to structure the resonator in a unidirectional ring geometry.

A simple ring resonator (such as in Figure 11.9) is not very different from a conventional resonator. A simple ring resonator will have longitudinal modes (the back-and-forth length of a conventional laser is equivalent to the round-trip length of a ring laser) and standing wave patterns (formed by the interaction between the left and right traveling waves in the ring).

However, ring lasers can also be made to operate in only one direction. Such unidirectional ring lasers no longer possess standing waves and do not create spatial hole

[45]D. A. Draegert, *IEEE J. of Quantum Electron.* QE-8:235 (1972).

[46]H. G. Danielmeyer, *Appl. Phys. Lett.* 16:124 (1970).

[47]H. G. Danielmeyer, *Appl. Phys. Lett.* 17:519 (1970).
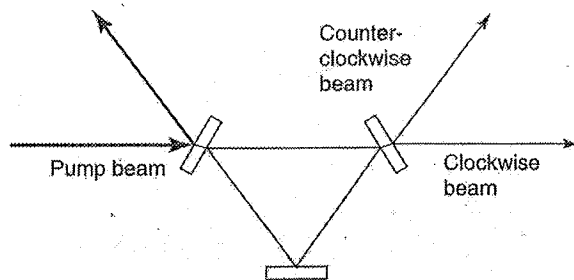
Figure 11.10   One of the advantages of a ring laser is that it is relatively easy to configure the resonator so that the back-reflected beam from a pump laser is not reflected into the resonator of the pump laser.

burning effects. Eliminating spatial hole burning provides several advantages. First, since the laser material is more homogeneous, there is more overall gain available to the longitudinal modes. This increases mode competition between adjacent longitudinal modes, making it possible to pump the laser harder and still retain single longitudinal mode operation. Additionally, since the gain is more homogeneous, more power can be extracted by a single operating mode. The combination of increased pumping range and increased gain means that unidirectional ring lasers can deliver significantly more power than conventional resonators.

Ring lasers possess some additional advantages. If a laser is being used as a pump for a ring laser, it is relatively easy to configure the resonator so that the back-reflected beam is not returned back into the resonator of the pump laser (see Figure 11.10). The optical system formed by a plane parallel mirror of a conventional resonator and the output mirror of the pump laser can act like a Fabry-Perot cavity attached to the laser. The interaction between this external Fabry-Perot and the resonator of the pump laser can significantly alter the frequency and intensity properties of the pump laser. (This is the origin of the oscillation that occurs when aligning a laser cavity with a HeNe laser and backreflecting the alignment beam precisely down the bore of the alignment laser.)

Ring lasers also possess more flexibility in cavity design, particularly for unstable resonators or for lasers that have a number of sensitive intracavity elements. Additionally, unidirectional ring lasers inherently have an ordering to the elements in the cavity. (For example, the gain material might be followed by a doubling crystal and then by a birefringent filter.) Inherent ordering of optical components is important in many applications.

Creating unidirectional oscillation.   One method for generating unidirectional oscillation is to create a small external cavity aligned with one of the propagating directions of the ring laser (see Figure 11.11). If the laser is running counter-clockwise (CCW), the traveling wave in the laser does not interact with the external cavity. However, if the laser is running clockwise (CW), the beam is back reflected into the CCW direction and supports the CCW mode.[48]

This method works for certain laser materials. However (even when it works) the method does not completely suppress the light in the unwanted direction. Perhaps more

---

[48]The terms cw (for continuous wave) and cw (for clockwise) are both commonly used in laser engineering. There is no standard notation to distinguish them, and so the meaning must be deduced from context. Here I will use CW for the latter.
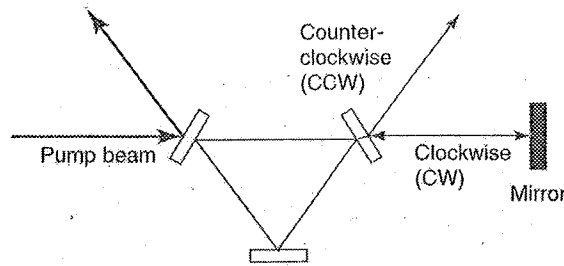
Figure 11.11   One method for generating unidirectional oscillation in a ring laser is to create a small external cavity aligned with one of the propagating directions of the ring laser.

importantly, the method can enhance mode-beating (particularly if there are multiple longitudinal modes running in the ring) and interferometric effects.

A more reliable method for generating unidirectional oscillation in a ring laser is to use an optical diode constructed from a Faraday rotator, a half-wave plate, and a Brewster plate or polarizer (see Figure 11.12).

A Faraday rotator (as used in a ring laser) is a device that changes the angle of linear polarization of light as a function of an applied DC magnetic field. The angle is changed in the *same* direction, independent of the direction of the wave propagation.

To explain this further, consider a vertically polarized wave traveling in the CCW direction and entering a Faraday rotator as shown in Figure 11.13. Assume the Faraday rotator changes the direction of linear polarization from vertical to 45 degrees to the vertical.
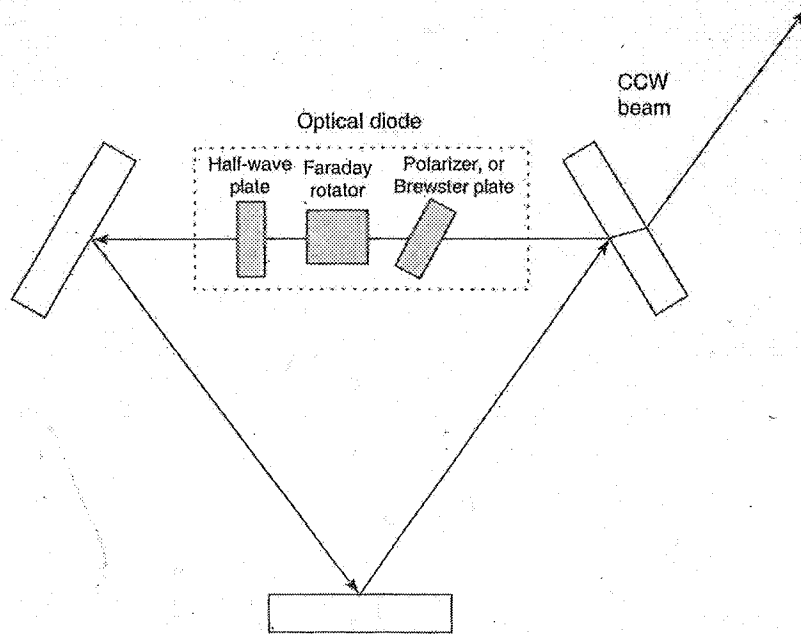
Figure 11.12   Another method for generating unidirectional oscillation in a ring laser is to place an optical diode (constructed from a Faraday rotator, a half-wave plate, and a Brewster plate or polarizer) in the resonator.
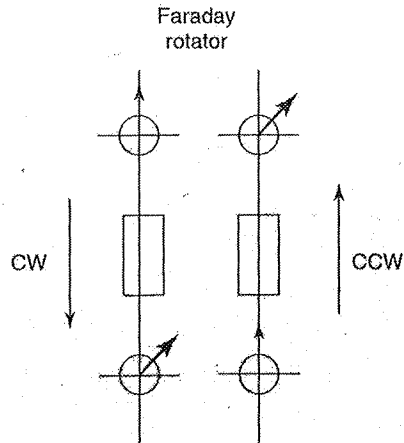
Faraday
rotator

Figure 11.13 Vertically polarized light passing through a Faraday rotator in clockwise (CW) and counter-clockwise (CCW) directions.

Now, assume a vertically polarized wave traveling in the CW direction is incident on the same Faraday rotator. The rotator will also change the direction of linear polarization from vertical to 45 degrees to the vertical. The angle has been changed in the same direction independent of the propagation direction of the wave.

Contrast this behavior with that of a half-wave plate. Consider a vertically polarized wave traveling in the CCW direction and entering a half-wave plate as shown in Figure 11.14. Assume the half-wave plate changes the direction of linear polarization from vertical to 45 degrees to the vertical. Now, assume a vertically polarized wave traveling in the CW direction is incident on the same half-wave plate. The rotator will change the direction of linear polarization from vertical to 315 degrees to the vertical (that is, 45 degrees in the *other direction* from vertical).

The unusual nature of Faraday rotators can be explained in another way. Assume that a Faraday rotator is configured with a mirror so that a beam enters the rotator, bounces off the mirror and enters the rotator again (but traveling the other direction). (See Figure 11.15.) Consider a vertically polarized wave traveling in the CCWdirection and entering the Faraday
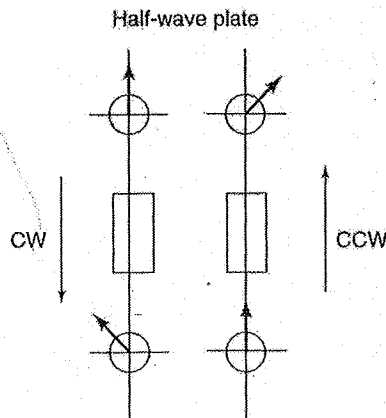
Half-wave plate

Figure 11.14 Vertically polarized light passing through a half-wave plate in clockwise (CW) and counter-clockwise (CCW) directions.

Faraday

CW   CCW
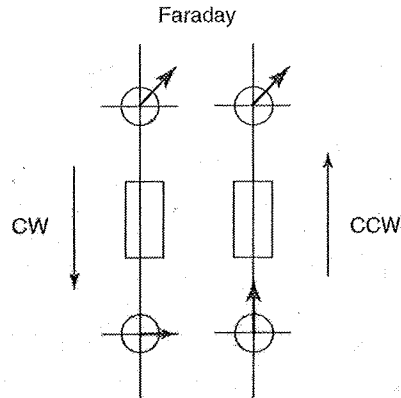
Figure 11.15   Vertically polarized light passing through a Faraday rotator in the CCW direction, being back-reflected, and passing back through the Faraday rotator in the CW direction.

rotator. Assume the rotator changes the direction of linear polarization from vertical to 45 degrees to the vertical. Now, the beam will be directed back through the rotator by the mirror, and will again be altered by 45 degrees in the same direction. The beam is now 90 degrees from its original polarization.

Contrast this with a half-wave plate. Assume that a half-wave plate is configured with a mirror so that a beam enters the half-wave plate, bounces off the mirror, and enters the half-wave plate again (but traveling the other direction). (See Figure 11.16.) Consider a vertically polarized wave traveling in the CCW direction and entering the half-wave plate. Assume the half-wave plate changes the direction of linear polarization from vertical to 45 degrees to the vertical. Now, the beam will be directed back through the half-wave plate by the mirror, and will be altered by 45 degrees in the reverse direction. The beam is at the same polarization as the original!

The contrasting properties of Faraday rotators and half-wave plates allow the creation of optical diodes. As an example, consider the optical system illustrated in Figure 11.17. Here, a Brewster plate (or polarizer) is oriented to pass vertical polarization. The Brewster plate is followed by a Faraday rotator and then by a half-wave plate. Consider the CCW wave first. A vertically polarized wave is first passed with no loss by the Brewster plate.

Half-wave plate

CW   CCW
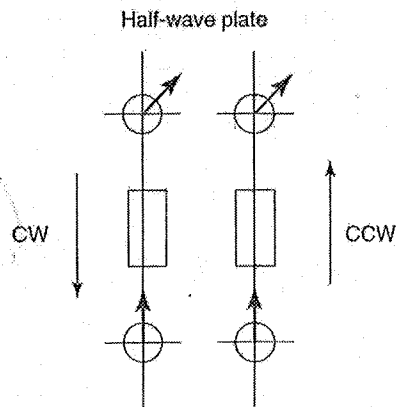
Figure 11.16   Vertically polarized light passing through a half-wave plate in the CCW direction, being back-reflected, and passing back through the half-wave plate in the CW direction.
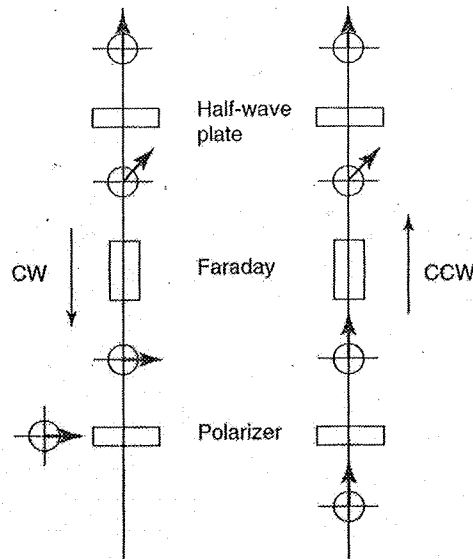
Figure 11.17   The contrasting properties of Faraday rotators and half-wave plates allow the creation of an optical diode. This system passes CCW light unchanged, but attenuates CW light.

Then, the Faraday rotator changes the direction from vertical to 45 degrees to the vertical. The half-wave plate then returns the polarization direction to the vertical. The original wave polarization has been recovered.

Now, consider the CW wave. A vertically polarized wave enters the half-wave plate and the direction is changed from vertical to 45 degrees to the vertical. The Faraday rotator then continues the change to 90 degrees to the vertical. The CW wave (now perpendicular to the CCW) experiences high loss from the Brewster plate (or polarizer) and is attenuated.

11.4.2 Birefringent Filters

A tunable laser (such as Ti:sapphire) requires some type of adjustable optical tuning element in order to run with a narrow linewidth. Spatially dispersive elements, such as prisms or gratings, can be used to provide this tuning. However, it is extremely difficult to design good tuning systems for wide bandwidth tunable lasers using spatially dispersive elements.[49]

An alternative strategy is to use etalons. Recall from Chapter 3 that a conventional etalon makes a very good high-resolution filter. However, a single etalon can only be tuned over its free spectral range. Thus, etalons are well-suited for isolating narrow linewidth features (such as a single argon-ion longitudinal mode) but are less well-suited for broad tuning.

Birefringent filters offer an effective alternative to dispersive elements or etalons. Multiple element birefringent filters offer excellent resolution over a very broad spectral tuning range. The first use of a birefringent filter as a tunable narrow band laser filter was

---

[49]A. L. Bloom, *Opt. Engineering* 11:1 (1972).

Birefringent plate at
Brewster's angle
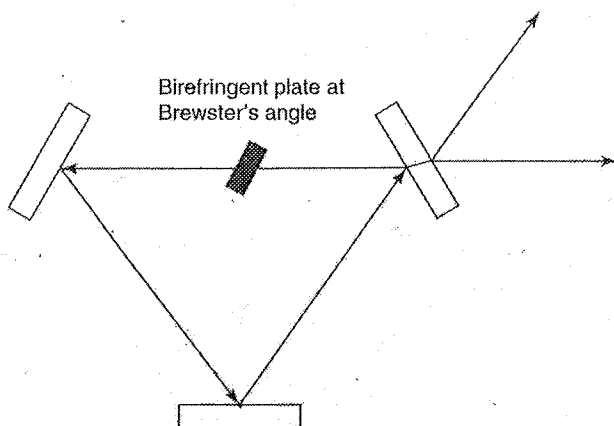
Figure 11.18   A birefringent filter is a plate of birefringent material placed inside a laser cavity at Brewster's angle. The birefringent filter will transmit a set of wavelengths corresponding to an integral number of full wave retardations in the crystal.

in 1972 by Yarborough.[50] Birefringent filters are analyzed by Bloom,[51] Preuss and Gole,[52] and Valle and Moreno.[53] Negus et al. hold a patent on a birefringent filter for use in a tunable pulsed laser cavity.[54]

A birefringent filter is a plate of birefringent material placed inside a laser cavity at Brewster's angle (see Figure 11.18). When the wavelength of the light incident on the filter corresponds to an integral number of full wave retardations in the birefringent element, then the beam emerges unchanged. However, if the wavelength of the incident light is anything other than an integral number of full wave retardations, then its polarization will be altered and it will suffer loss at the Brewster surface. Thus, the birefringent filter will transmit a set of wavelengths corresponding to an integral number of full wave retardations in the crystal (see Figure 11.19).

A birefringent filter can be tuned by rotation around its own axis (the rotational direction that does not change the Brewster angle orientation). This alters the index of refraction seen by the incident beam and thus the wavelength corresponding to an integral number of full wave retardations.

A single birefringent filter possesses a sinusoidal-like transmittance profile (see Figure 11.19) that is usually too broad for use as a tuning element in a Ti:sapphire laser. However, multiple birefringent filters can be used to provide greater selectivity. For example, Figure 11.20 illustrates the transmittance of a three-stage quartz birefringent filter with thicknesses of 0.5 mm, 1 mm, and 7.5 mm.

Birefringent filters can be analyzed with a matrix technique in a similar fashion to multilayer dielectric films.[55] Of special interest is the intensity transmittance for a single

---

[50] J. M. Yarborough and J. Hobart, post-deadline paper, CLEA meeting (1973).

[51] A. Bloom, *J. Opt. Soc. of Am.* 64:447 (1974).

[52] D. R. Preuss and J. L. Cole, *Appl. Opt.* 19:702 (1980).

[53] P. J. Valle and F. Moreno, *Appl. Opt.* 31:528 (1992).

[54] D. K. Negus et al., "Birefringent Filter for Use in a Tunable Pulsed Laser Cavity," U.S. Patent #5,164,946, Nov. 17, 1992.

[55] D. R. Preuss and J. L. Cole, *Appl. Opt.* 19:702 (1980).
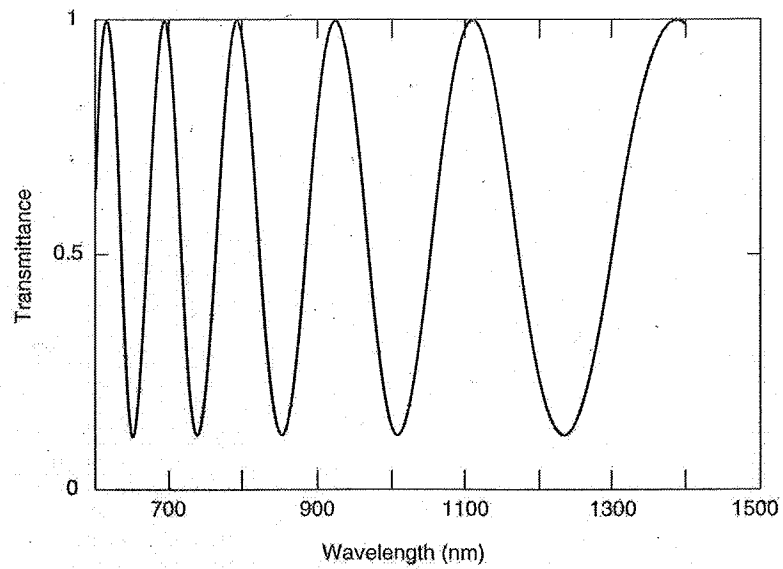
Figure 11.19 A single birefringent filter possesses a sinusoidal-like transmittance profile.
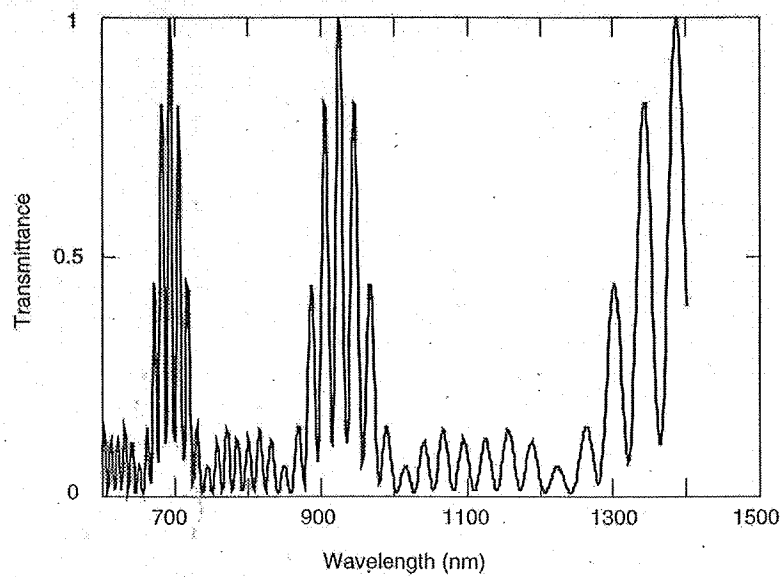
Figure 11.20 Multiple birefringent filters can be used to provide greater selectivity. This illustrates the transmittance of a three-stage birefringent filter with thicknesses of 0.5 mm, 1 mm, and 7.5 mm.

birefringent filter given by

$$I_{TM} = 1 - \sin^2(2\phi) \frac{n_o^4 - n_o^2 \cos^2(\theta)}{\left(n_o^2 - \cos^2(\phi)\cos^2(\theta)\right)^2} \cdot$$

$$\sin^2 \left(\frac{\pi d}{\lambda} \frac{n_e \left[1 - \cos^2(\theta)\cos^2(\phi)/n_e^2 - \cos^2(\theta)\cos^2(\phi)/n_o^2\right]}{\left[1 - \cos^2(\theta)\sin^2(\phi)/n_e^2 - \cos^2(\theta)\cos^2(\phi)/n_o^2\right]^{1/2}} - \frac{\pi d}{\lambda} \frac{n_o}{\left[1 - \cos^2(\theta)/n_o^2\right]^{1/2}} \right)$$

(11.1)

where $\theta = \pi/2 - \theta_B$ for Brewster angle incidence (where θ_B is Brewster angle), ϕ is the tuning angle (ranges from 0 to 90 degrees), and d is the thickness.[56]

Example 11.1

Calculate the transmittance for a three-stage birefringent filter fabricated from quartz. Assume the smallest element is 0.5 mm thick and that the elements are in the ratio 1:2:15. Assume the filter is in at Brewster's angle and that the rotational angle is 50 degrees. Plot the transmittance from 600 nm to 1400 nm.

Solution.   Programs such as Mathcad are well-suited for this type of calculation. Figure 11.20 illustrates the results of a Mathcad calculation for this problem.

11.4.3 Coherent Model 890 and 899 Ti:Sapphire Lasers

The Coherent Model 890 laser is a laser-pumped cw broadband Ti:sapphire laser (see Figure 11.21). The output power depends on the pump and can be as high as 2.5 watts with the SW mirror set and a 15 watt argon-ion pump.

Three sets of standard optics are used to access the Ti:sapphire tuning range. Using these three sets of optics, the wavelength can be tuned from 690 nm to beyond 1100 nm (see Figure 11.22).

In order to accommodate both low- and high-power pump lasers, the Model 890 can be configured for either high- or low-power pumping. The goal of the variable pump scheme is to optimize the overlap between the $TEM_{0,0}$ resonator mode and the pump beam. This maximizes the conversion efficiency and minimizes thermal lensing in the Ti:sapphire.

The laser wavelength is tuned with a birefringent filter (see Section 11.4.2). Smooth continuous tuning is accomplished by minimizing the competition between the birefringent tuning filter and the natural birefringence of Ti:sapphire. To achieve this, the crystal is mounted such that the polarization vector of the intracavity mode is aligned parallel to the c-axis of the crystal.

The alignment of the polarization and optic axis vectors is achieved via a face-normal rotation adjustment. This alignment prevents gaps or skips in the output tuning curve. The Model 890 resonator is a folded linear resonator (see Figure 11.23). The backbone of the 890 resonator is a 5 cm diameter, solid, stainless-steel bar. The bar has a high thermal mass, which reduces the system sensitivity to changes in the ambient temperature. Mirrors

---

[56]D. R. Preuss and J. L. Cole, *Appl. Opt.* 19:702 (1980).
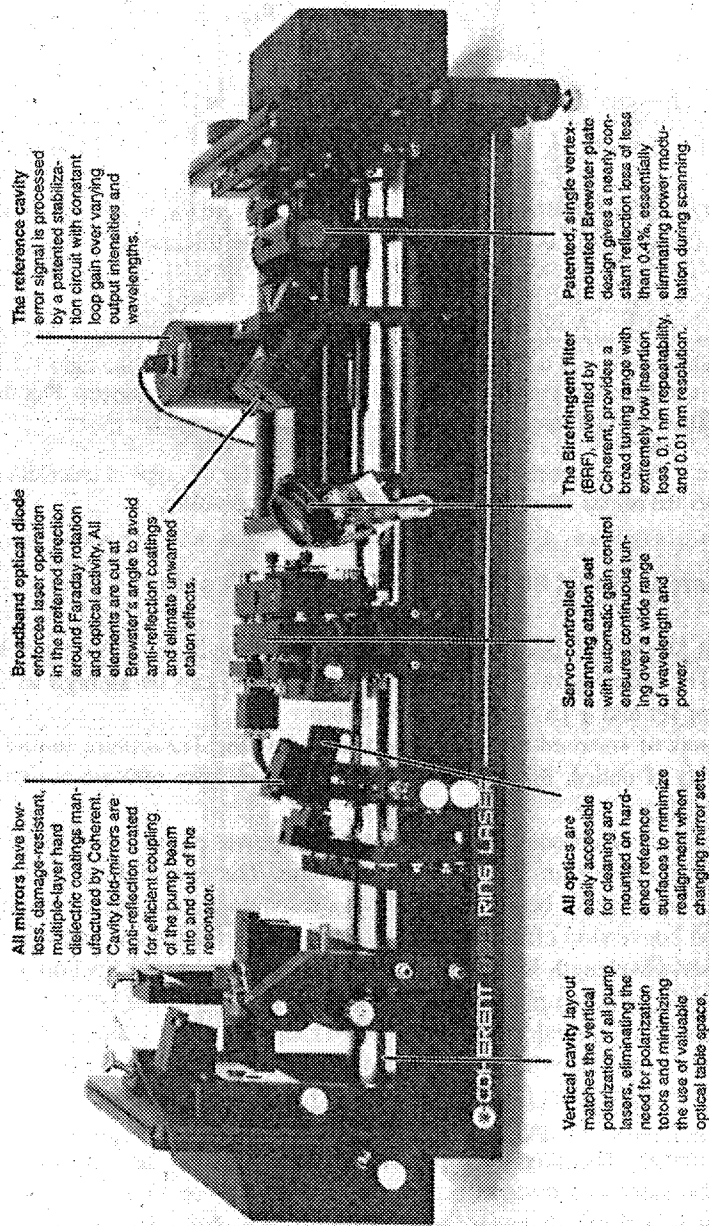
All mirrors have low-loss, damage-resistant, multiple-layer hard dielectric coatings manufactured by Coherent. Cavity fold-mirrors are anti-reflection coated for efficient coupling of the pump beam into and out of the resonator.

Broadband optical diode enforces laser operation in the preferred direction around Faraday rotation and optical activity. All elements are cut at Brewster's angle to avoid anti-reflection coatings and eliminate unwanted etalon effects.

The reference cavity error signal is processed by a patented stabilization circuit with constant loop gain over varying output intensities and wavelengths.

All optics are easily accessible for cleaning and mounted on hardened reference surfaces to minimize realignment when changing mirror sets.

Servo-controlled scanning etalon set with automatic gain control ensures continuous tuning over a wide range of wavelength and power.

The Birefringent filter (BRF), invented by Coherent, provides a broad tuning range with extremely low insertion loss, 0.1 nm repeatability, and 0.01 nm resolution.

Patented, single vertex-mounted Brewster plate design gives a nearly constant reflection loss of less than 0.4%, essentially eliminating power modulation during scanning.

Vertical cavity layout matches the vertical polarization of all pump lasers, eliminating the need for polarization rotors and minimizing the use of valuable optical table space.

Figure 11.21 The Coherent Model 890 laser is a laser-pumped cw broadband Ti:sapphire laser. The output power depends on the pump and can be as high as 2.5 watts with the SW mirror set and a 15 watt argon-ion pump. (Courtesy of the Coherent, Inc., Laser Group, Santa Clara, CA)
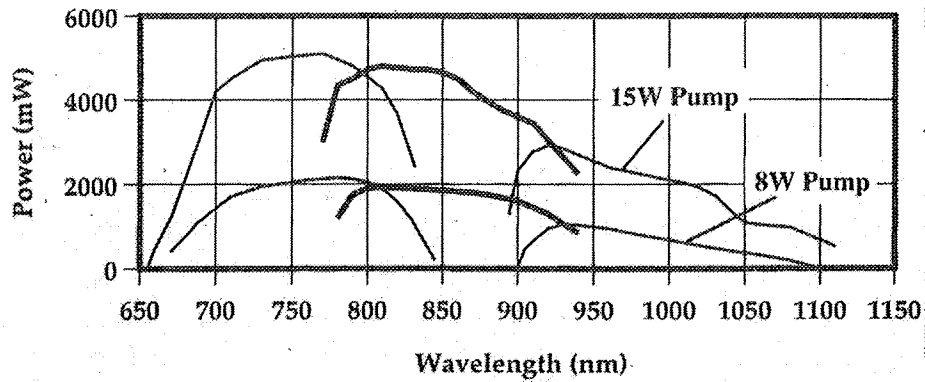
Figure 11.22 The Coherent Model 890 laser is a laser-pumped cw broadband Ti:sapphire laser. Three sets of standard optics are used to access the Ti:sapphire tuning range. Using these three sets of optics, the wavelength can be tuned from 690 nm to beyond 1100 nm. (Courtesy of the Coherent, Inc., Laser Group, Santa Clara, CA)
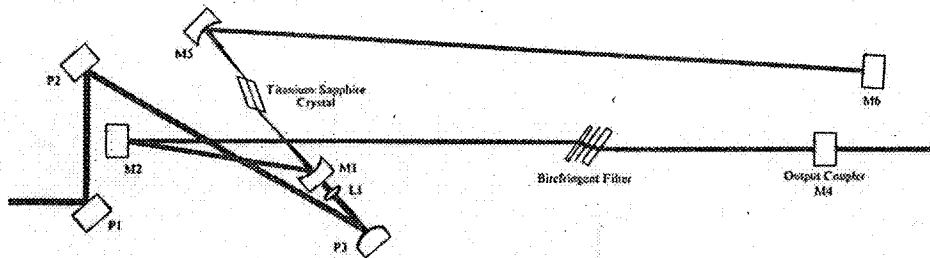
Figure 11.23 The Model 890 resonator is a folded linear resonator. (Courtesy of the Coherent, Inc., Laser Group, Santa Clara, CA)

M1 and M5 are transparent to the pump light. Mirrors M1, M2, M5, and M6 are highly reflective over the Ti:sapphire laser wavelengths. Mirror M4 is the output mirror for the laser. Mirrors P1, P2, and P3 are highly reflecting at the pump wavelengths. Thus, the pump beam enters the cavity along the M1 to M5 axis and the laser action occurs between the M4 and M6 output mirrors. The remaining mirrors are simply to assure that the pump beam can effectively pump the laser material without interacting with the Ti:sapphire laser output beam.

Coherent also sells a more elaborate version of the Model 890, which is the Model 899 Ti:sapphire ring laser. As with the model 890, three sets of standard optics are used to access the Ti:sapphire tuning range. Using these three sets of optics, the wavelength can be tuned from 700 nm to beyond 1000 nm (see Figure 11.24). The output power depends on the pump and can be as high as 3 watts with the SW mirror set and a 20 watt argon-ion pump.

The Model 899 resonator is a folded ring resonator (see Figure 11.25) using an Invar (rather than stainless-steel) backbone. Mirrors M1 and M5 are transparent to the pump light. Mirrors M1, M2, and M5 are highly reflective over the Ti:sapphire laser wavelengths.
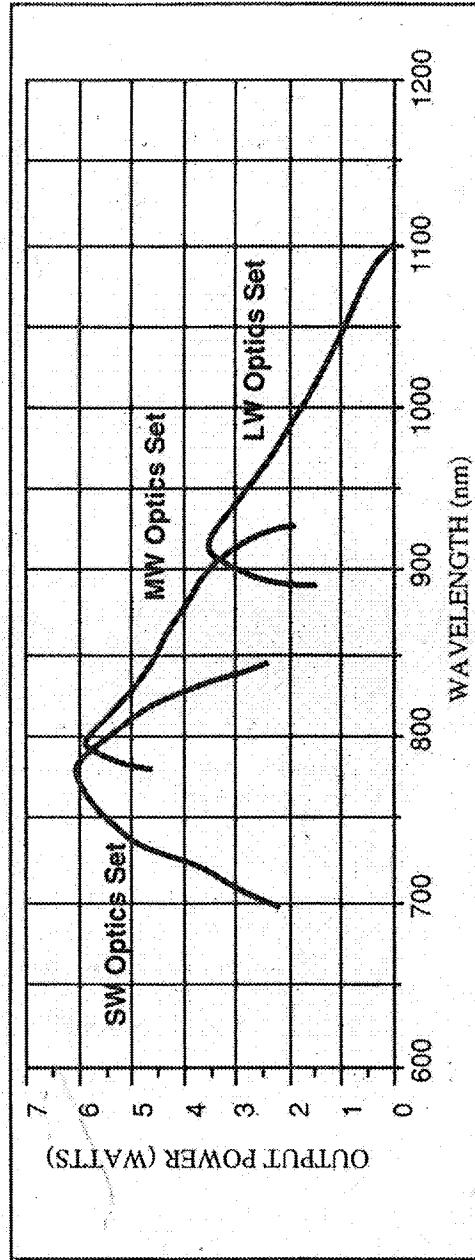
Figure 11.24 In the Model 899 Ti:sapphire ring laser, three sets of standard optics are used to access the Ti:sapphire tuning range. Using these three sets of optics, the wavelength can be tuned from 700 nm to beyond 1000 nm. (Courtesy of the Coherent, Inc., Laser Group, Santa Clara, CA).
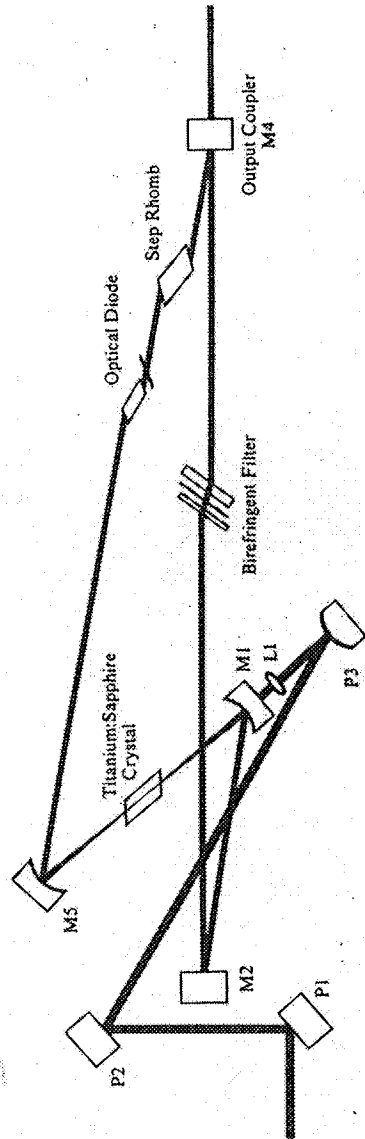
Figure 11.25 The Model 899 resonator is a folded ring resonator. (Courtesy of the Coherent, Inc., Laser Group, Santa Clara, CA)

Mirror M4 is the output mirror for the laser. Mirrors P1, P2, and P3 are highly reflecting at the pump wavelengths. Thus, the pump beam enters the cavity along the M1–M5 axis and the laser action occurs around the M1, M2, M4, and M5 ring. The optical diode and step rhomb are required to assure unidirectional operation around the ring (more on ring lasers in Section 11.4.1).

11.5 FEMTOSECOND PULSE LASER DESIGN

Since the discovery of mode-locking in 1964, there have been three generations of mode-locked lasers.

The first-generation lasers are in the subnanosecond regime, fabricated from solid-state materials such as Nd:YAG and Nd:glass, and using either active loss mechanisms (such as acousto-optic mode lockers) or passive loss mechanisms (such as saturable absorbers). These lasers are ultimately limited in pulsewidth by the relatively narrow spectral bandwidth of the gain material and the inability of the saturable absorbers to track with the pulse narrowing.

The second-generation lasers are in the femtosecond regime, using organic dyes as the gain materials, and with passive mode-locking using saturable absorbers in combination with rapid dye gain saturation. These lasers have demonstrated narrow pulse widths, but are difficult to align and maintain.

The third-generation lasers are in the low femtosecond regime, using solid-state vibronic materials such as Ti:sapphire, with passive soliton-like pulse shaping formed by balancing self-phase modulation against group velocity dispersion. These lasers also demonstrate narrow pulse widths, but are straightforward to construct.

Ultra-short pulse optical systems are an extremely rich research area. For the reader interested in learning more, there are a number of special issues on ultrafast optics,[57] as well as review papers such as Keller et al.,[58] Krausz et al.,[59] and Spielmann et al.[60]

11.5.1 Dispersion in Femtosecond Lasers

Dispersion is the ability of a material to alter the frequency character of light. There are two main dispersive properties important in the design of femtosecond pulse lasers.

The first dispersive property of interest is group velocity dispersion (GVD). Group velocity dispersion is the tendency of various frequencies of light to propagate at slightly

---

[57]*IEEE J. of Quantum Electronics,* Special Issues on Ultrafast Optics and Electronics: April 1983, January 1986, February 1988, December 1989, and October 1992.

[58]U. Keller, W. Knox, and G. 'tHooft, *IEEE J. of Quantum Electron.* 28:2123 (1992).

[59]F. Krausz, M. Fermann, T. Brabec, P. Curley, M. Hofer, M. Ober, C. Spielmann, E. Wintner, and A. Schmidt, *IEEE J. of Quantum Electron.* 28:2097 (1992).

[60]C. Spielmann, P. Curley, T. Brabec, and F. Krausz, *IEEE J. of Quantum Electron.* 30:1100 (1994).

different speeds in certain materials. In materials with a normal or positive GVD, the longer wavelengths travel faster than the shorter ones, thus red shifting the pulse.

The second dispersive property of interest is self-phase modulation (SPM). SPM is an intensity-dependent phase shift that manifests itself either spatially or temporally. (SPM is often termed the Kerr effect.)

Spatial SPM can also be described as self-focusing. As the intensity in the center of the pulse increases, the index of refraction of the material increases, and the pulse focuses.

Temporal SPM is a time-dependent phase shift that occurs as the pulse sweeps through the dispersive material. The rising intensity on the front edge of the pulse increases the index of refraction. This will delay the individual oscillations, and thus red shift the rising edge. The reverse effect occurs on the trailing edge (blue shifting the trailing edge). Thus, temporal SPM chirps the pulse.

For ultrashort pulse generation, the round-trip time in the resonator for all frequency components of the light must be the same. Otherwise, frequency components with different phase shifts will no longer add coherently and the mode-locking will break down (think of an unmode-locked laser with random phases).

In a normal laser, temporal SPM will cause a red shift of the pulse and the GVD will also cause a red shift of the pulse. Thus, in order to achieve transform-limited pulse widths, it is necessary to incorporate some type of dispersion compensation that blue shifts the pulse.

Prisms are the most common way of introducing GVD compensation. Although the glass in prisms has normal dispersion (red shifts the pulse), the geometry can be arranged so that the blue components transverse the prism path in a shorter length of time than the red components. An example of a prism pair where the GVD is a function of L is given in Figure 11.26.

11.5.2 Nonlinearities Used to Create Femtosecond Pulses

In an unmode-locked laser, all of the longitudinal modes will be running with random phases. These random phases may be synchronized by the addition of a suitable nonlinearity. A laser is referred to as passively or self-mode-locked when this nonlinearity is generated within the laser and does not depend on external influences.

For passive mode-locking to work, the introduced nonlinearity must create an amplitude or phase instability. If an amplitude instability is created, this amplitude instability should provide gain to the most intense initial fluctuation and loss to the others. In addition, this amplitude instability should be shorter than the minimum size of the initial fluctuation.

In lasers where the upper state lifetime is short in comparison to the cavity round-trip time (principally dye lasers) these requirements on the introduced nonlinearity are easily met
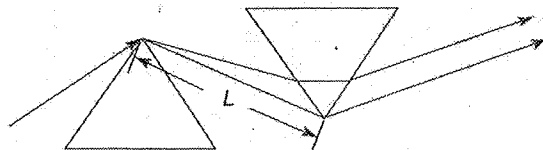
Figure 11.26   Prisms are the most common way of introducing GVD compensation. A prism geometry can be arranged so that the blue components transverse the prism path in a shorter length of time than the red components.

by using a slow saturable absorber. The combined action of the rapid saturable gain (due to the laser) and the slower saturable absorption (due to the dye) creates a gain window that follows the pulse width down to the dephasing time of the dye (usually tens of femtoseconds).

To illustrate this in more detail, visualize a short spontaneous fluctuation. As the fluctuation goes through the saturable absorber, the intensity of the pulse will bleach the absorber and the absorber loss will drop dramatically. As the fluctuation goes through the gain material (with a short upper state lifetime), it will dynamically reduce the available gain for a period following the pulse. Thus, there is a window between the drop in loss due to the dye bleaching and the drop in gain due to dynamic gain saturation. This window favors the more intense pulse (see Figure 11.27).

Now consider the situation with a typical solid-state laser. In solid-state lasers, the upper state lifetime is usually long and the lasers do not experience dynamic gain saturation on time scales compatible with mode-locked pulses. Thus, passive mode-locking techniques in solid-state lasers rely on saturable absorber dyes with extremely short lifetimes. In these systems, only the dynamic bleaching of the dye works to shorten the pulse. These systems are also limited by the finite-state excited lifetime of the saturable absorber dye. Such lifetimes are picoseconds in most organic dyes. Even the most exotic semiconductor saturable absorbers have lifetimes in the hundreds of femtoseconds (and are severely wavelength dependent).

However, it is also possible to mode-lock a laser using spatial or temporal SPM. SPM has the interesting characteristic that it almost instantaneously follows the variation in the optical field intensity. This ultra-fast effect can be transformed into a saturable absorber response by inclusion of compensating elements in the laser cavity.

For example, spatial SPM (self-focusing) can be used to create an intensity-dependent loss. Spatial SPM will introduce an intensity-dependent change in both the location and the width of the resonator mode beam waist. By introduction of a hard or soft aperture, the self-focusing effect can be converted into an intensity-dependent loss. (The process is also referred to as Kerr-lens mode-locking or KLM.)

Kerr-lens mode-locking can be used in many solid-state lasers, either by relying on the intrinsic self-focusing of the laser material or by adding a self-focusing material. In many cases (for example, Ti:sapphire) it is not even necessary to include a true aperture.
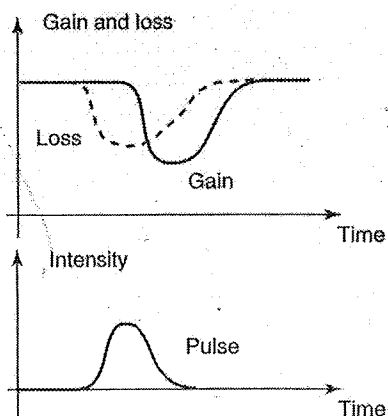
Figure 11.27 . In lasers where the upper state lifetime is short in comparison to the cavity round-trip time, there is a window between the drop in loss due to the dye bleaching and the drop in gain due to dynamic gain saturation. This window favors the more intense pulse.
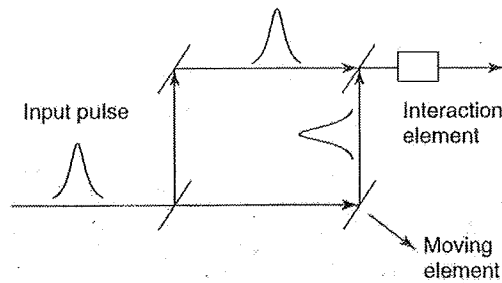
Figure 11.28   The majority of femtosecond pulse measurement techniques depend on the use of two pulses, with one delayed in time with respect to the other.

The higher gain seen by a smaller mode will experience gain saturation and this will serve as a soft aperture in the cavity.

11.5.3 Measuring Femtosecond Pulses

Once laser pulse widths drop below a few nanoseconds, it becomes difficult to measure them with conventional photodetectors and electronics. Thus, a variety of elegant techniques have appeared to measure these short pulses.

The majority of these techniques depend on use of two pulses, with one delayed in time with respect to the other (see Figure 11.28). These two pulses are typically created by a beam splitter and the relative time delay introduced by a moving mirror (such as a mirror on a speaker). The pulses are then allowed to re-interact in some way, and a trace obtained form this interaction. By changing the position of one pulse temporally with respect to the other, an autocorrelation pattern can be obtained (admittedly, at one point per pulse).

There are a number of possible interaction elements. Two of the most common are second harmonic crystals and two-photon phosphors. In the second-harmonic method, two arms of an interferometer are arranged so that the pulses have orthogonal polarizations. A second-harmonic crystal is cut so that harmonic light is only produced when both polarizations are present. The method thus measures the overlap of the pulse with its delayed replica. The two-photon method is somewhat simpler in concept than the second-harmonic method. In the two-photon method, the interaction material is simply a two-photon phosphor. When two photons are simultaneous absorbed in the fluorescent material, a single photon of twice the frequency is emitted and detected by a camera or photodetector.

11.5.4 Colliding Pulse Mode-Locking

Early work in femtosecond dye lasers primarily focused on resonator design. A large number of designs were proposed and tested. However, in 1981, Fork et al. came up with the seven-mirror colliding pulse mode-locking (CPM) ring laser.[61,62] CPM rings are so successful that all femtosecond dye lasers since then use some form of CPM ring geometry.

A typical set-up for a CPM system is shown in Figure 11.29. The laser gain material is a flowing jet of rhodamine 6G dye excited by an argon laser. The saturable absorber is a thin jet (10 μm) of absorber dye.

[61]R. L. Fork, B. I. Greene, and C. V. Shank, *Appl. Phys. Lett.* 38:671 (1981).

[62]R. L. Fork, C. V. Shank, R. Yen, and C. A. Hirlimann, *IEEE J. of Quantum Electron.* QE-19:500 (1983).
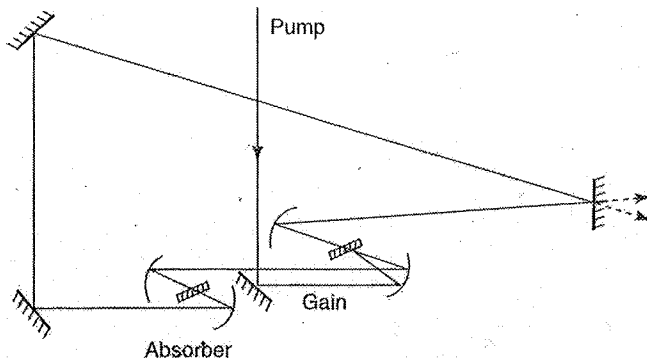
Figure 11.29   In colliding pulse mode-locking, two counter-propagating pulses are synchronized so as to overlap in a saturable absorber dye. (From R. L. Fork, C. V. Shank, R. Yen, and C. A. Hirlimann, "Femtosecond Optical Pulses," *IEEE J. of Quantum Electron.* QE-19:500 (1983). ©1983 IEEE.)

In CPM, two counter-propagating pulses are synchronized so as to overlap in a saturable absorber dye. The interference of the two pulses will create a standing wave pattern in the saturable absorber dye. The minimum loss condition in the dye corresponds to the maximum constructive interference for the laser pulses.

The system is self-synchronizing because the lowest loss condition always occurs when the two counter-propagating pulses overlap in the saturable absorber. Other conditions are more lossy and rapidly lose out to the lowest loss situation.

Competition between pulses for gain is minimal because the gain recovery time is swift in comparison to the round-trip cavity time. The interval between pulse arrival times in the gain media can be made large and equal for both pulses by separating the gain and absorber jets by one-quarter of the round-trip path length. (The idea here is for the pulses to overlap in the saturable absorber dye jet, but not in the gain media.)

A figure of merit for saturable absorber dye mode-locking is the ratio of the optical field intensity which saturates the absorber, to the optical field intensity which saturates the gain material. The higher this ratio, the more stable the laser. CPM rings offer a minimum of a factor of two improvement over conventional resonators (the factor of two is because two pulses saturate the absorber, while only one pulse saturates the gain material). An additional improvement results from the nonlinearity of the saturable absorber dye. Finally, the increased stability of CPM rings permits removal of dispersive cavity elements which may broaden the pulse. The net result is that CPM rings reduce the pulse width by a factor of 4 to 10 over conventional resonators.

11.5.5 Grating Pulse Compression

Grating pulse compression is a classical technique for reducing the temporal length of pulses by using self-phase modulation (see Figure 11.30).

An input pulse is directed through a dispersive material which broadens the spectrum of the pulse through self-phase modulation. (Single-mode fiber is the usual dispersive material because the fiber yields spatially uniform frequency broadening which is almost entirely due to self-phase modulation.) The resulting pulse (of the same temporal width, but with a factor of 3 to 5 broader spectrum) is then reflected between two gratings. The grating pair introduces a phase shift, which is a quadratic function of frequency and is opposite in
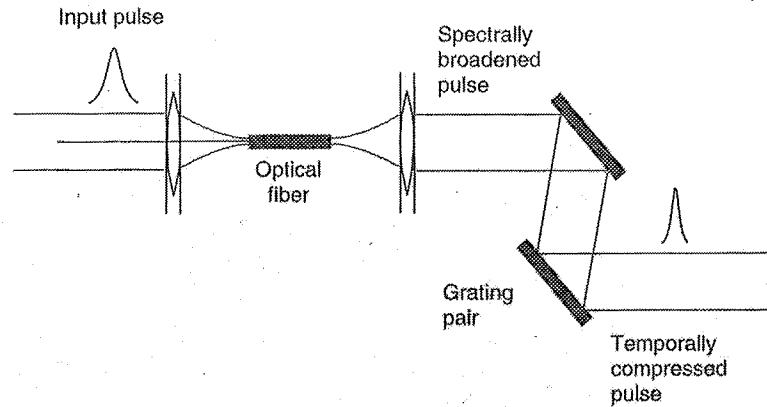
Figure 11.30 Grating pulse compression uses self-phase modulation in a fiber to broaden the spectrum of the pulse, followed by a grating pair to temporally compress the pulse.

sign to that of the dispersive medium. The end result is a temporally shorter pulse with a broader spectrum.

11.5.6 Solitons

Once the CPM ring laser geometries became well-established, research began to focus on dispersive properties of the resonator. In 1984, Martinez et al. proposed the idea that balancing group velocity dispersion (GVD) against self-phase modulation (SPM) might provide soliton-like pulse shaping and further reduce the temporal pulse width.[63] However, Martinez et al. observed that this effect was unlike to occur in conventional CPM ring lasers because of a competition between a negative contribution to the intracavity SPM, which arises from the time-dependent saturation of the absorber dye, and the positive SPM, which arises from the fast Kerr effect in the dye solvent. This causes an intracavity total SPM that is small and negative. Their suggestion was that one of these contributing sources would need to be reduced for the soliton behavior to be observed.[64]

This concept of balancing the GVD against the SPM to form solitons was first demonstrated by Valdmanis et al. in 1985 in a six-mirror CPM ring cavity with four prisms used as dispersion tuning elements[65,66] (see Figure 11.31). In this configuration, four fused-silica prisms were used with the beam running through the apex of each prism. The dispersion was tuned by changing the length L. With excess negative GVD, the laser maintained stable operation, but the pulse width gradually increased. For excess positive GVD, the laser was either not stable or ran with a stable mode but with long pulse widths. Valdmanis et al. hypothesized that the fast Kerr effect in the dye solvent was compensating for the negative

[63] O. E. Martinez, R. L. Fork, and J. P. Gordon, *Opt. Lett.* 9:156 (1984).

[64] O. E. Martinez, R. L. Fork, and J. P. Gordon, *J. Opt. Soc B,* 2:753 (1985).

[65] J. A. Valdmanis, R. L. Fork, and J. P. Gordon, *Opt. Lett.* 10:131 (1985).

[66] J. A. Valdmanis and R. L. Fork, *IEEE J. of Quantum Electron.* QE-22:112 (1986).
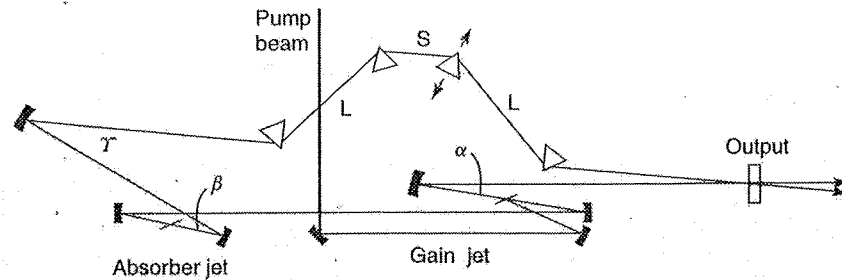
Figure 11.31 The concept of balancing the group velocity dispersion against the self-phase modulation to form solitons was first demonstrated by Valdmanis et al. in 1985 in a six-mirror CPM ring cavity with four prisms used as dispersion tuning elements. (From J. A. Valdmanis and R. L. Fork, "Design Considerations for a Femtosecond Pulse Laser Balancing Self Phase Modulation, Group Velocity Dispersion, Saturable Absorption, and Saturable Gain," *IEEE J. of Quantum Electron.* QE-22:112 (1986). ©1986 IEEE.)

introduced GVD by the prisms and thus creating the soliton formation. In essence, the Kerr effect generated a pulse with a positive chirp (a positive linear chirp has a phase greater than zero and can be considered qualitatively to have the red light coming first and the blue light coming second), which required the addition of a negative GVD to generate pulse compression.

11.5.7 Kerr-Lens Mode-Locking (KLM) in Ti:Sapphire

Prior to 1991, a variety of mode-locking techniques had been applied to Ti:sapphire. These included synchronous pumping, acousto-optic modulation, passive mode-locking, injection seeding, and additive pulse mode-locking. The only common feature was that the techniques were difficult and not very successful (the shortest pulse width was approximately 300 femtoseconds using injection seeding).

However, in 1991, Spence et al. demonstrated a new mode-locking technique in Ti:sapphire.[67] This technique was the first demonstration of Kerr-lens mode-locking and had the elegant feature that the critical nonlinearity was produced by the Ti:sapphire crystal itself (rather than by an additional optical element).

The cavity naturally mode-locked down to 100 fs and was astonishingly simple (containing only two prisms for dispersion compensation; see Figure 11.32). The simplicity of the set-up meant that his results were not well accepted until the same effect was confirmed in Ti:sapphire and observed in a variety of other lasers including Cr:LiSAF, Cr:LiCAF, Nd:glass, Nd:YAG, Nd:YLF, and Cr:forsterite (for a more complete review of Kerr lens mode-locking, see Krausz[68]).

The demonstration of self-mode-locking by Spence, coupled with the recognition of the importance of dispersion compensation in femtosecond pulse lasers, sparked a flurry of new activity in the early 1990s. Cavity designs simplified dramatically and research effort

[67]D. E. Spence, P. N. Kean, and W. Sibbett, *Opt. Lett.* 16:42 (1991).

[68]F. Krausz, M. Fermann, T. Brabec, P. Curley, M. Hofer, M. Ober, C. Spielmann, E. Wintner, and A. Schmidt, *IEEE J. of Quantum Electron.* 28:2097 (1992).
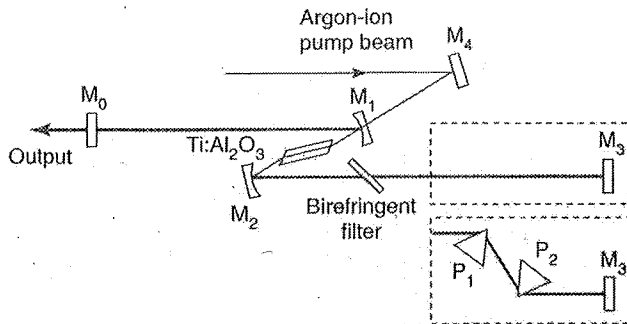
Figure 11.32 In 1991, Spence, Kean, and Sibbett first demonstrated Kerr-lens mode-locking in Ti:sapphire. (From D. E. Spence, P. N. Kean, and W. Sibbett, *Opt. Lett.* 16:42 (1991). Reprinted with the permission of the Optical Society of America.)

moved toward more sophisticated methods of dispersion compensation. The understanding of subtleties in material dispersion quickly led to Ti:sapphire lasers producing pulses in the 10 fs range without external pulse compression.[69, 70] The extraordinary mechanical simplicity of modern femtosecond pulse Ti:sapphire laser systems is stimulating commercial interest.[71]

11.5.8 Coherent Mira Femtosecond Lasers

The Coherent Mira lasers are ultrashort pulse Ti:sapphire lasers. The Mira 900-F is a femtosecond pulse laser with output pulse widths from 100 to 200 fs. The laser is tunable from less than 700 nm to more than 1000 nm by changing mirror sets. The Mira 900-P is very similar in overall design to the 900-F, except the optical cavity has been optimized for operation near 1 to 2 ps (see Figure 11.33).

The optical cavity for the femtosecond Mira 900-F is illustrated in Figure 11.34. The pump beam enters at M4, and mirrors M4 and M5 are transparent to the pump light. Mirrors M2, M3, M4, M5, M6, and M7 are highly reflective over the Ti:sapphire wavelengths. Mirror M1 is the output mirror for the laser. The cavity can also be run as a cw cavity by simply moving prism P1 and using the mirror combination M1, M2, M3, M4, M5, M8, and M9.

The Mira 900-F is typically pumped by an 8 to 15 W argon-ion laser. Average output power ranges from 270 mW (LW mirror set pumped by an 8 watt argon-ion laser) to 1100 mW (SW mirror set pumped by a 14 watt argon-ion laser). The repetition rate is 76 MHz with a beam diameter of 0.7 to 0.8 mm and a divergence of 1.5 to 1.7 mrad.

The Mira 900-F uses Kerr-lens mode-locking (see Section 11.5.7), where the nonlinear element is the Ti:sapphire crystal. A hard aperture is provided, rather than relying on the soft aperture of the nonlinear focusing. GVD compensation (see Section 11.5) is accomplished using a pair of prisms P1 and P2. A birefringent filter (see Section 11.4.2) is incorporated for broadband tuning.

Femtosecond Ti:sapphire lasers using GVD compensation do not start mode-locking spontaneously. Some transient change in cavity length is typically required to initiate the

---

[69]M. Asaki, C. Huang, D. Garvey, J. Zhou, H. Kapteyn, and M. Murnane, *Opt. Lett.* 18:977 (1993).

[70]I. Christov, M. Murnane, H. Kapteyn, J. Zhou, and C. Huang, *Opt. Lett.* 19:1465.

[71]W. Knox, "Practical Lasers Will Spawn Various Ultrafast Applications," *Laser Focus World* June: 135–41 (1996).
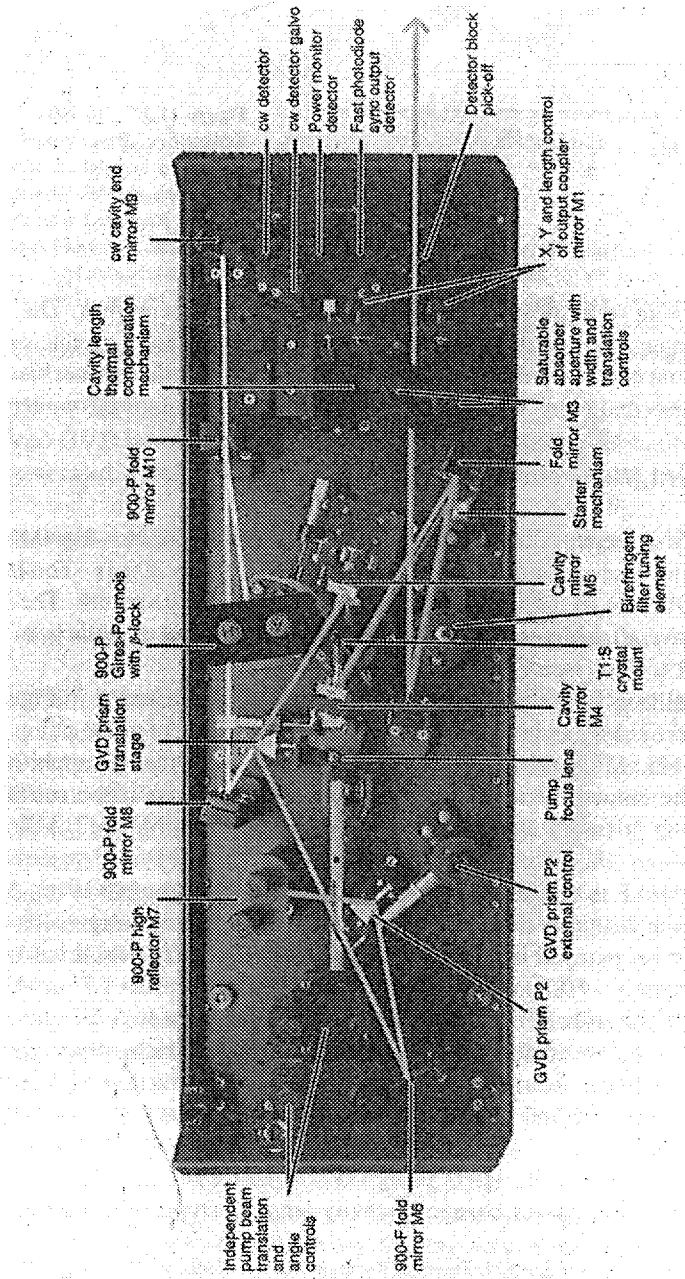
Figure 11.33 The Mira 900-P is a picosecond pulse Ti:sapphire laser. (Courtesy of the Coherent, Inc., Laser Group, Santa Clara, CA)
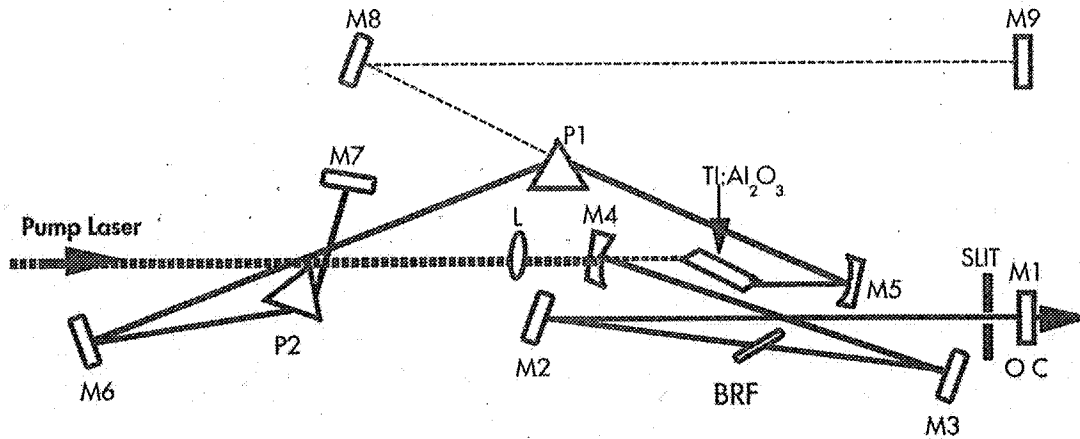
Figure 11.34 A schematic of the Mira femtosecond laser cavity. (Courtesy of the Coherent, Inc., Laser Group, Santa Clara, CA)

mode-locking process. (Ti:sapphire researchers typically start the lasers mode-locking by tapping on a mirror!) The Mira laser incorporates a novel transient-length variation technique that creates a sufficiently short pulse to start the mode-locking process.

The optical cavity for the picosecond Mira 900-P is illustrated in Figure 11.35. The pump beam enters at M4, and mirrors M4 and M5 are transparent to the pump light. Mirrors M2, M3, M4, M5, M8, and M10 are highly reflective over the Ti:sapphire wavelengths. Mirror M1 is the output mirror for the laser. The cavity can also be run as a cw cavity by simply moving prism P1 and mirror M10 and using the mirror combination M1, M2, M3, M4, M5, M8, and M9.
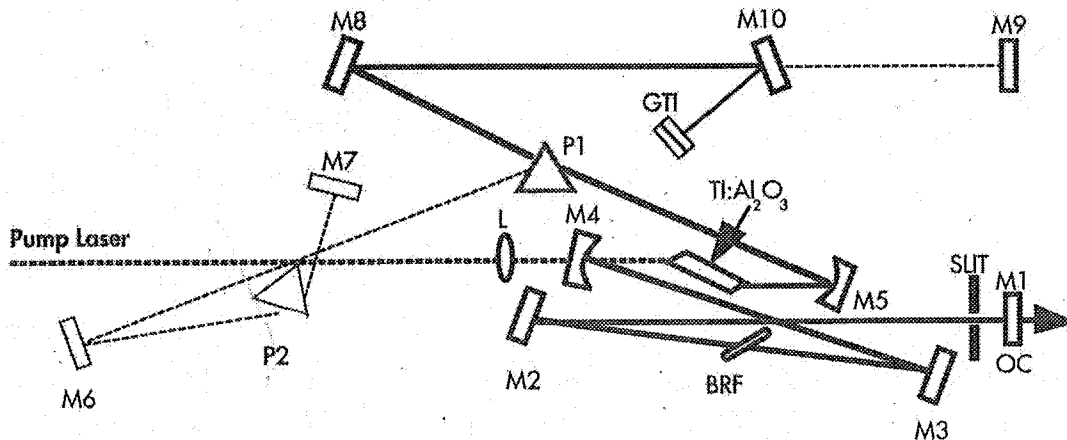
Figure 11.35 A schematic of the Mira picosecond laser cavity. (Courtesy of the Coherent, Inc., Laser Group, Santa Clara, CA)

The Mira 900-P is typically pumped by an 8 to 15 W argon-ion laser. Average output power ranges from 270 mW (LW mirror set pumped by an 8 watt argon-ion laser) to 1300 mW (SW mirror set pumped by a 14 watt argon-ion laser). The repetition rate is 76 MHz with a beam diameter of 0.7 to 0.8 mm and a divergence of 1.5 to 1.7 mrad.

The Mira 900-P also uses Kerr-lens mode-locking (see Section 11.5.7), where the nonlinear element is the Ti:sapphire crystal. Again, a hard aperture is provided rather than relying on the soft aperture of the nonlinear focusing alone. However (unlike the Mira 900-F) GVD compensation (see Section 11.5) is accomplished by removing prism P1 and using a Gires-Tournois interferometer.[72] A birefringent filter (see Section 11.4.2) is incorporated for broadband tuning.

EXERCISES

Overview of transition-metal solid-state tunable lasers

11.1 (design) Obtain a copy of B. D. Guenther and R. G. Buser, *IEEE Journal of Quantum Electronics* QE:18:1179 (1982). Read it and compare the predictions of 1982 with the actual development of tunable solid-state lasers between 1982 and today. Your answer should include:
   (a) a brief summary (one or two paragraphs) on how it was perceived in 1982 that tunable lasers would evolve,
   (b) a brief summary (one or two paragraphs) on the actual evolution, and
   (c) a table comparing the predicted development with the actual development.

11.2 (design) Obtain a copy of C. Pollock, D. Barber, J. Mass, and S. Markgraf, *IEEE Journal of Selected Topics in Quantum Electronics* 1:62 (1995). Read it and summarize the predictions for the future in the development of solid-state lasers. Your answer should be in the form of:
   (a) a few sentences describing the current perception on solid-state laser development, and
   (b) a table or list summarizing future developments.

Transition-metal solid-state tunable laser materials

11.3 (design) Obtain manufacturers' data sheets for ruby, Nd:YAG, alexandrite, and Ti:sapphire. (You may wish to coordinate with your classmates to avoid having a large number of people contacting the same vendor.) Construct a table comparing the optical and physical properties of these materials. Compare and contrast the materials. Your answer should include:
   (a) a summary table, and
   (b) several paragraphs discussing the relative advantages and disadvantages of the materials.

Ring lasers

11.4 (design) In using a HeNe laser as an alignment laser, it is quite common to observe a large oscillation when the back reflection from a flat optical component is redirected back into the alignment HeNe. Explain what is going on.

11.5 (design) Consider an optical system composed of a polarizer, a Faraday rotator, and a half-wave plate. Further assume that the Faraday rotator has been built so that it changes the linear polarization by 20 degrees. (For example, for a vertically polarized input CCW wave, the direction of the linear polarization emerging from the Faraday rotator is 20 degrees from the

---

[72]Anthony E. Siegman, *Lasers* (Mill Valley, CA: University Science Books, 1986), pp. 348–49.

normal.) Using diagrams similar to Figure 11.17, explain the effect that this element would have if installed in a typical ring laser.

11.6 (design) Creating unidirectional oscillation is a very important design issue in ring lasers. The text mentions using an external cavity or a Faraday rotator to create unidirectional oscillation. Propose at least one other method for achieving unidirectional oscillation in a ring laser. Your answer should include:

(a) a sketch of your idea,

(b) a reference if it is not an original idea, and

(c) a few sentences discussing the idea.

Birefringent crystals

11.7 Assume that you have two identical polarizers oriented with their polarization axes at 90 degrees to each other. Assume you have an incident unpolarized white light source of an intensity of 100 watts/cm^2. Assume both polarizers have $\Delta_0 = 0.5$ and $\Delta_{90} = 5.5$ over the range of the white light source. How much light is transmitted through the polarizers? Now, add a third identical polarizer in-between the two crossed polarizers, oriented at 45 degrees to each original polarizer. How much light is now transmitted through the three polarizers? How much light would be transmitted if the three polarizers were perfect? Explain.

11.8 (design) Use foam core and pins to construct a model of the indicatrix for a negative uniaxial crystal. (This can be done by cutting two foam-core ellipses with n_e and no major axes, and one foam-core circle with an n_o radius. Then, one of the ellipses is cut in half, and one is cut in quarters. The structure is then reassembled as an indicatrix using the pins. The model can be further enhanced by adding a k-vector and the associated ellipse using a different color of foam core.)

11.9 (design) Repeat the previous problem, but build a positive uniaxial indicatrix.

11.10 (design) Repeat the previous problem, but build an indicatrix for a biaxial crystal. Biaxial crystals have *two* optical axes. Locate them on the indicatrix once it is built.

11.11 Consider the general problem of propagation through a positive or negative uniaxial crystal. Determine an equation that allows the calculation of $n_o(\theta, \phi)$ and $n_e(\theta, \phi)$ for an arbitrary θ and ϕ given n_o and n_e of the original crystal.

11.12 Consider the following uniaxial crystals.

Crystal	n_o	n_e
Quartz	1.5443	1.5534
Rutile (TiO$_2$)	2.616	2.903
Calcite	1.6584	1.4864

Assume that you are propagating a beam at 35 degrees to the optic axis (as measured from the normal) and midway between the x- and y-axes (i.e., at 45 degrees to each axis). Determine the observed $n_o(\theta, \phi)$ and the $n_e(\theta, \phi)$ for all three systems.

Wave plates

11.13 Assume that you are on an interview for a job in optics and the interviewer hands you two identically appearing optical elements. She tells you that they are a quarter-wave plate and a polarizer. She asks you to figure out which is which. Describe what method you would use to distinguish between the elements using only items present in a conventional interviewer's office.

11.14 Consider a wave plate fabricated from calcite ($n_o = 1.6584$, $n_e = 1.4864$). How thick must the wave plate be in order to operate as a quarter-wave plate with a $\lambda/2$ phase shift? Assume the wave plate is to be used with a 632.8 nm laser.

Birefringent filters

11.15 Create a program that predicts the transmission of a birefringent filter. Use this program to calculate the transmittance of a three-stage filter fabricated from quartz. Assume the smallest element is 0.6 mm thick and that the ratio is 1:2:15. Assume the filter is installed at Brewster's angle and that the rotational angle is 50 degrees.

11.16 The calculated transmission function of a birefringent filter really does not illustrate the true value of the filters when installed inside a laser cavity. Combine the birefringent filter analysis of Section 11.4.2. with the pumping constraints discussed in Section 5.6 to predict the output intensity (as a function of wavelength) for a Ti:sapphire laser with a birefringent filter installed inside the laser. Assume the Ti:sapphire laser is the Coherent model 890, discussed in Section 11.4.3. Assume birefringent filter is the one in Exercise 11.15. Your answer should include:

(a) a brief (a few sentences) analysis of how you attacked the problem,

(b) a listing of your assumptions,

(c) a concise summary of your final equations, and

(d) a plot of intensity (y-axis) versus wavelength (x-axis) for the laser.

The Coherent model 890 and 899 Ti:sapphire lasers

11.17 (design) Obtain data sheets from two major manufacturers of cw Ti:sapphire lasers. Compare and contrast the laser systems. (You may wish to coordinate with your classmates to avoid having a large number of people contacting the same vendor.) Your answer should include:

(a) a table comparing the various features of the lasers, and

(b) several paragraphs discussing the relative strengths and weaknesses of the laser systems.

The design of femtosecond lasers

11.18 (design) Obtain copies of O. E. Martinez, R. L. Fork and J. P. Gordon, *Opt. Lett.* 9:156 (1984); J. A. Valdmanis, R. L. Fork, and J. P. Gordon, *Opt. Lett.* 10:131 (1985); and D. E. Spence, P. N. Kean, and W. Sibbett, *Opt. Lett.* 16:42 (1991). Each of these papers is representative of the state of the art at the time the paper was written. Read the papers, and develop a summary of the development of the state of the art in group velocity dispersion (GVD) compensation between 1984 and 1991. Your answer should include a brief (three to five paragraphs) summary of the development of the state of the state of the art in GVD compensation between 1984 and 1991.

11.19 (design) Measuring the width of femtosecond pulses is a real challenge! One type of indirect measurement technique is discussed in the text. Propose two other possible ways for measuring the pulse width of femtosecond pulses. Your answer should include

(a) two simple sketches of your proposed schemes for measuring the pulse width of femtosecond pulses, and

(b) a few sentences on each approach (with calculations as appropriate) describing the advantages and disadvantages of the approach.

11.20 (design) Do some library research (for example, check recent issues of trade journals such as *Laser Focus World* and *Photonics Spectra*, and recent issues of academic journals such as the *IEEE Journal of Quantum Electronics*, *Applied Physics Letters*, and *Optics Letters*) and determine the current state of the art in femtosecond-pulse lasers. What do you think is the shortest possible pulse length? Your answer should include:

(a) a one- to two-paragraph description of the state of the art in femtosecond pulse lasers (including references!), and

(b) a one- to three-paragraph summary of your opinion (supported by facts, references, and calculations) of the shortest possible pulse length from a femtosecond-pulse laser.

The Coherent Mira femtosecond lasers

11.21 (design) Obtain data sheets from two major manufacturers of femtosecond-pulse Ti:sapphire lasers. Compare and contrast the laser systems. (You may wish to coordinate with your classmates to avoid having a large number of people contacting the same vendor.) Your answer should include:

(a) a table comparing the various features of the lasers, and

(b) several paragraphs discussing the relative strengths and weaknesses of the laser systems.

12
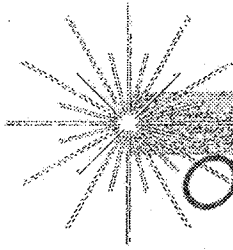
Other Major Commercial Lasers

Objectives

Carbon dioxide lasers

- To summarize the generic characteristics of the CO_2 laser.
- To describe the various energy states of the CO_2 laser and to summarize how these states interact with each other.
- To summarize the sequence of historical events leading to the development of the CO_2 laser.
- To describe the major characteristics of waveguide versus free space CO_2 lasers.
- To describe the construction of a commercial waveguide CO_2 laser.

Excimer lasers

- To summarize the generic characteristics of the excimer laser.
- To describe the various energy states of the excimer laser and to summarize how these states interact with each other.
- To summarize the sequence of historical events leading to the development of the excimer laser.
- To describe the general design principles underlying excimer lasers. These include preionization, corona discharge circuitry, and main discharge circuitry.
- To describe the construction of a commercial excimer laser.

Semiconductor diode lasers

- To summarize the sequence of historical events leading to the development of the semiconductor laser.
- To describe the energy band structure of the semiconductor diode laser.

384

- To summarize the process of pumping the semiconductor diode laser with a PN-junction.
- To describe the process of creating a semiconductor laser cavity by cleaving the semiconductor material.
- To describe the similarities and differences between homostructure and heterostructure semiconductor diode lasers.
- To describe the importance of vertical and horizontal confinement in designing semiconductor laser structures.
- To describe the major vertical and horizontal confinement structures.
- To describe the general physical principles governing the design of quantum wells, with special emphasis on the importance of the width of the quantum well in determining the optical properties of quantum well laser diodes.

12.1 THE DESIGN OF CARBON DIOXIDE LASERS

CO_2 lasers operate over a series of vibrational and rotational bands in the regions 9.4 and 10.6 μm. They are both high-average-power and high-efficiency laser systems. Commercially available cw CO_2 lasers range in power from 6 watts to 10,000 watts, and custom lasers are available at even higher powers. Small (2 to 3 feet long) CO_2 lasers can produce hundreds of watts of average power at an efficiency of 10%. Larger CO_2 lasers can produce many kilowatts of cw power. CO_2 lasers are widely used in such diverse commercial applications as marking of electronic components, wafers, and chips; marking on anodized aluminum; trophy engraving; acrylic sign making; rapid prototyping of 3D models; cutting of ceramics, textiles, and metals; carpet, sawblade, and sail cutting; drilling; thin film deposition; and wire stripping (see Figure 12.1). They find application in the medical field for laser surgery, and in research for spectroscopy and remote sensing. Military applications include imaging, mapping, and range-finding. They have also been used in inertial confinement fusion as an alternative to large glass lasers.

CO_2 is a laser material totally unlike the materials discussed so far in this text. Conventional lasers lase off of electronic transitions between various atomic states. CO_2 lasers lase off molecular transitions between the various vibrational and rotational states of CO_2. Among other things, this means that CO_2 lasers have a longer wavelength and higher efficiency than most conventional lasers. Additional information on CO_2 lasers can be found in Cheo,[1] Duley,[2] Tyte,[3] and Witteman.[4] Additional information on high peak power and gas dynamic CO_2 lasers can be found in Anderson,[5] Beaulieu,[6] and Losev.[7]

---

[1] Peter K. Cheo, *Handbook of Molecular Lasers* (New York: Marcel-Dekker Inc., 1987).

[2] W. W. Duley, *CO_2 Lasers: Effects and Applications*, (New York: Academic Press, 1976).

[3] D. C. Tyte, *Advances in Optical Electronics, Vol. 1*, ed D. W. Goodwin, (New York: Academic Press, 1970), pp. 129–198.

[4] W. J. Witteman, *The CO_2 laser* (Berlin: Springer-Verlag, 1987).

[5] John Anderson, *Gasdynamic Lasers: An Introduction* (New York: Academic Press, 1976).

[6] J. A. Beaulieu, *Proc. IEEE* 59:667 (1971).

[7] S. A. Losev, *Gasdynamic Laser* (Berlin: Springer-Verlag, 1981).
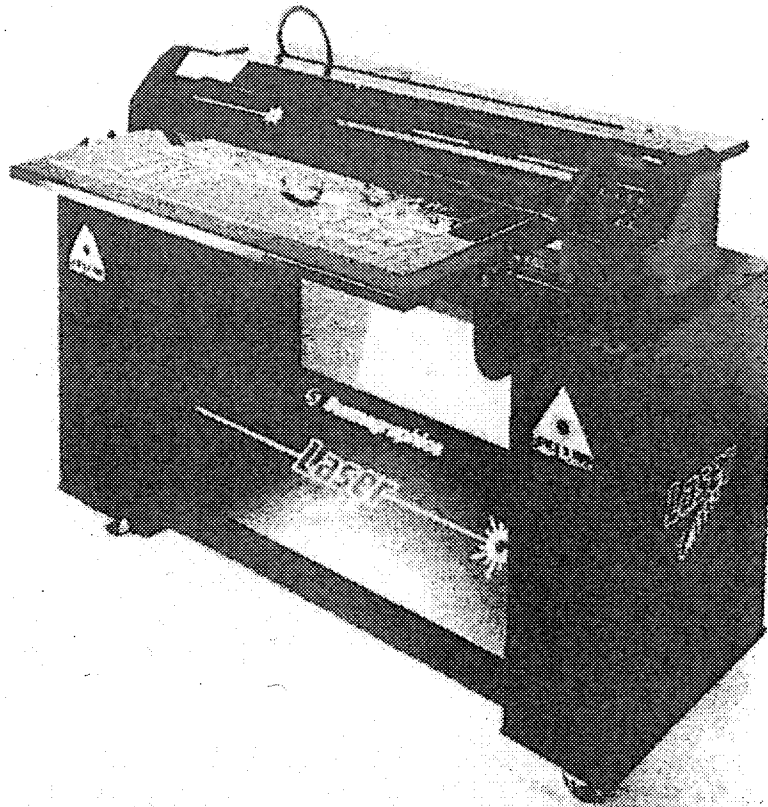
Figure 12.1 Carbon dioxide laser cutting system. (Courtesy of Synrad, Mukilteo, WA, and Summagraphics)

12.1.1 Introduction to CO_2 Laser States

Consider the CO_2 molecule as depicted in Figure 12.2. There are three normal modes of vibration possible in this molecule: the symmetric stretch mode, the bending mode, and the asymmetric stretch mode. The states are labeled by a notation (p_1, p_2, p_3) where the subscripts refer to the various normal modes and where p is an integer corresponding to the number of quanta in the mode. Thus (001) is the state with one quanta in the asymmetric stretch mode and (200) is the state with two quanta in the symmetric stretch mode. The total vibrational energy of the CO_2 molecule is expressed as

$$E(\nu_1, \nu_2, \nu_3) = h\nu_1\left(p_1 + \frac{1}{2}\right) + h\nu_2\left(p_2 + \frac{1}{2}\right) + h\nu_3\left(p_3 + \frac{1}{2}\right) \qquad (12.1)$$

where ν_1, ν_2, ν_3 represent the frequencies of the particular modes.[8]

---

[8] Amnon Yariv, *Optical Electronics*, 4th ed. (Philadelphia, PA: Saunders College Publishing, 1991), p. 242.

Carbon dioxide molecule

Symmetric stretch mode

Bending mode

Asymmetric stretch mode
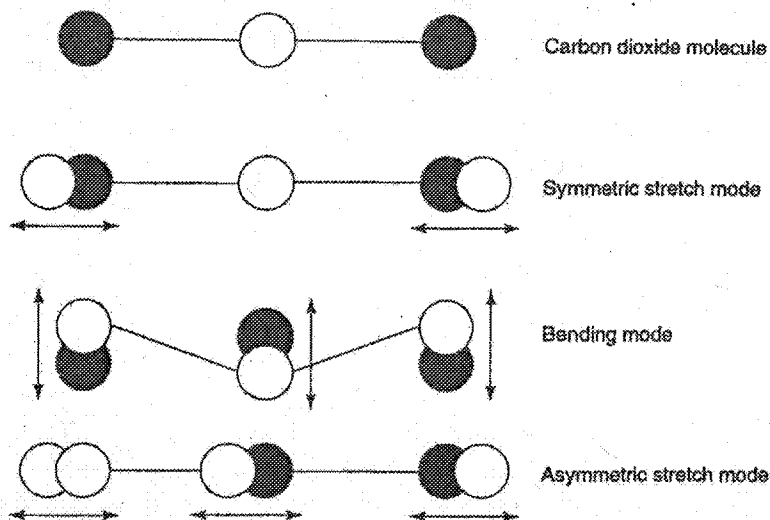
Figure 12.2   Normal modes of the carbon dioxide molecule.

The CO_2 molecules can also rotate, resulting in a series of closely spaced states characterized by the rotational quantum number J. The rotational energies of a given vibrational state i relative to the $J = 0$ level are given as

$$E_{i,J} = hc_o B_i J(J+1) - hc_o D J^2 (J+1)^2 \qquad (12.2)$$

where B_i and D are constants.[9]

The principal laser transitions in CO_2 are the (001) to (100) 10.6 μm transitions and the (001) to (020) 9.4 μm transitions (see Figure 12.3). Each of the levels (001), (100), and (020) consists of a series of rotational states. Transitions in CO_2 occur between states where $J_{odd} \to (J+1)_{even}$ (termed the P-branch) and $J_{odd} \to (J-1)_{even}$ (termed the R-branch). (See Figure 12.4.)

If no wavelength discrimination is provided in the cavity, the P-branch of the (001) to (100) 10.6 μm transition will dominate. However, if wavelength selection is provided (by a grating, for example), it is possible to lase on any of the allowed P- or R-branch transitions. Notice, however, that since both the (001)$\to$(100) and the (001)$\to$(020) transitions share the same upper laser level, then the (001)$\to$(100) transition must be suppressed for the (001)$\to$(100) transition to lase.

The majority of CO_2 lasers contain a mixture of three gases (CO_2, N_2, and He) in a roughly 0.8:1:7 ratio.[10] The CO_2 is the laser gain material. The N_2 has only one excited mode (the symmetrical stretch mode) and the energy of the (1) N_2 vibration nicely aligns with the (001) upper state of the CO_2 molecule (see Figure 12.3). Since the N_2 vibrational states are metastable (very long lifetimes) the energy in the (1) N_2 transition (plus a little kinetic energy) can be transferred to a CO_2 molecule as a means of populating the (001)

---

[9] Amnon Yariv, *Quantum Electronics*, 2d ed. (New York: John Wiley and Sons, 1975), p. 213, Appendix 3.

[10] W. W. Duley, *CO_2 Lasers: Effects and Applications* (New York: Academic Press, 1976), p. 16.
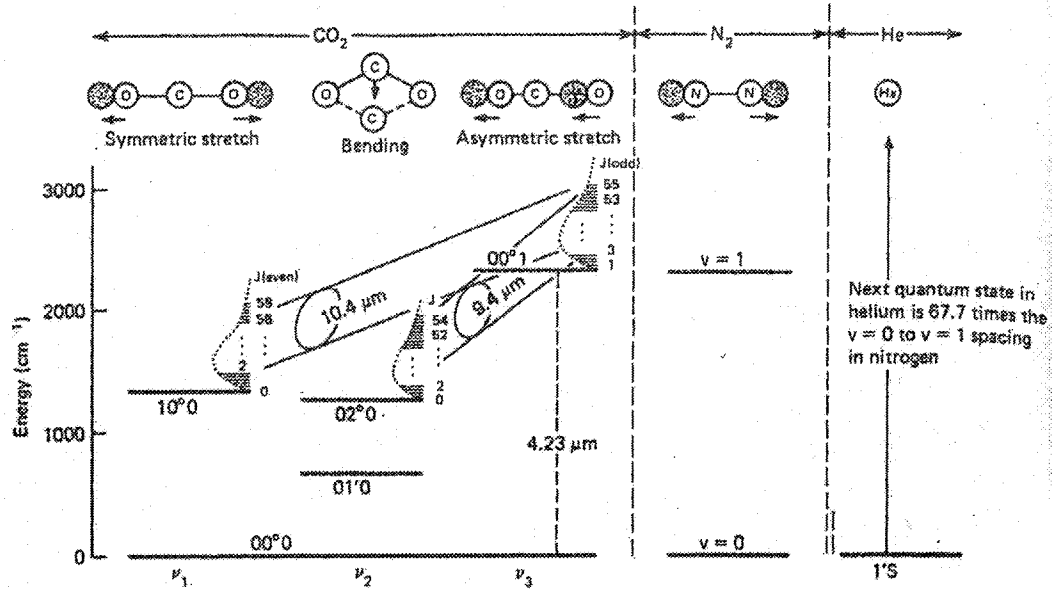
Figure 12.3 Laser states of the carbon dioxide molecule. (From LASER ELECTRONICS 2E. by VERDEYEN, J.T. ©1989, Figure 10.14, p. 336. Adapted by permission of Prentice-Hall, Inc., Upper Saddle River, NJ.)
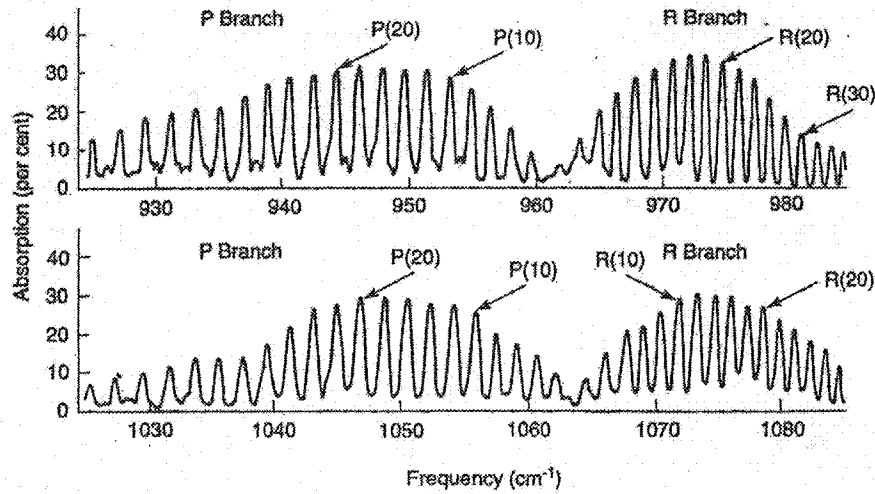
Figure 12.4 Absorption spectrum of the carbon dioxide molecule. (From E. F. Barker and A. Adel, *Phys. Rev.* 44:185 (1933))

upper CO_2 level (notice that the N_2–CO_2 energy transfer is very similar to the He–Ne energy transfer in HeNe lasers; see Section 9.1.3). The helium in the gas mixture provides cooling by means of thermal transfer to the walls (helium is a very thermally conductive gas). Helium also plays a role in optimizing the kinetic energy of the N_2 molecules for maximum energy transfer between the N_2 and CO_2.

Because of the metastable N_2 and the match between the (1) N_2 level and the (001) CO_2 level, the conversion efficiency between input electrical power to power in the upper laser state is 50 to 70%. Since the quantum efficiency is roughly 45%, this means that CO_2 lasers can operate at extremely high efficiencies (10 to 35%).

12.1.2 The Evolution of CO_2 Lasers

The first demonstration of laser action from CO_2 was reported by Patel in 1964.[11,12,13] The concept of using N_2 to transfer vibrational energy from the electrical discharge to the CO_2 was recognized by Legay and Legay-Sommaire in the same year[14] and the idea of incorporating helium for cooling was first proposed by Patel a year later.[15] During this period of rapid development on the CO_2 laser, Patel and other researchers were able to improve Patel's original 1 mW output to roughly 100 watts.[16,17,18]

The first CO_2 lasers were constructed from long tubes of glass where the desired laser mixture flowed through the glass tube (see Figure 12.5). Electrodes in the gas generated a plasma arc to excite the N_2 molecules into their symmetrical stretch mode. Although the very first demonstration of laser action from CO_2 used RF excitation, systems soon converted to DC excitation for increased power.[19]

The original glass tube CO_2 lasers operated at low pressures with the electrical discharge running longitudinally down the cavity. As a consequence, operating pressures were low due to the necessity to create and maintain a plasma over a long distance. However, in 1970, Beaulieu[20] first reported operation of an atmospheric pressure CO_2 laser by exciting the discharge transversely to the cavity (see Figure 12.6). These Transverse Excited Atmospheric (TEA) lasers offered higher gains and greater output powers than longitudinally excited lasers.

[11] C. K. N. Patel, *Phys. Rev. Lett.* 12:588 (1964).

[12] C. K. N. Patel, *Phys. Rev. Lett.* 13: 617 (1964).

[13] C. K. N. Patel, *Phys. Rev.* 136:A1187 (1964).

[14] F. Legay and N. Legay-Sommaire, *C. R. Acad. Sci.* 259B:99 (1964).

[15] C. K. N. Patel, P. K. Tien, and J. H. McFee, *Appl. Phys. Lett.* 7:290 (1965).

[16] C. K. N. Patel, *Phys. Rev.* 136:A1187 (1964).

[17] N. Legay-Sommaire, L. Henry, and F. Legay, *C.R. Acad. Sci.* 260B:3339 (1965).

[18] C. K. N. Patel, P. K. Tien, and J. H. McFee, *Appl. Phys. Lett.* 7:290 (1965).

[19] C. K. N. Patel, *Appl. Phys. Lett.* 7:15 (1965).

[20] A. J. Beaulieu, *Appl. Phys. Lett.* 16:504 (1970).
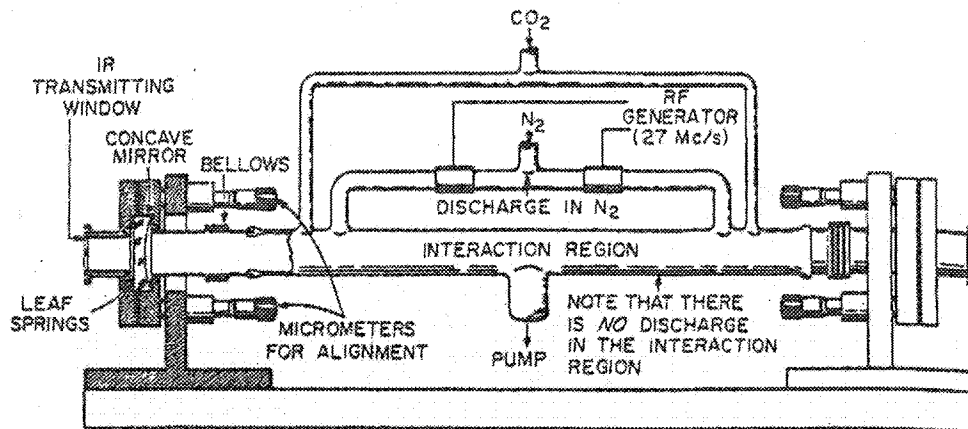
Figure 12.5 Early carbon dioxide laser construction. (From C. K. N. Patel, *Phys. Rev. Lett.* 13: 617 (1964). Reprinted with the permission of the author.)

The CO_2 laser Q-switches exceptionally well and Q-switched operation was reported in 1966 by a number of researchers including Flynn,[21,22] Kovacs,[23] Bridges,[24] and Patel.[25] However, the narrow bandwidth of CO_2 (approximately 50 MHz), means that physically long lasers are required to effectively demonstrate mode-locking. In spite of this difficulty, the first mode-locking of a conventional CO_2 laser was reported in 1968 by Caddes,[26] and Wood and Schwartz.[27] High-peak power can also be obtained from CO_2 lasers by pulsing or gain switching the lasers.[28]   TEA lasers are especially well-suited for production of high-peak power CO_2 laser pulses.[29]

In a conventional CO_2 laser, the output power will increase as the gas flow is increased. This increased power is thought to be due to enhanced cooling and more effective removal of dissociation products such as CO and O_2 from the CO_2 discharge.[30] However, in many applications, it is not possible to support the peripheral equipment for handling flowing gases and a sealed laser configuration is required. In a sealed laser, the lack of gas flow means that some mechanism must be provided to regenerate the dissociated gas products

[21]G. W. Flynn, M. A. Kovacs, C. K. Rhodes, and A. Javan, *Appl. Phys. Lett.* 8:63 (1966).

[22]G. W. Flynn, L. O. Hocker, A. Javan, M. A. Kovacs, and C. K. Rhodes, *IEEE J. Quan. Elec.* QE-2:378 (1966).

[23]G. W. Flynn, L. O. Hocker, A. Javan, M. A. Kovacs, and C. K. Rhodes, *IEEE J. Quan. Elec.* QE-2:378 (1966).

[24]T. J. Bridges, *Appl. Phys. Lett.* 9:174 (1966).

[25]C. K. N. Patel, *Phys. Rev. Lett.* 16:613 (1966).

[26]D. E. Caddes, L. M. Osterink, and R. Targ, *Appl. Phys. Lett.* 12:74 (1968).

[27]O. R. Wood and S. E. Schwartz, *Appl. Phys. Lett.* 12:263 (1968).

[28]A. E. Hill, *Appl. Phys. Lett.* 12:324 (1968).

[29]W. W. Duley, *CO_2 Lasers: Effects and Applications* (New York: Academic Press, 1976), Chapter 2.

[30]Tyte, D. C., in *Advances in Optical Electronics*, Vol 1, ed D.W. Goodwin (New York: Academic Press, 1970), pp. 167–168.
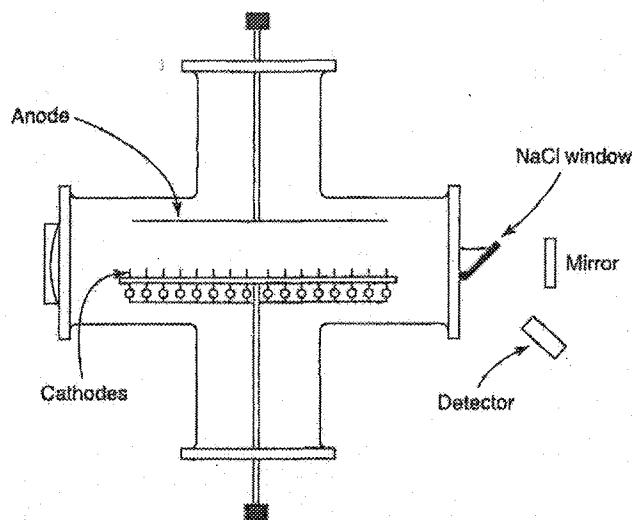
Figure 12.6 A schematic of an early Transverse Excited Atmospheric (TEA) laser. (Reprinted with permission from A. J. Beaulieu, *Appl. Phys. Lett.* 16:504 (1970). ©1970 American Institute of Physics.)

(particularly the oxygen species) back into CO_2. If these products are permitted to react with the tube walls, the chemical equilibrium of the plasma is disturbed and additional dissociation products are formed. Various regeneration methods include adding additional gases, periodically heating the tube, or incorporating catalyst alloys on the electrodes. Sealed lasers demonstrating such regeneration methods were first developed by Wittman in 1965[31] and further developed by Wittman[32] and Carbone.[33]

The initial use of flowing gases to improve the output performance of CO_2 lasers led to the development of another fascinating way to pump CO_2. The basic idea is to begin with a hot equilibrium gas mixture and then to expand the mixture through a supersonic nozzle. This lowers the temperature and pressure of the gas mixture in a time short compared to the upper state lifetime. When this occurs, the upper laser level cannot track with the temperature and pressure changes and so remains at its initial values. In contrast, the lower level population drops dramatically. The result is a population inversion that extends some distance downstream of the supersonic nozzle (see Figure 12.7). Lasers using this type of pumping are called gas dynamic lasers and were first suggested by Konyukhov and Prokhorov[34] in 1966 and demonstrated by Gerry[35] and Konyukhov.[36]

The most spectacular forms of gas dynamic lasers are those run using jet or rocket engines as the pump source. The basic idea is to create a laser gas mixture by burning some type of fuel that generates the CO_2. The fuel source is often ignited with a methanol burner,

[31]W. J. Witteman, *Phys. Lett.* 18:125 (1965).

[32]W. J. Witteman, *IEEE J. Quan. Electron.* QE-5:92 (1969).

[33]R. J. Carbone, *IEEE J. Quan. Electron.* QE-5:48 (1969).

[34]V. K. Konyukhov and A. M. Prokhorov, *JETP Lett.* 3:286 (1966).

[35]E. T. Gerry, *IEEE Spectrum* 7:51 (1970).

[36]V. K. Konyukhov, I. V. Matrosov, A. M. Prokhorov, D. T. Shalunov, and N. N. Shirokov, *JETP Lett.* 12:321 (1970).
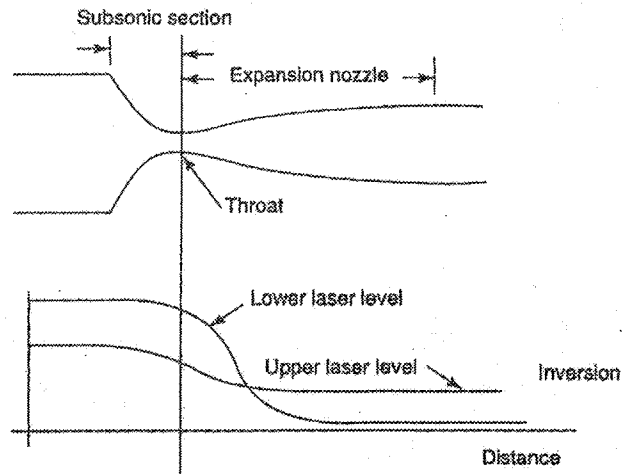
Figure 12.7 Gas dynamic lasers operate by creating a population inversion via gas expansion through a nozzle. (From E. T. Gerry, "Gasdynamic Lasers," *IEEE Spectrum* 7:51–58 (1970). ©1970 IEEE.)
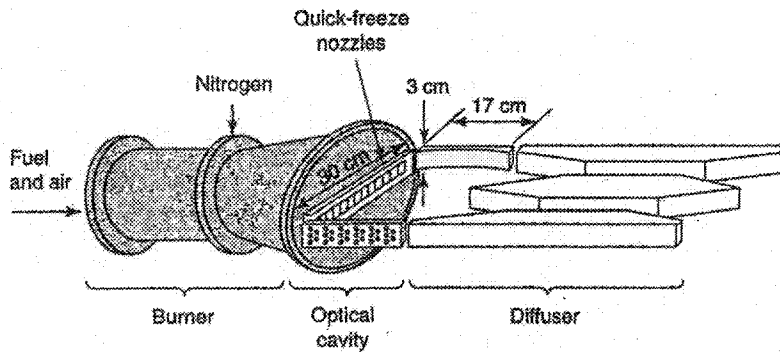
Figure 12.8 The most spectacular forms of gas dynamic lasers are those run using jet or rocket engines as the pump source. (From E. T. Gerry, *IEEE Spectrum* 7:51 (1970). ©1970 IEEE.)

which also injects water into the mixture. (The water is used to decrease the lifetime of the lower laser state.) Extra nitrogen is added to improve the excitation of the CO_2. The resulting mixture is then compressed by the engine and allowed to expand out through a series of supersonic nozzles. The optical cavity is then located sideways across the expansion chamber (see Figure 12.8).[37]

---

[37] E. T. Gerry, *IEEE Spectrum* 7:51 (1970).
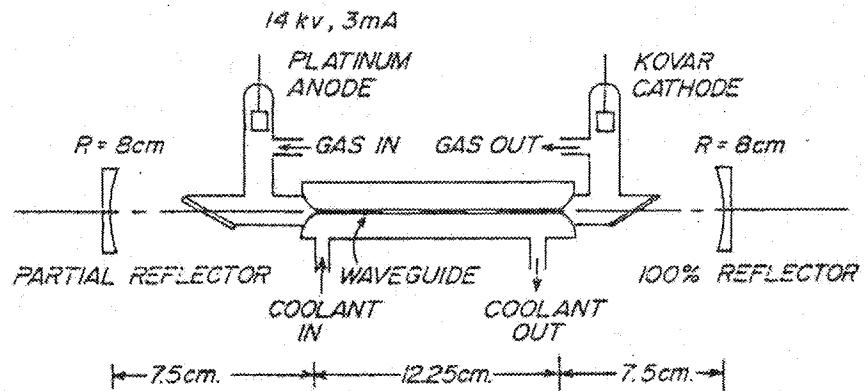
Figure 12.9 The construction of an early waveguide carbon dioxide laser. (Reprinted with permission from T. J. Bridges, E. G. Burkhardt, and P. W. Smith, *Appl. Phys. Lett.* 20:403 (1972). ©1972 American Institute of Physics.)

12.1.3 Waveguide CO_2 Lasers

One very good method for improving CO_2 laser performance is to decrease the bore size of the laser. This increases the number of gas collisions with the bore and significantly enhances the cooling rate (see Figure 12.9). If the electrodes are located transversely (rather than longitudinally) in the laser cavity, then the possibility also exists of using the electrodes themselves as an optical waveguide, thus permitting an even smaller bore size. The use of such a waveguide allows increased gas pressure with the attendant advantages of improved gain and larger linewidth. Operation in a waveguide mode also offers some additional advantages in alignment stability. The concept of a waveguide CO_2 laser was first proposed in 1964 by Marcatili and Schmeltzer[38] and later demonstrated by Steffen and Kneubuhl[39] and Smith.[40] Transverse-excited waveguide lasers are disclosed by Smith in U.S. Patent #3,815,047.[41]

Waveguide lasers use a small bore to confine the laser beam. The bore is itself an optical element, composed of two or four optically reflecting walls. Conventional mirrors are placed on either end of the cavity, but (unlike a conventional free space laser) these mirrors do not define a Gaussian beam in the cavity. Instead, the laser establishes various stable modes inside the bore (not unlike the modes in a laser fiber or a zig-zag slab laser). It is also possible to control the mode formation by introducing artifacts inside the bore that force the development of stable reflecting points.[42]

---

[38] E. A. J. Marcatili and R. A. Schmeltzer, *Bell Sys. Tech. J.* 43:1783 (1964).

[39] H. Steffen and F. K. Kneubuhl, *Phys. Lett.* 27A:612 (1968).

[40] P. W. Smith, *Appl. Phys. Lett.* 19:132 (1971).

[41] Peter W. Smith, "Transversely Excited Waveguide Gas Laser," U.S. Patent #3,815,047, June 4, 1974.

[42] Peter Laakmann, "Sealed Off RF-Excited Gas Lasers and a Method for Their Manufacture," U.S. Patent #5,065,405, November 12, 1991.

Waveguide lasers are typically differentiated from free space lasers by a number called the Fresnel number. This is defined as

$$F = \frac{a^2}{L\lambda_o} \qquad (12.3)$$

where a is the beam radius (for a cylindrical laser) or 1/2 the beam width (for a square laser), L is the length, and λ_o the free space wavelength. A laser with a Fresnel number of less than 0.5 is a true waveguide laser. A laser with a Fresnel number of greater than about 10 is a true free space laser. Lasers with Fresnel numbers around 1 are intermediate lasers that have some of the features of both classes.[43]

Waveguide lasers are typically smaller, lighter, easier to align, and cheaper than their glass tube ancestors. They also have significantly lower operating voltages, as the gas discharge must only be sustained transversely across the bore (a few millimeters) rather than longitudinally along the tube (many centimeters).

12.1.4 A Typical Modern CO_2 Industrial Laser

The remainder of this chapter will focus on a family of sealed low-power CO_2 lasers representative of modern commercial lasers used for industrial laser machining applications such as cutting and marking (see Figure 12.10). The specific units under discussion are the very popular series 48 sealed CO_2 lasers manufactured by Synrad in Mukilteo, Washington, U.S.A. These lasers represent an excellent example of modular design and are available in three power levels (10W, 25W, and 50W). (See Figure 12.11.)

CO_2 lasers can be operated with flowing gases or in a sealed configuration. Sealed lasers (such as the series 48 lasers) have obvious advantages in the industrial workplace as they do not require complex gas handling systems. Sealed lasers are only commercially available up to approximately 250 watts. The cross-over point between sealed laser technology and flowing gases technology is roughly 1 kW, and driven primarily by size and manufacturing constraints.[44]

Water-cooling is another critical issue in CO_2 laser design. Although CO_2 lasers are exceptionally efficient, 10% efficiency still means that 90% of the input power ends up somewhere else, usually as heat in the chassis. If the laser gets too hot, then the lower state population increases, and the laser performance drops. With good heat sink design, sealed CO_2 lasers can be operated in air-cooled mode up to approximately 25 watts. Past that power level, water-cooling is typically required.[45]

Design and manufacture of the series 48 module.   The basic series 48 module is described in U.S. Patent #5,065,405 (Peter Laakmann, "Sealed Off RF-Excited Gas Lasers and a Method for Their Manufacture," November 12, 1991) and the technology is discussed in U.S. Patent #4,805,182 (Peter Laakmann, "RF-Excited All-Metal Gas laser," February 14,

---

[43]Peter Laakmann, "Sealed Off RF-Excited Gas Lasers and a Method for Their Manufacture," U.S. Patent #5,065,405, November 12, 1991.

[44]Peter Laakmann, "Using Low Power CO_2 Lasers in Industrial Applications," Synrad Application Note.

[45]Peter Laakmann, "Using Low Power CO_2 Lasers in Industrial Applications," Synrad Application Note.

Figure 12.10 Typical products marked by a carbon dioxide laser. (Courtesy of Synrad)

1989). The key points of the design and manufacturing are described below and additional details may be found in the patents.

The basic series 48 module consists of two extruded aluminum electrodes and two extruded aluminum ground plane strips (see Figure 12.12). The inner surfaces of the electrodes and ground strips are optically reflective at 10.6 μm. (The electrodes are typically anodized with a 5 μm hard anodization to improve discharge stability and RF breakdown characteristics.[46]) The top and bottom electrodes are identical and measure approximately 1 cm by 2 cm by 40 cm long. The left and right ground plane strips are also identical and measure approximately 2 cm by 4 cm by 40 cm long. To reduce costs, the overall shape of the electrodes and ground planes is predefined by the extrusion process and only minor post-extrusion machining operations need to be performed.

The inner surfaces of the electrodes and the ground strips define the optical cavity of the laser. The bore of this cavity measures roughly 5 mm square, which gives the overall

---

[46]Y. F. Zhang, S. R. Byron, P. Laakmann, and W. B. Bridges, *Cleo '94*, 1994; *Tech. Digest Series*, Vol. 8, 94CH3463-7, pp. 358–9.
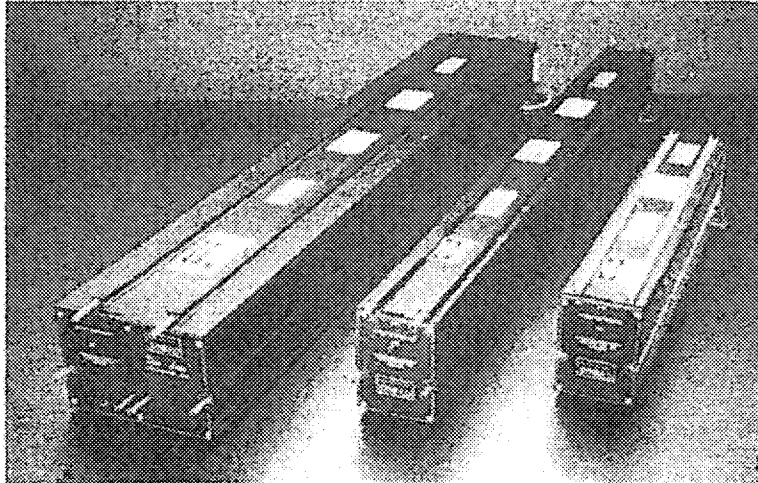
Figure 12.11   The Synrad series 48 sealed carbon dioxide lasers. (Courtesy of Synrad)
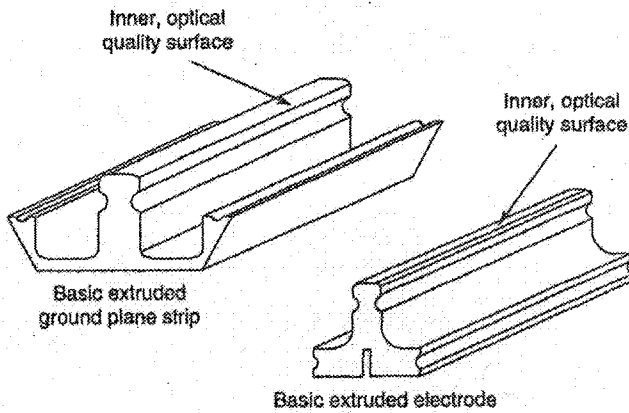
Figure 12.12   The Synrad electrodes and ground plane strips.

laser system a Fresnel number of approximately 1.5 and a diameter to length ratio of approximately 0.015. Thus, the laser operates in the intermediate regime between full waveguide operation and full free space operation. In this intermediate regime, only a fraction of the power of the optical wave interacts with the walls of the cavity. This fraction is high enough to obtain a good optical fill factor, but not so high as to create large losses due to absorption in the optical cavity structure.

If the optical surfaces of the electrodes and the ground strips are perfectly flat and aligned, then spurious reflections from the surfaces may cause aberrations in the output mode pattern. By deliberately introducing artifacts into the cavity geometry, these aberrations may be reduced or eliminated. Two types of artifacts have been found to be successful in reducing mode aberrations. The first artifact consists of slightly tapering the walls of the bore. In this method, the bore is made slightly larger near the end mirror than at the
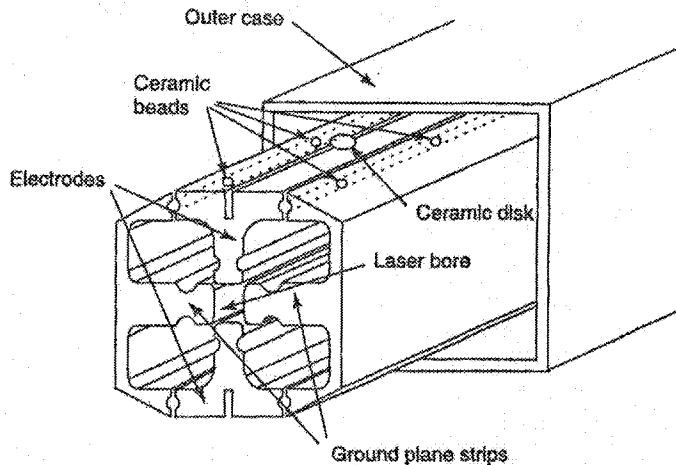
Figure 12.13   The Synrad series 48 cross-section.

front mirror. The taper angle is quite small, typically less than a milliradian. The second artifact consists of introducing small, sharp bends in the optical surfaces. The bends can be in one electrode and its adjacent ground strip, or in two opposing electrodes (or ground strips). If the bend is introduced into the electrode and its adjacent ground strip, then it is a bend on the order of 5 to 10 milliradians. If the bend is introduced into opposing electrodes (or ground strips), then it is on the order of 1 milliradian. These bends prevent reflections off all four walls from adding in phase to produce competing modes and parasitic oscillations.

The two electrodes and two ground planes are assembled in a clean room. The electrodes and ground plane strips are slipped into an outer case as shown in Figure 12.13. Small ceramic beads are used to isolate the electrodes from the ground plane strips. Larger ceramic disks are used to isolate the electrodes from the outer case. Electrical feedthroughs (which also serve as gas fill ports) are provided in the outer case.

A common cause of short lifetimes in CO_2 lasers is the accumulation of water vapor. Water vapor can migrate through the o-ring mirror seals, or be formed by hydrogen combining with dissociated oxygen. An effective way to minimize contamination due to water vapor is to introduce a getter into the cavity. A molecular sieve getter for removal of water vapor is typically inserted into the cavity during the initial assembly. Following the initial assembly, aluminum mirror mounts are welded to both ends of the tube. The laser module is then subjected to a high vacuum bake-out process. This process removes water as well as the majority of volatile contaminants such as hydrocarbons and hydrogen.

The bake-out process is followed by a passivation process where the laser module is exposed to an oxygen-helium plasma. The passivation process produces numerous oxygen species that react with the exposed aluminum parts and create aluminum oxides. (Al_2O_3, sapphire, is one of the many aluminum oxides formed by this process.) These oxides serve to

prevent oxygen loss in the finished laser and extend the operating lifetime. The passivation process also serves to clean the bore of the laser and prevent contamination of the mirrors during operation.

The passivation is performed by generating an oxygen plasma within the laser bore. To create all the oxides necessary for effective passivation, the plasma is operated at several different temperatures, and at peak excitation powers that exceed those the laser will experience in operation.

After the passivation is complete, the laser mirrors are added to the module. Although nearly perfect mirror alignment is required for effective operation of a true waveguide laser, the best mode quality and output power performance of an intermediate regime laser is often obtained when the end mirrors are aligned slightly off-axis. The back mirror is a 100% dielectric coating on silicon (3 meter concave for the 10 watt series 48 laser). The front mirror is flat with a partially reflective dielectric coating on ZnSe (95% reflectivity for the 10 watt series 48 laser). The mirrors are mounted against an o-ring seal and three small screws provide alignment adjustment. (Although the o-ring seal at first glance seems like a potentially unsatisfactory element, Synrad experience has shown them to work quite well. The leak rate is approximately 1 cm^3 of helium per year, not the limiting factor in the laser lifetime. The o-ring mounts do not fail catastrophically, and provide a simple and straightforward means to make alignment adjustments.[47])

Once the mirrors have been installed, the laser is again subjected to a short vacuum bake-out. This bake removes water vapor introduced by the mirror mounting operation. The bake is relatively short (120°C for 8 hours for the 10 watt series 48 laser) to avoid damaging the passivation layer.

Once the bake-out is completed, the laser is carefully realigned and permanently filled with the operating gas mixture. The operating mixture consists of roughly 7% xenon, 10% CO_2, 13% N_2, and 67% He.[48] (The xenon is added to lower the overall electron temperature and improve the cross-section of the (1) transition in N_2).[49] The basic laser module is now complete.

The finished laser module can be mounted in one of several different housings. The most common is to mount the laser in a simple housing incorporating an integral heat exchanger. The laser tube fits in the bottom of the housing, and the RF electronics to drive the electrodes mounts in the top (see Figure 12.14).

Expanding the basic module.   The basic 10 watt laser is designed to effectively scale to higher powers. Two electrodes, two ground strips, and an RF driver define a 10 watt module. Four electrodes (of the same length as the 10 watt electrodes), two ground strips (twice as long as the 10 watt ground strips), and two RF modules define the 25 watt module.

The two 25 watt modules are combined together in a simple but effective way to form the 50 watt module. The standard 25 watt module lases with its polarization vector

---

[47]P. Laakmann, *Lasers and Optronics* March: 35–41 (1989)

[48]P. Laakmann, "Using Low Power CO_2 Lasers in Industrial Applications," Synrad Application Note.

[49]W. J. Witteman, *The CO_2 Laser* (Berlin: Springer-Verlag, 1987), pp. 74–75.
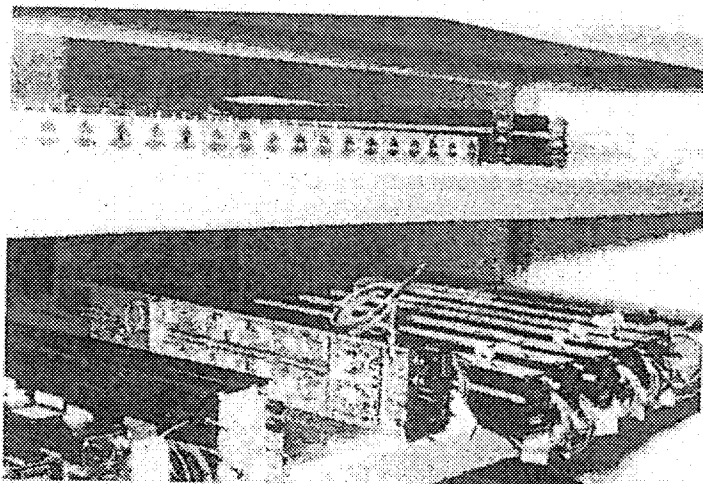
Figure 12.14 Synrad CO_2 series 48 internal modules and housings. (Courtesy of Synrad)
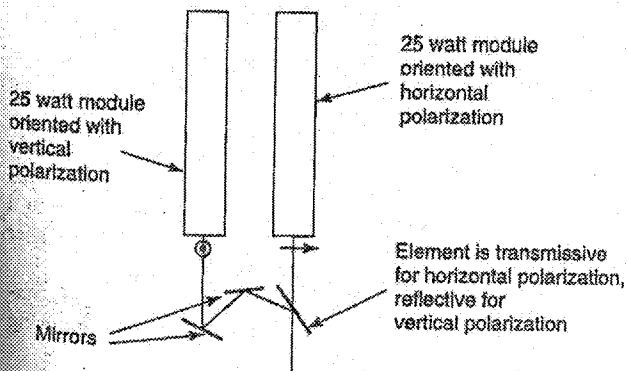
Figure 12.15   Combining the 25 watt beams together for the 50 watt unit.

parallel to the ground planes.[50] If one 25 watt module is installed with its polarization vector vertical, and the second installed with its polarization vector horizontal, then the orthogonally polarized beams can be combined at the output using a polarizing beam splitter (see Figure 12.15).

The same modular scaling strategies are applied to the RF drive electronics. The single 10 watt module uses one RF driver board. The 25 watt module uses two identical driver boards, and the 50 watt module uses four identical driver boards.

---

[50]Y. F. Zhang, S. R. Byron, P. Laakmann, and W. B. Bridges, *Cleo '94*, 1994; *Tech. Digest Series*, Vol. 8, 94CH3463-7, pp. 358–9.

Design of the RF driver board.   Although the very early CO_2 lasers frequently used a radio frequency (RF) discharge,[51,52,53,54,55] this was considered by most researchers to be an inefficient and inconvenient excitation source.[56]   It was not until 1977, when Katherine Laakmann began re-examining the use of RF-excitation for waveguide lasers,[57] that the potential value of RF-excitation for small sealed waveguide lasers became apparent.

Conventional CO_2 lasers use a longitudinal high voltage DC current to create the plasma. In a DC longitudinally excited laser, the output power is difficult to control electrically. Changing the voltage across the electrodes changes the character of the plasma. This, in turn, alters the plasma impedance and the ability of the plasma to excite the CO_2 molecules. Thus, a rather small change in the exciting voltage can result in large changes in the laser performance. Furthermore, the length and stability characteristics of the longitudinal excitation make rapid changes in the laser performance difficult.

In the late seventies, Laakmann Electro-optics (started by Peter and Katherine Laakmann) developed the transverse RF-excited CO_2 laser. The major advantage of transverse RF-excited lasers is that the output power can be electrically controlled over a wide range, at rates of up to 20 kHz. (Figure 12.16 illustrates the control of the output power by alteration of the duty cycle for 5 kHz and 20 kHz operation from a 65 watt Synrad CO_2 laser.) Other advantages of RF-excitation include significantly lower voltages (hundreds compared to thousands of volts) and the possibility of longer laser lifetimes due to reductions in gas-dissociation-related damage.

RF-excitation does have its costs. In particular, transistor controlled RF-excited devices have roughly half the wallplug efficiency of similar DC-excited units.[58] Additionally, the power supplies required for RF-excitation are typically more expensive than those in an equivalent DC-excited unit.

The excitation frequency of the RF discharge ranges from a value of approximately $v/2a$ to $50v/a$, where a is the width of the laser bore, and v is the drift velocity of electrons in the laser gas. The drift velocity ranges from approximately $5 \cdot 10^6$ to $1 \cdot 10^7$ cm/sec in a typical CO_2 laser gas mixture.[59] Thus, for a typical transversely excited RF discharge laser system, appropriate excitation frequencies lie in the UHF-VHF region.

In order to avoid radio interference with other services, certain ISM (Industrial, Scientific, Military) frequencies have been set aside by the FCC for industrial uses requiring

[51]C. K. N. Patel, *Phys. Rev.* 136:A1187 (1964).

[52]P. Barchewitz, L. Dorbec, R. Farrenq, A. Truffert, and P. Vautier, *C. R. Hebd. Seanc. Acad. Sci.* 260:3581 (1965).

[53]P. Barchewitz, L. Dorbec, A. Truffert, and P. Vautier, *C. R. Hebd. Seanc. Acad. Sci.* 260:5491 (1965).

[54]R. Farrenq, C. Meyer, C. Rossetti, L. Dorbec, and P. Barchewitz, *C. R. Hebd. Seanc. Acad. Sci.* 261:2617 (1965).

[55]C. Rossetti, R. Farrenq, and P. Barchewitz, *J. Chim. Phys.* 64:93 (1967).

[56]Tyte, D. C., in *Advances in Optical Electronics*, Vol. 1, ed D. W. Goodwin (New York: Academic Press, 1970), p. 172.

[57]Katherine Laakmann, "Waveguide Gas Laser with High Frequency Transverse Discharge Excitation," U.S. Patent #4,169,251, September 25, 1979.

[58]P. Laakmann, *Lasers and Optronics* (1989), pp. 35–41.

[59]Katherine Laakmann, "Waveguide Gas Laser with High Frequency Transverse Discharge Excitation," U.S. Patent #4,169,251, September 25, 1979.
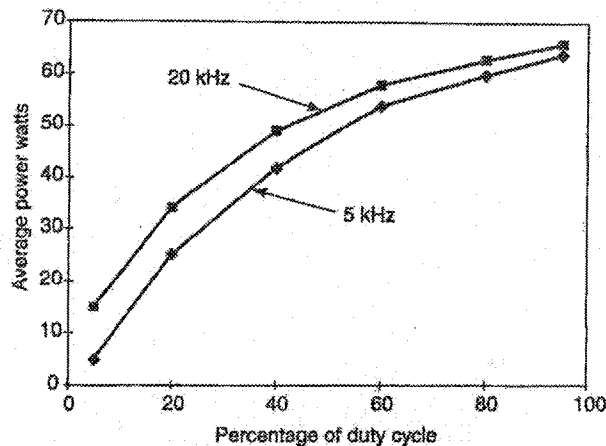
Figure 12.16   Output power versus duty cycle for the 57G Synrad laser. (Courtesy of Synrad)

large amounts of RF power. These ISM frequencies are used for larger RF CO_2 lasers and are 27.12 MHz and 40.68 MHz. Smaller lasers may operate outside of the ISM frequency limits if the shielding is sufficiently good so that RF leakage is below FCC minimums.[60]

Supplying power to the plasma of an RF-excited transversely pumped CO_2 waveguide laser requires careful design. The RF voltage source typically has a very low impedance, while the laser tube may have an impedance of hundreds to thousands of ohms at its operating frequency. A laser tube with a square bore 4.8 mm in width and 37 cm long, with a laser gas pressure of 60 torr, will have an impedance of approximately 200 ohms when operating with an output of approximately 15 watts.[61] The impedance increases as the power decreases, and is several thousand ohms if the plasma is not ignited.

An impedance matching network typical of the Synrad series 48 lasers is described in U.S. Patent #5,008,894, "Drive System for RF-Excited Gas Lasers," by Peter Laakmann. The basic concept is illustrated in Figure 12.17. An RF power supply output stage is connected through a transmission line to the pair of electrodes and ground strips forming the waveguide laser. The collector of the upper transistor in the push-pull output stage of the RF power supply is connected to the top electrode of the laser through the core of a 1/4 wavelength (at the laser operating frequency) transmission line. The lower transistor in the push-pull output stage is connected through the cladding of the transmission line to ground via a blocking capacitor. A coil connects the top electrode to the bottom electrode of the waveguide laser. (This coil serves to neutralize the capacitive reactance and to generate bi-phase excitation of the plasma.[62]) A transformer is used to match the impedance of the final stage to the preceding circuitry in the RF source.

In a small RF-excited CO_2 laser (such as the Synrad 10-50 watt series 48 lasers) the entire power supply and impedance matching networks can be integrated into a single

---

[60]P. Laakmann, "Using Low Power CO_2 Lasers in Industrial Applications," Synrad Application Note.

[61]P. Laakmann, "Drive System for RF-Excited Gas Lasers," U.S. Patent #5,008,894, April 16, 1991.

[62]P. Laakmann, "Electrically Self-Oscillating RF-Excited Gas Laser," U.S. Patent #4,837,772, June 6, 1989.
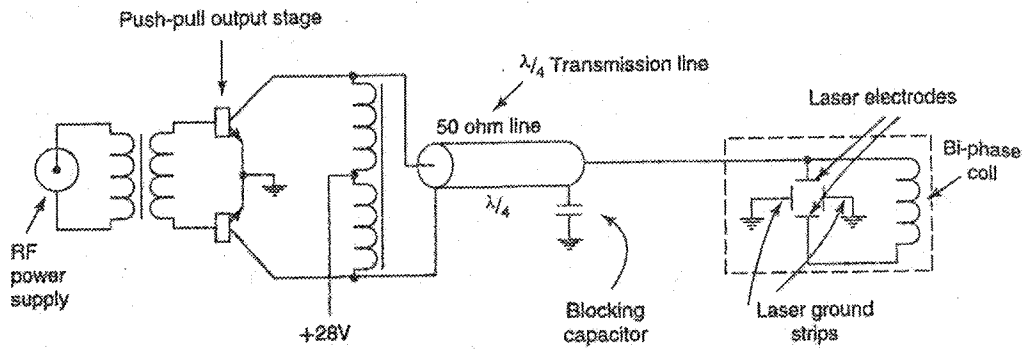
Figure 12.17 An impedance matching network typical of the Synrad series 48 lasers. (From Peter Laakmann, "Drive System for RF-Excited Gas Lasers," U.S. Patent #5,008,894.)
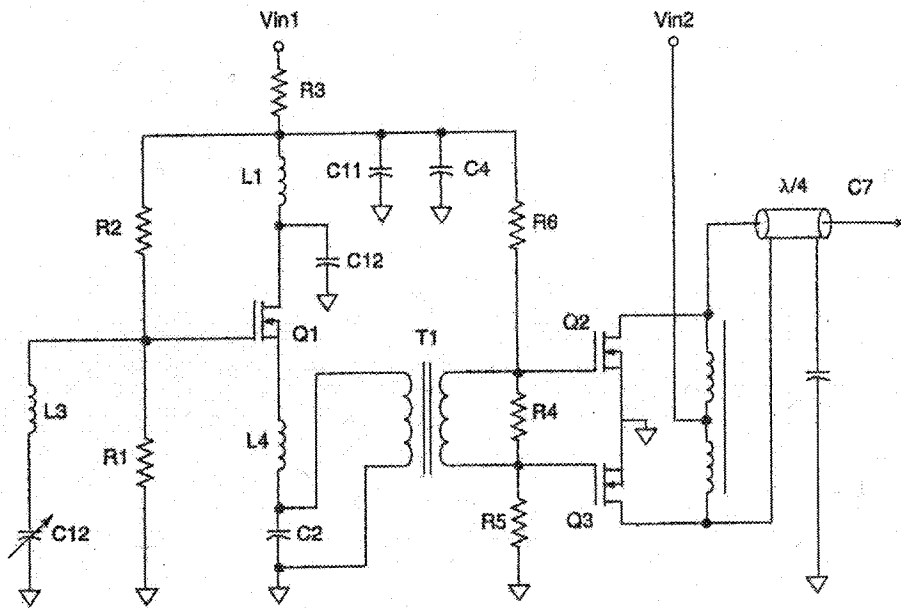
Figure 12.18 A typical RF drive circuit for a waveguide carbon dioxide laser.

unit as illustrated in Figure 12.18. The input stage of the power supply is a relatively conventional RF oscillator circuit. The output stage is a push-pull stage and is integrated into the impedance matching network as described in the previous paragraph and in U.S. Patent #5,008,894.[63]

---

[63]P. Laakmann, "Drive System for RF-Excited Gas Lasers," U.S. Patent #5,008,894, April 16, 1991.

12.1.5 Optical Components and Detectors for CO_2 Lasers

Window, mirrors and lenses.   The long (10.6 μm) wavelength and high average power of CO_2 lasers lead to some difficulties in construction of optical systems. Conventional glass optics cannot be used at CO_2 wavelengths due to high optical absorption and low thermal conductivity. Table 12.1 summarizes the important optical properties of materials typically used for transmissive optics in CO_2 lasers. The alkali halides (such as KBr) tend to have very low absorption, but are hygroscopic and require special coatings to survive in moist environments. The semiconductors (such as ZnSe and GaAs) are much more robust, but with correspondingly higher absorption coefficients. Unfortunately, both germanium (Ge) and silicon (Si) suffer from a thermal runaway problem. Above a certain critical laser intensity, as the sample heats, the absorption increases, and the sample heats more. This feedback mechanism rapidly results in destruction of the sample.

TABLE 12.1   PROPERTIES OF MATERIALS USED IN CO_2 LASERS

Material	Thermal expansion ($\times 10^6$ / °C)	Thermal conductivity ($\times 10^{-2}$ W / cm °C)	α (at 10.6 μm cm^{-1})
NaCl	38.9	6.5	$1.34 \cdot 10^{-3}$
KBr	43	4.8	$5 \cdot 10^{-5}$
ZnSe	7.7	13	$6 \cdot 10^{-3}$
GaAs	5.7	37	$1.2 \cdot 10^{-2}$
Si	4.2	120	2.5
Ge	6	59	$3.6 \cdot 10^{-2}$

W. W. Duley, *CO_2 Lasers: Effects and Applications* (New York: Academic Press, 1976), p. 104, Table 3.4.

Zinc selenide (ZnSe), a well-behaved semiconductor with a relatively high thermal conductivity and low absorption, is the typical choice for CO_2 transmissive optics. ZnSe does not suffer from thermal runaway and has the major advantage of being transmissive from 600 nm to 11 μm. (This allows low power HeNe lasers to be used for alignment of CO_2 systems.) ZnSe is available commercially as in the form of windows, dielectric-coated partially-transmitting mirrors, and lenses.

The very high average power typical of CO_2 lasers means that CO_2 reflecting optics must be thermally conductive as well as poor optical absorbers at 10.6 μm. Dielectric- or metal-coated mirrors with single-crystal silicon substrates are the mirrors of choice for lower-power CO_2 lasers. Higher power lasers use metal coatings (typically silver or gold) on molybdenum or copper substrates. Molybdenum (with a thermal conductivity of 1.33 W/cm °C) offers roughly equivalent thermal conductivity as silicon, but is a much more durable refractory material. Molybdenum may also be used without a surface metal coating of gold or silver. (Uncoated molybdenum mirrors typically have reflectances on the order of 98%.) Copper (with a thermal conductivity of 3.9 W/cm °C) is much more thermally conductive than either silicon or molybdenum, but significantly less rugged. Copper is also difficult to polish and exceptionally easy to scratch during cleaning.

The long wavelength of CO_2 lasers does offer certain advantages during fabrication of optics. Diffraction and focusing effects of scratches are roughly proportional to $(1/\lambda)^4$.

Thus, a relatively poor finish by visible optics standards may be perfectly suitable for CO_2 laser optics. Additionally, the longer wavelength permits fabrication of optics using such methods as diamond turning. If properly fabricated, a diamond turned CO_2 reflector may not need to be polished after fabrication.

CO_2 laser detectors. The long wavelength and high average power of CO_2 lasers also lead to difficulties in optical detection and laser power measurement. Several detection technologies are commonly employed with CO_2 lasers to overcome these problems. These technologies include thermopiles, bolometers, pyroelectric crystals, and long wavelength semiconductor photovoltaic and photoconductive detectors. (For more details on thermopiles, bolometers, and pyroelectric crystals, see Section 8.4.)

The majority of photovoltaic and photoconductive semiconductor devices are fabricated from silicon and have a roughly 400 nm to 1.1 μm response range. A simple example of a photodetector of this type is a PIN photodiode. However, photovoltaic or photoconductive devices do exist with responses in the 10.6 μm range. To move the detector into the 10.6 μm range requires switching to more exotic semiconductors with narrower bandgaps than silicon. Examples include HgCdTe, CdTe, and PbSnTe. However, 10.6 μm infrared photovoltaic or photoconductive detectors do suffer from a special problem. Semiconductor energy states that absorb in the 10.6 μm range are separated by approximately 0.1 eV. Thus, thermal population of the energy states from sources other than the laser beam is quite likely. Therefore, the detectors are often cooled using liquid helium, liquid nitrogen, or thermoelectric coolers.

10.6 μm radiation is far outside of the human visual response. Thus, a number of techniques have been developed to enable humans to locate the beam and make qualitative measurements. The simplest include such things as absorption in foamed polystyrene, wood, or metal. More complex methods include the use of color changes in liquid crystals and visible fluorescence from various materials. One of the most elegant and effective methods is the thermal-quenching of visible luminescence from a ZnCdS phosphor excited continuously with UV light. The usual configuration is to use a UV light to excite the back of a small screen coated with the phosphor. The phosphor glows a brilliant yellow until it interacts with a CO_2 beam. The CO_2 beam quenches the fluorescence and leaves dark areas on the screen.

12.2 THE DESIGN OF EXCIMER LASERS

Excimer[64] lasers operate on the radiative transition between the excited state of a molecule and its ground state. Commercial excimer lasers typically use molecules formed from the combination of heavy noble gases (such as Xe, Kr, and Ar) and halogens (such as F, Cl, Br, and I). Common excimer laser combinations include ArCl (175 nm), ArF (193 nm), KrCl (222 nm), KrF (249 nm), XeBr (282 nm), XeCl (308 nm), and XeF (351 nm). Excimer lasers operate pulsed and are available in energies ranging from several millijoules to handfuls of

---

[64]In the most correct usage, the word *excimer* is limited to homopolar molecules such as Xe_2. Heteropolar molecules such as XeF are more correctly termed *exciplex* molecules. However, since it is quite difficult to pronounce exciplex laser, the term excimer has grown to mean both classes of lasers.

joules per pulse. Repetition rates range from a few kHz to hundreds of Hz and output average powers are available up to 500 watts.

Excimer lasers are prized for their ability to efficiently produce coherent UV and deep UV radiation. They are used in such diverse commercial applications as laser hole drilling, laser chemical vapor deposition, laser photochemistry, creation of soft x-ray plasmas, semiconductor wafer cleaning, laser machining, laser ablative sputtering, excimer laser surface annealing, deep UV lithography, and laser planarization. They find application in the medical field for coronary angioplasty and photorefractive keratectomy. Research applications include spectroscopy, laser photochemistry, laser doping of semiconductors, and remote sensing.

Excimer lasers, like CO_2 lasers, are very different from the other lasers discussed in this text. Conventional lasers lase off electronic transitions between various atomic states. Excimer lasers lase off the transition between a molecular excited state and a molecular ground state. This means that excimer lasers tend to have a shorter wavelength and higher efficiency than most conventional lasers. Additional information on excimer lasers can be found in Rhodes,[65] Laude,[66] Elliot,[67] and Weber.[68]

12.2.1 Introduction to Excimer Laser States

Consider a gas mixture of a rare gas A (such a krypton) and 0.1 to 0.3% of a halogen gas X (such as fluorine). Assume that the mixture is pumped by an intense electron beam, which forms A^+ and X^- ions.[69] The ions then recombine to form the excited $(A^+X^-)^*$ state as:[70]
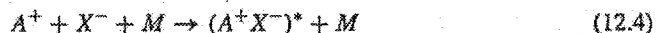
$$A^+ + X^- + M \rightarrow (A^+X^-)^* + M \qquad (12.4)$$

where A is the rare gas ion, X is the halogen ion and M is any third body (usually another rare gas ion) to assure momentum conservation.

The $(A^+X^-)^*$ molecules are the excited molecules and form the upper state population (with a lifetime on the order of 5 to 15 ns). The AX molecules form the lower state population. However, the lifetime of the AX molecule is extremely short (on the order of tens of femtoseconds). Thus, even though the upper state lifetime is short by the standard of most lasers (tens of nanoseconds as compared to tens or hundreds of microseconds), it is still three orders of magnitude greater than the lifetime of the ground state. (For excimer lasers to operate correctly, it is necessary for the ground state molecule to dissociate rapidly. Systems for which the molecule dissociates slowly do not make successful lasers because the laser bottlenecks in the ground state.)

---

[65]C. K. Rhodes, ed, *Excimer Lasers* (Berlin: Springer-Verlag, 1984), particularly Chapter 4, pp. 87–138.

[66]Lucien Laude, *Excimer Lasers* (Netherlands: Kluwer Academic Publishers, 1994).

[67]David Elliot, *Ultraviolet Laser Technology and Applications* (San Diego: Academic Press, 1995).

[68]Marvin J. Weber, ed, *Handbook of Laser Science and Technology, Vol. II, Gas Lasers* (Boca Raton, FL: CRC Press, Inc., 1982), particularly Section 3, pp. 273–491; and Marvin J. Weber, ed, *Handbook of Laser Science and Technology, Supp. I, Lasers* (Boca Raton, FL: CRC Press, Inc., 1991), particularly Section 3.3.1, pp. 341–387.

[69]The A^+ and X^- ions are A and X atoms which have lost or gained one electron respectively.

[70]The excited $(A^+X^-)^*$ is a molecule with the same number of electrons as AX, but with one of the electrons in a higher energy state.
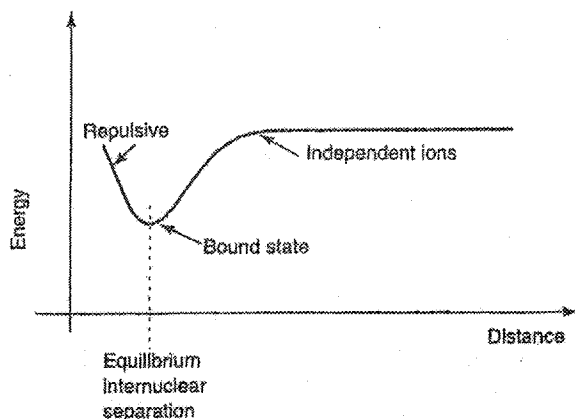
Figure 12.19 The formation of a molecule is driven by a balance between the coulombic attraction of the ions and the repulsive potential that keeps two ions from occupying the same space.

The physics of excimer laser operation is inherently connected to the basic processes of molecule formation. Recall that the formation of a molecule is driven by a balance between the coulombic attraction of the ions and the repulsive potential that keeps two ions from occupying the same space. Thus, the formation of a molecule is a function of the distance between the two ions (see Figure 12.19). If the two ions are widely separated, there is no molecule. If the two ions are trying to occupy the same space, there is no molecule. The balance between the coulombic attraction and the repulsive potential creates a *well* or *pocket* in the potential energy curve. When the two ions are at a distance (the equilibrium internuclear separation) corresponding to this energy well they are *bound* and form the molecule.

The situation in a rare-gas halogen laser is somewhat more complicated than that illustrated in Figure 12.19. This is because of the simultaneous existence of atoms, ions, molecules, and their various excited states. A simplified potential energy diagram of a rare gas halogen excimer laser is illustrated in Figure 12.20. Notice that the upper state manifold has two kinds of potential energy curves. There are covalent curves corresponding to the bonding of an excited atom with another atom ($A^* + X$ or $A + X^*$). There are also ionic curves corresponding to the bonding of two ions ($A^+ X^-$). The ionic curves actually form a family of curves, because there are a variety of electron configurations possible in the $(A^+ X^-)^*$ excited state.

Practical excimer laser systems are those for which the ionic $(A^+ X^-)^*$ states are the lowest states of the upper manifold. These are systems where the crossings between the ionic and covalent state energies occur for larger internuclear separations than the equilibrium distance. In these systems the dynamics of the reactions lead inevitably to molecules residing in the bound metastable $(A^+ X^-)^*$ state. From the $(A^+ X^-)^*$ state, the only available downward energy transition is by radiation. There are no competing alternative paths.

The lower state manifold is similar to the upper state manifold, but somewhat less complex. Since the lower state does not have ions, the only potential energy curves are those associated with the various electronic states of the covalent AX. The lower state may (or may not) have a potential well indicating the existence of a bound molecule.

Structure of rare gas monohalides
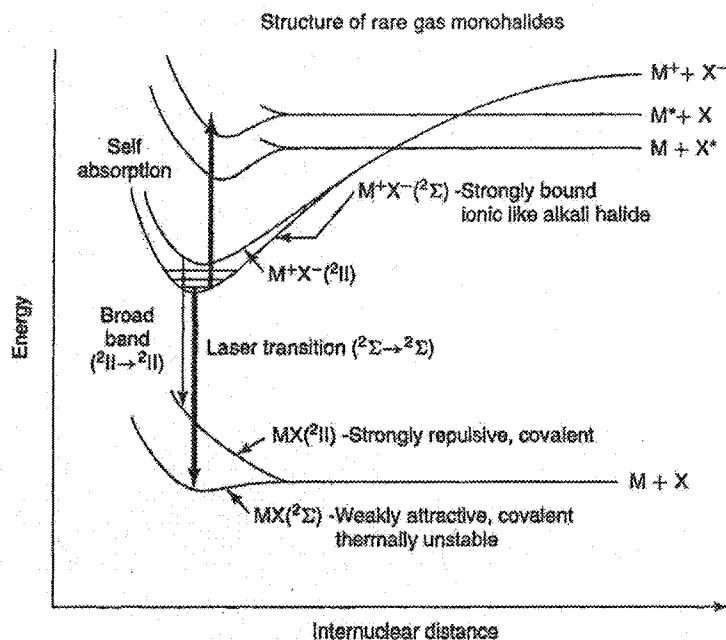
Figure 12.20 A simplified potential energy diagram of a rare-gas halogen laser. (From C. K. Rhodes, ed, *Excimer Lasers* (Berlin: Springer-Verlag, 1984), Figure 4.1, p. 88. ©1984 Springer-Verlag.)

The emission spectrum of KrF illustrates the radiative characteristics of a typical rare gas-halogen transition (see Figure 12.21). The largest peak corresponds to the transition from the bottom of the potential well of the $(A^+ X^-)^*$ excited state to the bottom of the potential well of the AX excited state.

Commercially interesting rare gas halide lasers are pumped by electron beam excitation or by electrical discharge. In electron beam excitation, an energetic electron beam is created in vacuum and directed through a thin metal or polymer membrane into the gas mixture. High energy electrons scattering off atoms in the gas create ions, excited atoms, and secondary electrons. The secondary electrons, in turn, create more ions, excited atoms, and electrons. The ions and excited atoms react to form the excited molecules. Under electron beam excitation, ions are produced in preference to excited states (by about a 3:1 ratio) and the primary reaction is
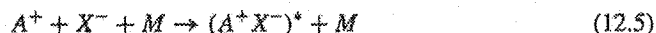
$$A^+ + X^- + M \rightarrow (A^+ X^-)^* + M \tag{12.5}$$

where A is the rare gas ion, X is the halogen ion, and M is any third body (usually another rare gas ion), to assure momentum conservation.

Pulsed electrical discharges are more commonly used for commercial lasers because they offer the potential for higher pumping efficiency and higher average power. In an electrical discharge, the low energy electrons drift along in the electric field and increase in energy. Eventually, they reach the energy threshold for excitation of the first excited state
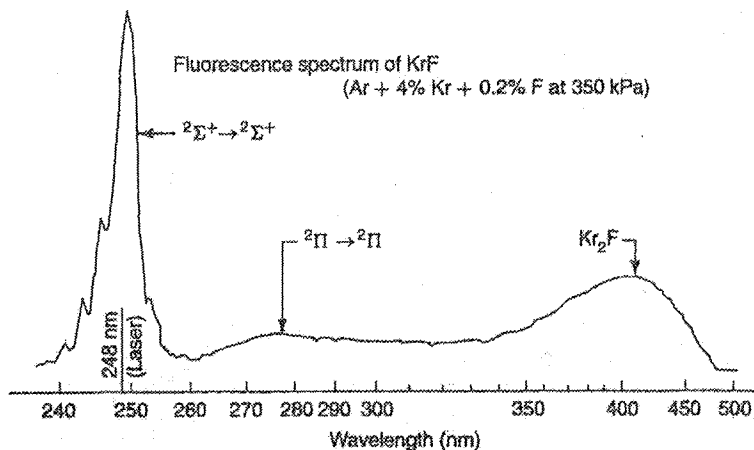
Figure 12.21 The emission spectrum of KrF illustrates the radiative characteristics of a typical rare gas-halogen transition. (From C. K. Rhodes, ed, *Excimer Lasers* (Berlin: Springer-Verlag, 1984), Figure 4.2, p. 91. ©1984 Springer-Verlag.)

of the rare gas atoms. Then, they collide inelastically with the rare gas atom, leaving the gas atom in an excited state and returning the electron to low energy. Under these conditions, a very fast and efficient reaction termed a *harpoon* collision is involved.[71]

$$A^* + MX \rightarrow (A^+ X^-)^* + M \tag{12.6}$$

12.2.2 The Evolution of Excimers

The first excimer was demonstrated in 1970 by Basov et al. at the Lebedev Physics Institute.[72] This laser was an Xe_2 excimer that lased at 176 nm and was excited by a relativistic electron beam directed into liquid xenon. In 1972, Koehler et al. at Lawrence Livermore National Laboratories demonstrated an Xe_2 laser using electron beam pumping of gaseous xenon.[73] Laser action from XeBr at 282 nm was first reported in 1975 by Searles and Hart at the Navel Research Laboratory.[74] Searles and Hart measured the optical gain of the XeBr to be 4% per pass over 15 cm of active length. The experiment was originally run at 1 to 4% Br_2, but this was reduced to 0.1 to 1% Br_2 when the Br_2 was discovered to quench the XeBr excited state.

A few weeks later, Ewing and Brau reported laser action from XeCl at 308 nm and KrF at 249 nm.[75] An independent observation of laser action in KrF was also reported by Tisone

---

[71]D. R. Herschbach, *Adv. Chem. Phys.* 10:319 (1966); pp. 367–379 in particular.

[72]N. G. Basov, V. A. Danilychev, Yu. M. Popov, and D. D. Khodkevich, *JETP Lett.* 12:329 (1970).

[73]H. A. Koehler, M. A. Ferderber, D. L. Redhead, and P. J. Ebert, *Appl. Phys. Lett.* 21:198 (1972).

[74]S. K. Searles and G. A. Hart, *Appl. Phys. Lett.* 27:243 (1975).

[75]J. J. Ewing and C. A. Brau, *Appl. Phys. Lett.* 27:350 (1975).

et al.[76] and Mangano and Jacob.[77] In the Ewing and Brau experiments, laser action was obtained from a mixture of Ar, Xe, and Cl_2 at 89.9:10:0.1 and from a mixture of Ar, Kr, and F_2 at 98.9:1.0:0.1. The output energy was approximately 50 μJ from the XeCl laser and approximately 4 mJ from the KrF laser. Tisone et al. used a mixture of 3000 torr of Ar, 150 torr of Kr, and 6 torr of F_2 and were able to obtain 5.6 J by using 5 cm diameter cavity mirrors. In the Mangano and Jacob experiments, laser action was obtained from a mixture of Ar, Kr, and F_2 at 97.9:2.0:0.1. The maximum output energy in the Mangano and Jacob experiments was 6 mJ. All three experiments used a pulsed electron gun to excite the gas mixture.

Reports of laser action from XeF soon followed, first discovered by Brau and Ewing,[78] but first published by Ault et al.[79] Brau and Ewing used a mixture of Ar, Xe, and F_2 at 99.6:0.3:0.1 where the mixture was excited with a cold cathode electron gun. Ault et al. used a mixture of Ar, Xe, and NF_3 at 250:25:1. The use of NF_3 in the Ault experiments was to both minimize the corrosive effects of F_2 and to avoid quenching due to self-absorption. The measured output energy from the Ault experiments was 5 mJ per pulse, the peak power was 500 kW, and the pulse width was 10 ns.

All of the early excimer and exciplex lasers were electron beam pumped. However, the efficiency advantages of using electrical discharge pumping were recognized very early. Since excimer lasers require very high voltages, longitudinal discharge excitation of excimers was never successfully attempted. Instead, excimer technology leveraged off the existing developments in transversely excited CO_2 lasers. A major advancement occurred in 1975, when Burnham and Djeu at the Navel research laboratories modified a TEA CO_2 laser and demonstrated excimer laser action with an electrical discharge.[80]

12.2.3 General Design Background

Gas flow.   In order to operate an electrically discharge excited excimer laser, it is necessary to provide an electric field that exceeds the DC breakdown voltage of the gas mixture by a factor of 2 to 3. This typically requires voltages of 10 to 15 kV/cm. Furthermore, this pulse must be applied in a time short compared to the electronic avalanche time of 20 to 30 ns. This implies a rise time of several kV/nanosecond. Finally, there must be sufficient electrons in the circuit to supply the growing plasma. This requires a very low impedance electrical excitation circuit.

The discharge pulse of an excimer laser creates a number of ionized and excited species. Many of these species are quite long-lived. If another discharge pulse is attempted before these secondary species have decayed, the resulting electrical discharge will be unstable. Therefore, in most commercial excimers, the gas flows across the electrodes. In general, the best results are achieved when the flow rate is high enough to flush the dis-

[76]G. C. Tisone, A. K. Hays, and J. M. Hoffman, *Opt. Commun.* 15:188 (1975). (The Ewing paper was received on June 17, 1975, and the Tisone paper on July 7, 1975.)

[77]J. A. Mangano and J. H. Jacob, *Appl. Phys. Lett.* 27:495 (1975). (The Ewing paper (footnote #75) was received on June 17, 1975, and the Mangano paper on July 7, 1975.)

[78]J. J. Ewing and C. A. Brau, *Appl. Phys. Lett.* 27:350 (1975); and C. A. Brau and J. J. Ewing, *Appl. Phys. Lett.* 27:435 (1975).

[79]E. R. Ault, R. S. Bradford, and M. L. Bhaumik, *Appl. Phys. Lett.* 27:413 (1975).

[80]Jeff Hecht, *Laser Pioneers*, revised ed. (Boston, MA: Academic Press, 1992), p. 46.

charge volume between the electrodes 2 to 3 times before the next pulse. In the case of high power lasers with pulse repetition rates of 500 Hz to 2 kHz, this gas replacement means that velocities of 50 to 150 m/sec are required. Thus, aerodynamics becomes a critical part of excimer laser design.

Preionization.   Good electrical discharge uniformity is essential for the successful operation of a pulsed excimer laser. In order to provide a uniform high voltage discharge in high pressure gases, the gas must be preionized immediately prior to the application of the main electrical discharge pulse. Preionization means that a uniform ion or electron cloud is generated in the gas in the discharge region. This cloud serves to *seed* the discharge and prevent the formation of arcs or streamers in the discharge. Once the initial cloud (approximately 10^7 electrons/cm^3) is created, the main discharge will proceed by avalanche ionization to create densities near 10^{15} electrons/cm^3.

Preionization is a very challenging problem because a large number of electrons must be created quickly. Preionization can be accomplished in a variety of ways.[81,82] The two most common are UV light and x-rays. UV light can be generated by spark gaps or by corona discharges. However, UV light does have the limitation that the ionizing range is restricted to a few cm.[83] X-rays can be created in x-ray tubes by collisions of energetic electrons with a high Z material (such as tungsten). X-rays have a much deeper penetration depth, but are more difficult to create. In addition, the use of x-rays in a commercial system requires special licensing and approval.

Multiple spark gaps are commonly used to create UV light for preionization.[84] Early excimer laser systems used a linear sparkboard where each spark gap was separately discharged to create a traveling spark wave down the length of the cavity. Later designs used multiple parallel pins, where the pins were fired simultaneously. Spark gaps provide excellent preionization, but at the cost of some structural complexity. More importantly, spark gaps erode and tend to contaminate the laser gas and optical components of the resonator. Spark gaps are much less frequently used today, as they have been replaced by corona or x-ray preionization methods.

Corona discharges tend to provide lower electron concentrations, but are structurally simpler and do not contaminate the gas. Corona discharges have the additional advantage that they can be easily integrated with the main electrode structure. Thus corona discharges are most commonly used with commercial excimers (such as XeCl) that do not require high electron preionization concentrations.

Another alternative is to use x-ray preionization.[85] Although x-ray preionization was not used in the early development of excimer lasers (due to the difficulty and expense of making short x-ray pulses) advances in x-ray generation technology for lasers have made x-ray preionization a very viable alternative to corona technology. This is especially true for the more exotic excimers which may require higher preionization electron densities.

[81] A. J. Palmer, *Appl. Phys. Lett.* 25:136 (1974).

[82] S. C. Lin, *J. Appl. Phys.* 51:210 (1980).

[83] K. Midorikawa, M. Obara, and T. Fujiokam, *IEEE J. of Quantum Electron.* QE-20:198 (1984).

[84] K. Miyazaki et al., *Rev. Sci. Instrum.* 52:201 (1985).

[85] S. Sumida, M. Obara, and T. Fujiokam, *Appl. Phys. Lett.* 33:913 (1978).
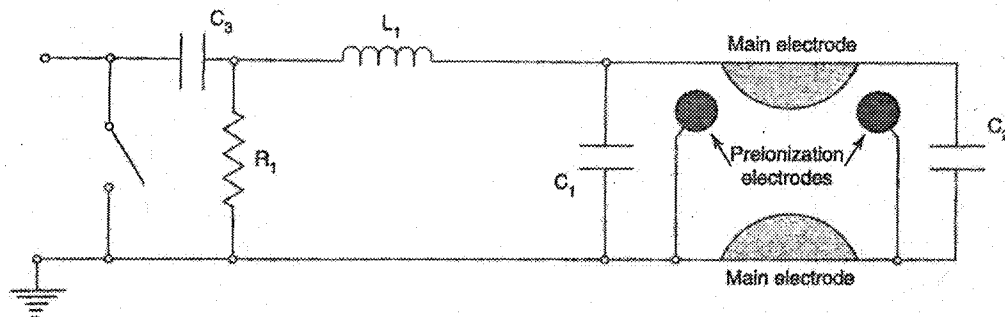
Figure 12.22 A typical corona discharge circuit. The two main electrodes are oriented transversely. The two preionization electrodes are also oriented transversely, and are parallel to the main electrodes. (From E. Müller-Horsche, "Apparatus for Preionizing a Pulsed Gas Laser," U.S. Patent #5,247,531, Sept. 21, 1993.)

Corona discharge circuitry.   The corona discharge method is one of the most common commercial preionization techniques.[86,87] In the corona discharge method, UV light is generated by a gas discharge between a metal and a dielectric. The UV light then creates a weak ionization in the discharge region of the electrodes. One of the major advantages of corona preionization is that the dielectric prevents formation of spark channels to the preionization electrodes. Thus, the contamination effects of the sparks are eliminated.

A typical corona discharge circuit is shown in Figure 12.22.[88] The two main electrodes are oriented transversely. The two preionization electrodes are also oriented transversely, and parallel to the main electrodes. The preionization electrodes consist of a conductor with a surrounding dielectric (for example, a quartz sleeve). The preionization electrodes are placed near one of the main electrodes and are connected to the potential of the other electrode. A high-voltage source charges the storage capacitor, and the pulse is triggered by a thyratron (or equivalent high-voltage switching element). The preionization potential is thus driven by the main discharge pulse.

Another option is shown in Figure 12.23.[89] The geometry is similar to Figure 12.22. However, with this system, the preionization potential is driven by a separate set of circuitry from the main discharge pulse. This permits more subtle tuning of the timing between the two events, but at the cost of additional circuitry.

Still another option is shown in Figure 12.24.[90] Here, the clever use of inductors and capacitors generates a very rapid starting spike across the preionization electrodes, which is followed by the main discharge pulse. Suitable choice of inductor and capacitor values permit this circuit to be tuned for optimum output power.

---

[86]G. J. Ernst and A. G. Boer, *Opt. Commun.* 27:105 (1978).

[87]U. Hasson and H. M. Bergmann, *Rev. Sci. Instrum.* 50:59 (1979).

[88]E. Müller-Horsche, "Apparatus for Preionizing a Pulsed Gas Laser," U.S. Patent #5,247,531, Sept. 21, 1993.

[89]E. Müller-Horsche, "Apparatus for Preionizing a Pulsed Gas Laser," U.S. Patent #5,247,531, Sept. 21, 1993.

[90]E. Müller-Horsche, "Apparatus for Preionizing a Pulsed Gas Laser," U.S. Patent #5,247,531, Sept. 21, 1993.
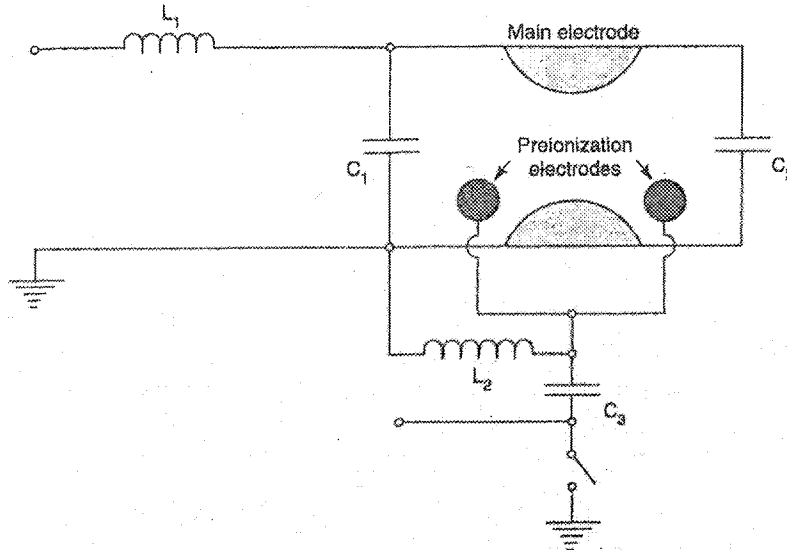
Figure 12.23   Another type of corona discharge circuit. In this circuit, the preionization potential is driven by a separate set of circuitry from the main discharge pulse. This permits more subtle tuning of the timing between the two events, but at the cost of additional circuitry. (From E. Müller-Horsche, "Apparatus for Preionizing a Pulsed Gas Laser," U.S. Patent #5,247,531, Sept. 21, 1993.)
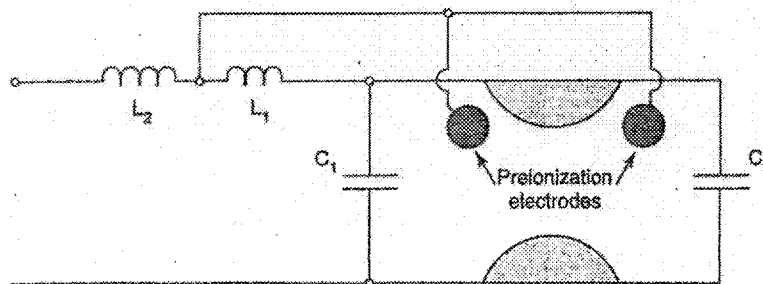
Figure 12.24   In this circuit, the clever use of inductors and capacitors generates a very rapid starting spike across the preionization electrodes, which is followed by the main discharge pulse. (From E. Müller-Horsche, "Apparatus for Preionizing a Pulsed Gas Laser," U.S. Patent #5,247,531, Sept. 21, 1993.)

Main discharge circuitry.   Once the preionization stage is complete, the main discharge pulse must be generated. The electrical discharge requirements on discharge excited pulsed excimer lasers are quite stringent. The rise time is short (10^{11} A/sec) and the voltage and power are high (50 kV and 5 kW). Furthermore, the gas (after breakdown) has a very low impedance.
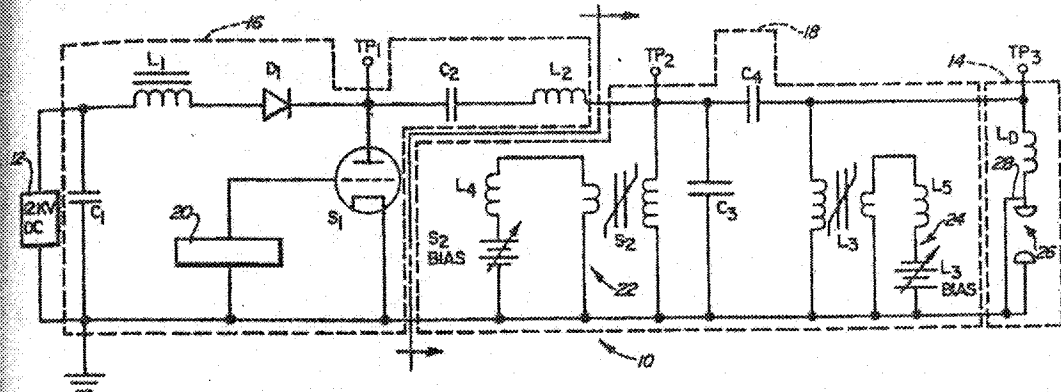
Figure 12.25 A typical discharge circuit for an excimer laser. This circuit provides an electrical interface between a high-voltage, high-impedance power source, and a relatively low-impedance laser load. (From T. S. Fahlen and B. Mass, "Electrical Excitation Circuit for Gas Lasers," U.S. Patent #4,549,091, Oct. 22, 1985.)

An example of a typical discharge circuit is shown in Figure 12.25.[91] The electrical circuit provides an electrical interface between a high-voltage, high-impedance power source and a relatively low-impedance laser load. The circuit includes an electrical excitation circuit 10, a charging circuit 16, a pulse forming network 18, and a laser load 14.

The charging circuit includes a power source capacitor C_1, a charging capacitor C_2 series-connected with an inductor L_2, a charging choke L_1 and an isolating diode D_1. The choke L_1 and charging diode D_1 isolate the power source 12 from the pulse forming network 18. (The capacitor C_1 is significantly larger than the capacitor C_2.) A thyratron S_1 is also included in the charging circuit. The control electrode of the thyratron is connected to a pulse generator.

The pulse-forming network (PFN) includes a saturable inductor switch S_2, a bias power source for S_2, and a choke L_4 connected in series with the bias winding of the saturable inductor switch. The PFN also includes a PFN capacitor C_3 shunted across the saturable inductor switch S_2 and a second PFN capacitor C_4 connected between TP_2 and TP_3. Additionally, the PFN includes a magnetic diode charging inductor L_3, a bias power source for L_3 and a choke L_5 connected in series with the bias winding of the magnetic diode charging inductor. (The choke L_5 provides isolation of the bias power source for L_3 from high-voltage pulses produced by transformer action on the bias winding of the magnetic diode-charging inductor L_3.) The laser load 14 is connected between TP_3 and common. The inductance L_D represents the distributed inductance of the electrode structure of the laser load 14. A preionization circuit 28 is also included.

The electrical excitation circuit performs four relatively separate operations: a slow resonant charge of the charging capacitor C_2, a medium-speed charge of the pulse forming

[91] T. S. Fahlen and B. Mass, "Electrical Excitation Circuit for Gas Lasers," U.S. Patent #4,549,091, Oct. 22, 1985.
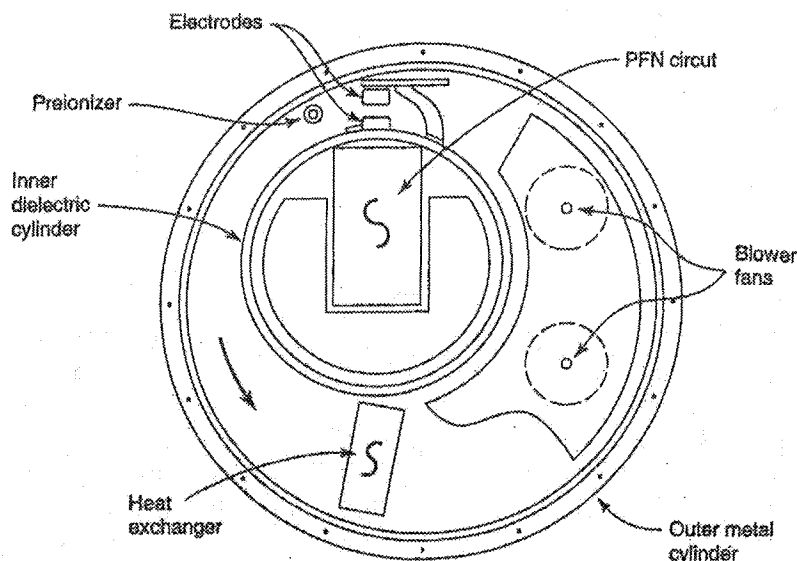
Figure 12.26 The heart of the 5300 is a pressure vessel consisting of two eccentrically mounted cylinders. (From D. J. Clark and T. S. Fahlen, "Gas Transport Laser System," U.S. Patent #4,611,327, Sept. 9, 1986.)

network 18, an inversion of the voltage on half of the pulse forming network, and finally the laser discharge.

12.2.4 A Typical Modern Excimer Laser

The remainder of this section will focus on an industrial excimer laser intended for industrial materials processing applications. The specific unit under discussion is the XMR 5300 laser manufactured by XMR, Inc., in Fremont, CA. This laser is representative of a high-end industrial materials processing excimer laser.

The XMR 5300 is a XeCl laser operating at 308 nm and producing 200 watts at 300 Hz for an energy of approximately 660 mJ/pulse. The repetition rate is selectable from 1 to 300 Hz and the pulse width is 40 to 50 ns. The output beam incorporates a beam homogenizer and is 1.5 cm by 3.3 cm with less than a 5 mrad divergence. The laser operates at a pressure of 5.76 atmospheres with a buffer gas of neon and uses an HCl precursor to generate the chlorine. The design of this laser is discussed in D. J. Clark and T. S. Fahlen, "Gas Transport Laser System," (U.S. Patent #4,611,327), and in T. S. Fahlen, "Gas Discharge Laser Having a Buffer Gas of Neon," (U.S. Patent #4,393,505), and is only summarized here.[92,93]

The heart of the 5300 is a pressure vessel consisting of two eccentrically mounted cylinders (see Figure 12.26). The outer cylinder is metal and constitutes the outer wall of the pressure vessel. The inner cylinder is a dielectric and contains the PFN for the electrodes.

---

[92]D. J. Clark and T. S. Fahlen, "Gas Transport Laser System," U.S. Patent #4,611,327, Sept. 9, 1986.

[93]T. S. Fahlen, "Gas Discharge Laser Having a Buffer Gas of Neon," U.S. Patent #4,393,505, July 12, 1983.

The gas flow is between the inner cylinder and the outer cylinder and is driven by a set of blower fans. A gas-to-liquid heat exchanger is located near the bottom of the pressure vessel.

The electrodes are placed on the top of the inner dielectric cylinder and the laser is excited transversely. Two pairs of preionizing corona electrodes are located slightly to both sides of the main electrodes. The main discharge plasma is created between the two electrodes near the top of the pressure vessel. Thus, the optical cavity is located parallel to these electrodes.

Physically, the 5300 pressure vessel consists of a nickel-plated stainless-steel cylinder that is 100 cm long and 60 cm in diameter. The vessel contains approximately 200 liters of laser gas. The stainless-steel cylinder has a welded flange with an o-ring groove on each end. End plates are bolted to the welded flanges. Although the system operates at a pressure of roughly 70 psig, the heavy stainless construction has been pressure tested up to 180 psig.

The laser system is designed for easy repair and maintenance. All of the components inside the pressurized vessel are readily accessible. A removable cantilevered arm hinged to the flange holds the end plate so that it can be swung away from the flange. Once removed, the end plate is supported on a wheeled cradle. The inner dielectric cylinder, electrodes, PFN, blowers, and heat exchangers are attached to the end plate and are removed with it. This configuration provides ready access to the sub-assemblies for servicing. Each of the sub-assemblies is a module and can be replaced independently of the others.

The electrodes are two solid-rail electrodes, 79 cm long and 2.5 cm wide, spaced by 2.5 cm. The material of both electrodes is solid nickel. The electrodes are mounted to the outside of the internal dielectric cylinder. Each of the electrodes is bolted to eighteen feedthroughs penetrating the inner dielectric cylinder. Each feedthrough is o-ring-sealed as it enters the inner cylinder. However, the electrodes can be adjusted or removed without replacing the o-rings.

Five to 10 kW of heat is generated in the laser gas from the electrical discharge, the corona preionization, and the blower fans. The gas to liquid heat exchanger maintains the gas temperature at 90°F with a 65°F input coolant temperature at a flow of 3 to 5 gallons per minute. The heat exchanger is a finned tube construction, nickel-plated to minimize damage from the gas mixture. In order to minimize feedthroughs, the heat exchanger is welded to a flange, which is sealed to the end plate with an o-ring.

Figure 12.27 is a perspective figure illustrating the entire system. The outer metal cylinder defines the shape of the entire system. The inner dielectric cylinder can be seen toward the back of the drawing (somewhat hidden by the fans). The window for the optical cavity can be seen near the front top of the pressure vessel. The large triangular housings on each side of the pressure vessel contain the drive assembly for the blower fans.

The double cylinder structure offers a number of advantages. To begin with, it places the pulse-forming network inside of a large steel structure. This serves as an ideal *Faraday cage* and minimizes the laser generating damaging electromagnetic interference from the extremely high voltage and current pulses. The Faraday cage construction similarly reduces the possibility of accident triggering of the PFN by external sources. Locating the PFN close to the electrodes minimizes the overall inductance of the electrical system. Finally, locating the PFN within the pressure vessel minimizes the number of feedthroughs.
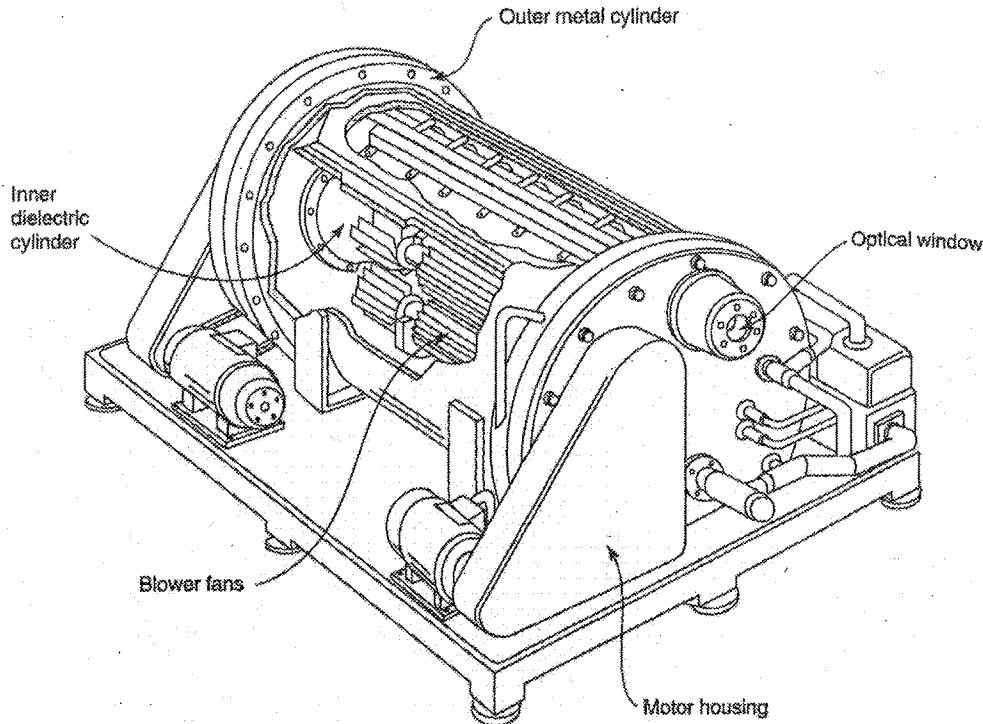
Outer metal cylinder

Inner
dielectric
cylinder

Optical window

Blower fans

Motor housing

Figure 12.27 A perspective figure illustrating the laser chamber of the XMR 5300. The outer metal cylinder defines the shape of the entire system. The inner dielectric cylinder can be seen toward the back of the drawing (somewhat hidden by the fans). (From D. J. Clark and T. S. Fahlen, "Gas Transport Laser System," U.S. Patent #4,611,327, Sept. 9, 1986.)

The eccentric placement of the cylinders is also a critical part of the design. Notice that the electrodes are located at the narrowest part of the structure. This increases the velocity of the gas over the electrodes and enhances the uniformity of the gas flow. The flow velocity is maximized in the double-cylinder geometry because there are no sharp bends, constrictions, or changes in direction. Additionally, the cylindrical geometry minimizes the surface area exposed to the gas mixture.

One of the major challenges in constructing excimer laser systems is the corrosion caused by the halogen ions. Early excimers were notorious for blowing seals and destroying electrical components. Thus, excimer laser design must include a number of features to simultaneously reduce leakage and enhance the laser lifetime. The 5300 incorporates magnetic couplings for the blowers in order to provide a hermetic seal with no mechanical contact. Within the pressurized vessel, bearings are lubricated with fluorinated lubricants. The blower and coupling bearings inside the vessel are enclosed in a housing, which is pressurized with a small flow of halogen-free gas. In addition, materials used inside the pressure vessel have been selected carefully. The majority of the metals are nickel-plated. Insulating materials are quartz or ceramic.
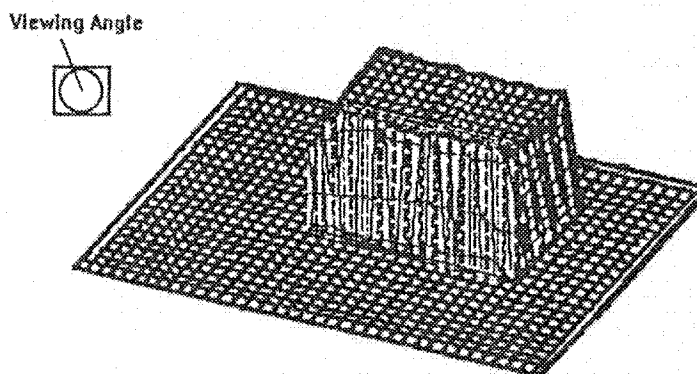
Viewing Angle

Figure 12.28 Materials processing applications (such as laser planarization or laser annealing) frequently require a "top hat" beam profile with adjustable x and y dimensions. (Courtesy of XMR, Fremont, CA)

The pressure vessel has an input and exhaust port for gas replenishment. Although the 5300 can run for approximately 10^7 pulses without replenishment, eventually parasitic chemical reactions will deplete the halogen and the system will need to be recharged.

The preionization is supplied by a corona wire. The corona wire is a quartz insulated conductor. The discharge volume created by the corona wire is approximately $70 \times 2.5 \times 2$ cm^3.

It is usually necessary to provide a buffer gas in an excimer laser mixture in order to initially support the discharge. Many excimers use helium, because it is chemically inert, inexpensive, has a high ionization potential, and forms stable low pressure discharges. It is also light and has a high specific heat for cooling. However, the 5300 uses neon as a buffer gas. Neon offers many advantages over helium in a system with corona wire preionization. Use of neon as a buffer gas increases both the output power and efficiency of the laser. This enhanced performance appears to be related to increased stability of the plasma.

The electrodes are pulsed at 20 to 50 kV. The rise time of the electrical pulse must be shorter than the upper state lifetime (5 to 15 ns). All of the circuit elements in the PFN are preferably insulated by a bath of transformer oil. The insulating oil is cooled by circulation through a heat exchanger. Electrical connections from the pulse forming network to the external circuitry are made with continuous cables sealed by compression o-rings.

The laser resonator uses a conventional high-reflecting rear mirror and partially transparent front mirror. The laser runs in a pseudowaveguide mode in the vertical direction and in a free-space mode in the horizontal. This creates a beam profile that is Gaussian only in the horizontal direction.

12.2.5 Laser Beam Homogenizers

Materials processing applications (such as laser planarization or laser annealing) frequently require a "top hat" beam profile (see Figure 12.28) with adjustable x and y dimensions.

Since most materials processing lasers lase on some combination of Gaussian modes, an optical element (called a homogenizer) is necessary to convert the Gaussian beam into the "top hat" profile. A large number of techniques have been used to homogenize laser beams. One class of techniques consists of using lenses, white cells, or waveguides to divide the beam into small parts and then recombine the parts into the desired shape.[94,95] A second class of techniques uses prisms or mirrors to fold the beam onto itself.[96]

XMR uses a homogenizer of the beam dividing type. In their homogenizer,[97] two sets of arrays of crossed cylindrical lenses (four groups of cylindrical lenses in total) are used to divide the incoming beam into an array of "beamlets" (see Figure 12.29). A focusing lens then recombines the beamlets into a "top hat" distribution on the exposure plane. In the XMR commercial unit, arrays 3 and 4 (and the focusing lens) are fixed. Arrays 1 and 2 are free to move. The separation of array 1 from array 3 determines the x dimension of the homogenized beam, while the separation of array 2 from array 4 determines the y dimension. Notice that the homogenized "top hat" distribution is always formed at the same location from the homogenizer, independent of the location of the arrays.

12.2.6 Application Highlight

Excimer lasers are employed in a large number of laser materials processing applications. The short wavelength, high energy, and high average power of excimer lasers present unique materials processing benefits.

For example, the polysilicon thin film transistor (poly-Si TFT) is considered to be the next technological step in the development of active-matrix liquid crystal displays.[98] Polysilicon has a number of advantages over amorphous silicon. As one example, polysilicon possesses more than 100 times the carrier mobility of amorphous silicon, thus enabling CMOS peripheral display drivers to be integrated right into the display. Displays with built-in drivers are more reliable than conventional displays, because electrical connections are implemented in metallization layers on the substrate itself instead of with thousands of TAB-bonded interconnects. Another benefit of eliminating TAB-bonding is that screen pitch is no longer limited by interconnection pitch, thus opening the door to super-high-resolution displays suitable for imaging and graphics applications. In addition, high mobility poly-Si TFT transistors offer fast charging speeds to compensate for RC time delays in larger displays.

However, commercializing the use of poly-Si TFT devices for active-matrix liquid-crystal displays has been difficult. The customary approach to creating poly-Si TFT devices is to use a quartz substrate with a layer of deposited amorphous silicon and slowly anneal ($700°C$ for 24 hours) the amorphous silicon into a polysilicon thin film. However, the high cost of quartz substrates and the long process times required for furnace annealing have made

---

[94] Geary, *Optical Engineering* 27:972 (1988).

[95] Iwasaki et al., *Applied Optics* 29:1736 (1990).

[96] Bruno and Liu, *Lasers and Applications* (1987), p. 91.

[97] T. S. Fahlen, S. B. Hutchison, and T. McNulty, "Optical Beam Integration System," U.S. Patent #4,733,944, March 29, 1988.

[98] D. Zankowsky, *Laser Focus World* (1994).
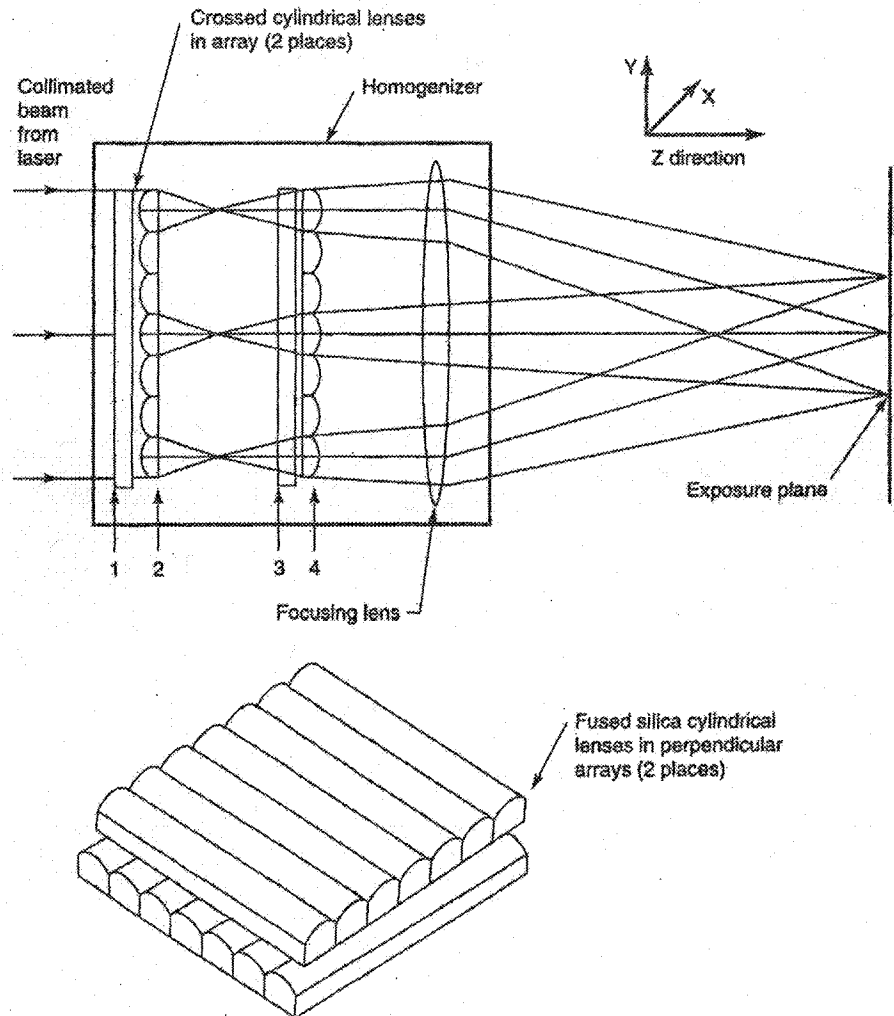
Figure 12.29 In XMR's homogenizer, two arrays of crossed cylindrical lenses (four groups of cylindrical lenses in total) are used to divide the incoming beam into an array of "beamlets." A focusing lens then recombines the beamlets into a "top hat" distribution on the exposure plane. (Courtesy of XMR, Fremont, CA)

this process impractical for high-volume production of large displays. Unfortunately, lower-priced glass substrates cannot be used, because the high temperatures used in conventional annealing processes also melt the glass substrate.

Laser annealing offers an alternative to furnace annealing for creating economical poly-Si TFT devices (see Figure 12.30). In laser annealing, the laser only heats the surface of the material, thus allowing materials other than expensive quartz to be used as substrates.

Figure 12.30 Schematic of an excimer laser annealing system for manufacturing poly-Si TFT devices. (Courtesy of XMR, Fremont, CA)

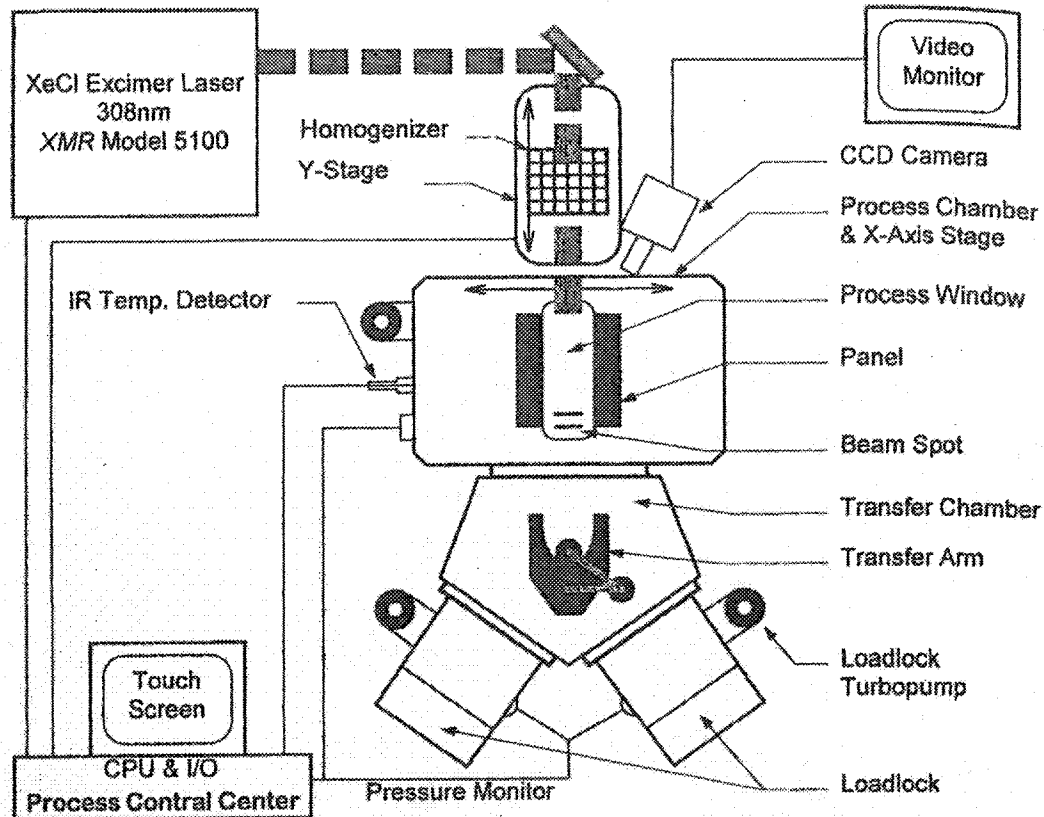Both argon and excimer lasers have been used to anneal amorphous silicon to polysilicon. However, excimer lasers have a significant advantage over argon lasers in this application. This is because excimers are high power (200+ watt), short pulse (20- to 50-ns) lasers. As a consequence, they only locally heat the surface of the film. The melt region extends just 50 to 100 nm below the surface. Excimer laser annealing is the only current annealing technology that can reliably transform amorphous silicon into polysilicon while the substrate remains at room temperature.

The basic process for creating polysilicon thin films by laser annealing is quite straightforward. Before processing, the substrate is covered with an amorphous silicon thin film. The excimer then scans the glass substrate with a spatially uniform pattern of overlapping rectangular pulses. The UV energy is strongly absorbed by the surface layer of amorphous silicon, which rapidly melts and recrystallizes into polysilicon. The instantaneous local temperature in the surface layer is high enough to achieve excellent crystallinity. However, the

average temperature of the glass substrate remains substantially below the damage threshold and is unaffected by the laser crystallization process.

Since laser annealing is a scanning process, it offers considerable present and future process flexibility. The manufacturer has the option of selectively annealing designated areas or moving to larger or smaller substrates. In addition, laser annealing provides the high throughputs required for high-volume active-matrix liquid crystal display manufacturing. The high peak energy of the excimer laser, combined with a 300 Hz pulse repetition rate, enables 360 × 450 mm substrates to be processed in as little as three minutes.

12.3 OVERVIEW OF SEMICONDUCTOR DIODE LASERS

12.3.1 History of Semiconductor Diode Lasers

There are often periods in science when major discoveries are made simultaneously by a number of different researchers. The early history of semiconductor diode lasers follows this pattern.

Consider the research environment for lasers in mid-1962. The existing lasers were lasers with long path lengths and large external resonators. These lasers lased on narrow transitions between well-defined discrete states. Semiconductors (with a high free carrier absorption, wide bandwidth optical transition, and relatively small size) were assumed to have inefficient radiative recombination and were considered an improbable material for laser action.

However, in July 1962 Keyes and Quist presented a paper, "Recombination Radiation Emitted by Gallium Arsenide Diodes," at the Solid State Device Research Conference (SSDRC) in Durham, NH.[99,100] This paper described intense luminescence with a quantum efficiency of approximately 85% from GaAs junctions at 77°K. These results were so startling that they energized a number of research groups to consider the question of semiconductor lasers. These included research groups at General Electric, IBM, and MIT Lincoln Laboratories. (Notice that all of these groups achieved semiconductor laser operation in the latter half of 1962!)

The General Electric group used n-type GaAs wafers with a zinc diffusion to form a degenerate PN-junction. (The importance of the degenerate junction was pointed out by Bernard and Duraffourg in 1961.[101]) The resulting wafers were cut into strips approximately 0.5 mm wide and cemented to plates so that the edges could be lapped and polished. These polished edges formed the Fabry-Perot resonator structure. The resulting diodes were cooled to 77°K and operated in pulsed mode. The paper announcing the first semiconductor laser operation was the General Electric paper submitted in September 1962 and appearing in the November 1, 1962, edition of *Physical Review Letters.*[102]

---

[99]R. J. Keyes and T. M. Quist, "Recombination Radiation Emitted by Gallium Arsenide Diodes," presented at the *Solid State Device Res. Conf.,* 1962.

[100]The material in these papers was later published in R. J. Keyes and T. M. Quist, *Proc. IRE* 50:1822 (1962).

[101]M. G. A. Bernard and G. Duraffourg, *Phys. Stat. Sol.* 1:699 (1961).

[102]R. N. Hall, G. E. Fenner, J. D. Kingsley, T. J. Soltys, and R. O. Carlson, *Phys. Rev. Lett.* 9:366 (1962).

The IBM group also used n-type GaAs wafers with a zinc diffusion to form a degenerate PN-junction. The IBM group was struggling with the concept of how to make a resonator, and so decided to attempt to demonstrate stimulated emission without a resonator. The IBM *Applied Physics Letter* reporting the coherent stimulated emission from a GaAs PN-junction was submitted in October 1962, appearing within days of the publication of the General Electric *Physical Review Letter*.[103]

The MIT Lincoln Laboratories group also used n-type GaAs wafers with a zinc diffusion. They elected to use mechanical polishing to form the resonator structure and achieved laser action within a few weeks of the other groups. Their first paper was submitted in November 1962, and their results were reported in a pair of experimental and theoretical papers.[104, 105] The MIT Lincoln Laboratories group was also noteworthy for being the first group to address the question of applications for the new lasers by demonstrating TV transmission from a rooftop, and then from a nearby mountain top.[106]

Very shortly after the first demonstration of laser action in a degenerate GaAs PN-junction, a number of interesting and important advancements occurred. Just a few weeks after the initial announcement of GaAs diodes by the General Electric group,[107] Holonyak and Bevacqua demonstrated the first visible (710 nm) laser diode in $GaAs_{1-x}P$, using polished facets[108] (the Holonyak and Bevacqua paper was submitted in October 1962). The first cw operation (at 2°K) was observed by Howard et al.,[109] and the first pulsed room-temperature operation by Burns et al.[110]

The issue of polishing versus cleaving to create the small Fabry-Perot cavities was a critical one in early semiconductor laser development. Although cleaving is now considered to be somewhat easier than polishing, the first three lasers to be demonstrated all incorporated polished Fabry-Perot cavities. Holoyak originally attempted cleaving, but returned to polishing after difficulties in cleaving $GaAs_{1-x}P$. The first reported use of cleaving is by Bond et al. in 1963.[111] Dill and Rutz patented the cleaving concept from a disclosure filed on October 20, 1962.[112]

Laser research then began to diverge into a number of separate areas. The idea of using heterostructures in semiconductor diode lasers was a very powerful idea and was

---

[103]M. I. Nathan, W. P. Dumke, G. Burns, R. H. Dill, Jr., and G. Lasher, *Appl. Phys. Lett.* 1:62 (1962).

[104]T. M. Quist, R. H. Rediker, R. J. Keyes, W. E. Krag, B. Lax, A. L. McWhorter, and H. J. Zeiger, *Appl. Phys. Lett.* 1:91 (1962).

[105]A. L. McWhorter, H. J. Zeiger, and B. Lax, *J. Appl. Phys.* 34:235 (1963).

[106]R. H. Rediker, R. J. Keyes, T. M. Quist, M. I. Hudson, C. R. Grant, and R. G. Burgess, "Gallium Arsenide Diode Sends Television by Infrared Beam," *Electron.* 35: 44–45 (1962); and R. J. Keyes, T. M. Quist, R. H. Rediker, M. I. Hudson, C. R. Grant, and J. W. Meyer, "Modulated Infrared Diode Spans 30 Miles," *Electron.* 36: 38–39 (1963).

[107]R. N. Hall, G. E. Fenner, J. D. Kingsley, T. J. Soltys, and R. O. Carlson, *Phys. Rev. Lett.* 9:366 (1962).

[108]N. Holonyak, Jr., and S. F. Bevacqua, *Appl. Phys. Lett.* 1:82 (1962).

[109]W. E. Howard, F. F. Fang, F. H. Dill, Jr., and M. I. Nathan, *IBM J. Res. Develop.* 7:74 (1962).

[110]G. Burns and M. I. Nathan, *IBM J. Res. Develop.* 7:68 (1962).

[111]W. L. Bond, B. G. Cohen, R. C. C. Leite, and A. Yariv, *Appl. Phys. Lett.* 2:57 (1963).

[112]F. H. Dill, Jr., and R. F. Rutz, "Method of Fabrication of Crystalline Shapes," U.S. Patent #3,247,576, filed October 30, 1962; issued April 16, 1966.

first proposed by Kroemer in 1963.[113] However, the heterostructure concept required the development of appropriate materials-processing technologies, such as liquid phase epitaxy (LPE), metal-organic chemical vapor deposition (MOCVD), and molecular beam epitaxy (MBE). Therefore, the original proposal of Kroemer went relatively unnoticed.

In 1963, Nelson first demonstrated the liquid phase epitaxy growth of GaAs on GaAs.[114] In 1967, Woodall et al. demonstrated the growth of the heterostructure $Al_xGa_{1-x}As$ on GaAs.[115] The first LPE pulsed room temperature heterostructure lasers soon followed in 1969[116,117,118] and then cw room temperature heterostructure lasers.[119,120] Quantum confinement was the next major advancement in heterostructures. In 1978, Dupuis et al. first demonstrated a room-temperature quantum well laser.[121] Strained quantum well lasers soon followed.[122,123,124]

Distributed feedback lasers (DFB lasers) were another major track in laser development. DFB lasers incorporate an intrinsic grating to force single longitudinal mode operation. Kogelnik and Shank first developed the experimental and theoretical ideas behind DFB lasers.[125] Nakamura et al. reported the DFB semiconductor laser oscillation by photopumping GaAs.[126] Scifres et al.[127] reported the first AlGaAs/GaAs single heterostructure DFB junction lasers. Casey et al.[128] and Nakamura et al.[129] used an AlGaAs/GaAs separately confined heterostructure to achieve the first DFB cw oscillation at room temperature. Room-temperature cw operation of a DFB laser at the fiber-optical communication wavelength of 1.5 μm in InGaAsP/InP was first reported by Utaka et al.[130]

Distributed Bragg reflector lasers (DBR lasers) are a variation on DFB lasers where the reflectors are outside (rather than inside) the active region. Lasing occurs between the

[113]H. Kroemer, *Proc. IEEE* 51:1782 (1963).

[114]H. Nelson, *RCA Rev.* 24:603 (1963).

[115]J. M. Woodall, H. Rupprecht, and G. D. Pettit, *Solid-State Device Conf.*, 1967. Abstracts reported in *IEEE Trans. Electron. Devices* ED-14:630 (1967).

[116]H. Kressel and H. Nelson, *RCA Rev.* 30:106 (1969).

[117]I. Hayashi, M. B. Panish, and P. W. Foy, *IEEE J. Quantum Electron.* QE-5:211 (1969).

[118]Zh. I. Alferov, V. M. Andreev, E. L. Portnoi, and M. K. Trukan, *Fiz. Tekh. Poluprovodn.* 3:1328 (1969) [*Sov. Phys. Semicond.* 3:1107 (1970)].

[119]I. Hayashi, M. B. Panish, P. W. Foy, and S. Sumuski, *Appl. Phys. Lett.* 17:109 (1970).

[120]Zh. I. Alferov, V. M. Andreev, D. Z. Garbuzov, Yu. V. Zhilyaev, E. P. Morozov, E. L. Portnoi, and V. G. Trofim, *Fiz. Tekh. Poluprovodn.* 4:1826 (1970). [*Sov. Phys. Semicond.* 4:1573 (1971)].

[121]D. Dupuis, R. D. Dapkus, N. Holonyak, Jr., E. A. Rezek, and R. Chin, *Appl. Phys. Lett.* 32:295 (1978).

[122]E. Yablonovitch and E. O. Kane, *J. Lightwave Technol.* LT-4:504 (1986); 6:1292 (1988).

[123]D. P. Bour, D. B. Gilbert, L. Elbaum, and M. G. Harvey, *Appl. Phys. Lett.* 53:2371 (1988).

[124]P. J. A. Thijs and T. van Dongen, *Electron. Lett.* 25:1735 (1989).

[125]H. Kogelnik and C. V. Shank, *Appl. Phys. Lett.* 18:152 (1971); and H. Kogelnik and C. V. Shank, *Appl. Phys. Lett.* 43:2327 (1972).

[126]M. Nakamura, A. Yariv, H. W. Yen, and S. Somekh, *Appl. Phys. Lett.* 22:515 (1973).

[127]D. R. Scifres, R. D. Burnham, and W. Streifer, *Appl. Phys. Lett.* 25:203 (1974).

[128]H. C. Casey, Jr., S. Somekh, and M. Ilegems, *Appl. Phys. Lett.* 27:142 (1975).

[129]M. Nakamura, A. Aiki, J. Umeda, and A. Yariv, *Appl. Phys. Lett.* 27:403 (1975).

[130]K. Utaka, S. Akiba, K. Sakai, and Y. Matsushima, *Electron. Lett.* 17:961 (1981).

grating mirrors, or between one grating and a conventional facet. The first DBR laser was an AlGaAs/GaAs laser demonstrated by Reinhart et al.[131]

Vertical-cavity surface-emitting lasers (VCSEL) were later developments in semiconductor laser technology.[132] Soda et al. demonstrated the first VCSEL.[133] This was a double heterostructure InGaAsP device operating at 1.3 μm. It used metal mirrors and lased at 77°K. In 1982, Burnham, Scifres and Streifer filed a patent on various designs for VCSEL devices.[134] Epitaxial mirrors for VCSEL devices were first demonstrated in 1983.[135] In 1989, the first cw room temperature VCSEL device was demonstrated by Jewell et al.[136] This device was an quantum well active region sandwiched between n- and p-doped semiconductor Bragg reflectors.

Historical details of this era from the perspective of the major participants are available in a series of review papers in volume QE-23 of the *IEEE Journal of Quantum Electronics*.[137] Additional historical details can be found in the reviews by Hall,[138] Rediker,[139] and in the books by Kressel and Butler,[140] and by Casey and Panish.[141] IEEE has also published a summary of seminal papers on semiconductor diode lasers.[142]

12.3.2 The Basics of the Semiconductor Diode Laser

Energy band structure.   The semiconductor laser can be modeled as a two-level laser system. The upper laser state is the conduction band, and the lower laser state is the valence band. The laser wavelength is emitted at the bandgap of the semiconductor.

In order for the semiconductor to have sufficient gain to operate as a laser, it is usually necessary for the electron transition from the conduction band to the valence band to be a direct radiative transition. Gallium arsenide (GaAs) is an example of a direct semiconductor. Silicon is an example of an indirect semiconductor. The distinction between a direct and indirect semiconductor material is often explained using the E (energy) versus k (momentum)

[131]F. K. Reinhart, R. A. Logan, and C. V. Shank, *Appl. Phys. Lett.* 27:45 (1975).

[132]J. Jewell, *Scientific American* November: 86–94 (1991).

[133]H. Soda, K. Iga, C. Yitahara, and Y. Suematsu, *Jpn. J. Appl. Phys.* 18:2329 (1979).

[134]R. Burnham, D. R. Scifres, and W. Streifer, U.S. Patent #4,309,670, Jan. 1982.

[135]A. Chailertvanitkul, S. Uchiyama, Y. Kotaki, Y. Kokubun, and K. Iga, *Annual Meet. Jpn. Sec. Appl. Phys.* (1983).

[136]J. L. Jewell, A. Scherer, S. L. McCall, Y. H. Lee, S. Walker, J. P. Harbison, and L. T. Florez, *Electron. Lett.* 25:1123 (1989).

[137]R. N. Hall, *IEEE J. of Quantum Electron.* QE-23:674 (1987); M. I. Nathan, *IEEE J. of Quantum Electron.* QE-23:679 (1987); N. Holonyak, *IEEE J. of Quantum Electron.* QE-23:684 (1987), and R. H. Rediker, *IEEE J. of Quantum Electron.* QE-23:692 (1987).

[138]R. N. Hall, "Injection lasers," *IEEE Trans. Electron Dev.* ED-23:700 (1976).

[139]R. H. Rediker, I. Melngailis, and A. Mooradian, "Lasers, Their Development and Applications at M.I.T. Lincoln Laboratory," *IEEE J. Quantum Electron.* QE-20:602 (1984).

[140]H. Kressel and J. K. Butler, *Semiconductor Lasers and Heterojunction LEDs* (New York: Academic Press, 1977).

[141]H. C. Casey, Jr., and M. B. Panish, *Heterostructure Lasers, Parts A and B* (New York: Academic Press, 1978).

[142]W. Streifer and M. Ettenberg, eds, *Semiconductor Diode Lasers* (New York: IEEE Press, 1991).
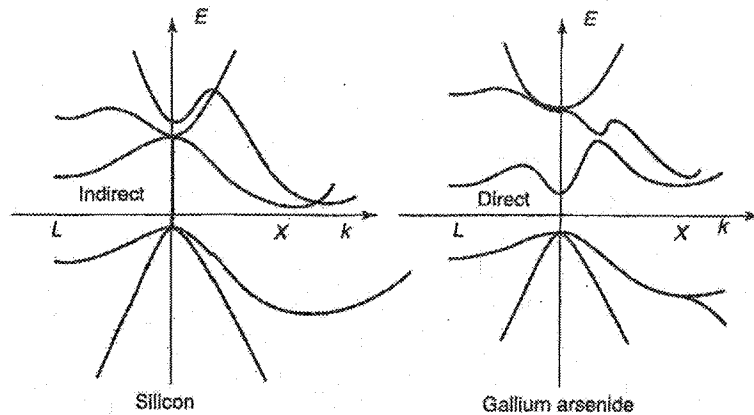
Figure 12.31 The distinction between a direct and indirect semiconductor material is often explained using the E (energy) versus k (momentum) diagram for the semiconductor. If the minima of the conduction band and the maxima of the valence band both occur at $k = 0$, then the semiconductor is direct. If the minima and maxima do not overlap at all, or overlap at $k \neq 0$, then the semiconductor is indirect.

diagram for the semiconductor. If the minima of the conduction band and the maxima of the valence band both occur at $k = 0$, then the semiconductor is direct. If the minima and maxima do not overlap at all or overlap at $k \neq 0$, then the semiconductor is indirect. Examples of E versus k diagrams for indirect and direct materials are given in Figure 12.31.

Pumping the semiconductor diode laser.   In order for the semiconductor to lase, it is necessary to create a population inversion between the valence and the conduction bands. Such a population inversion can be created by external pumping (lasers, electron beams, or flashlamps) or by internally pumping (with a PN-junction).

The simplest way to create a population inversion is to pump the semiconductor with another light source. This technique is termed photopumping and is commonly used to test new semiconductor laser materials in order to determine their suitability for laser operation. One way to photopump a semiconductor laser is to use a conventional gas laser source (such as a HeNe or an argon-ion) as a pump source. This has the advantage of simplicity, but tends to overheat the laser material. For this reason, photopumped laser slices are generally thinned and mounted in thermally conductive holders. Another way to photopump is to use a conventional pulsed laser source (such as a Nd:YAG or glass laser). This not only solves the thermal problems, but also permits testing of recombination rates in the material. A very clever way to photopump a diode laser material is with another diode laser. The sample is thinned and mounted directly on the output window of the diode laser. Although the actual diode laser power is relatively small, the coupling efficiency between the diode laser and the photopumped laser is excellent.

However, the majority of commercial semiconductor lasers are electrically pumped using a PN-junction. Under conditions of high current injection in a PN-junction, a re-
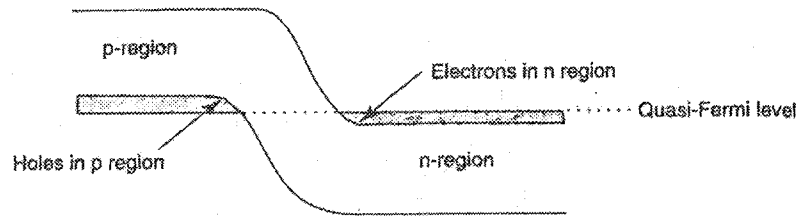
Figure 12.32 In equilibrium, the quasi-Fermi levels of the degenerate p- and n-junction laser material align.
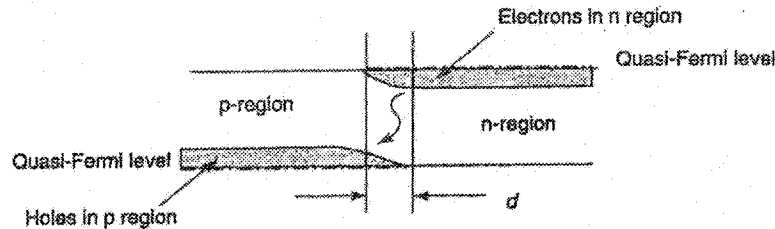

Figure 12.33 The quasi-Fermi levels will misalign by the value of the applied voltage. Under the influence of the forward bias, the holes will drift to the n-region and the electrons will drift into the p-region. The holes and electrons are now spatially coincident and hole-electron recombination occurs.

gion near the depletion region will contain an inverted population of electrons and holes. Appropriate alignment of this region with the cleaved facets will result in laser operation.

Consider the energy band diagram for a simple PN-junction intended for use in a semiconductor photon source. Initially, one side of the junction is heavily doped n and the other side is heavily doped p. In general, both materials are doped degenerately (meaning that the quasi-Fermi level is above the bandedge). In equilibrium the quasi-Fermi levels align as shown in Figure 12.32.

When a positive voltage is applied to the p-region and a negative voltage is applied to the n-region, then the diode is forward biased. The quasi-Fermi levels will misalign by the value of the applied voltage. Under the influence of the forward bias, the holes will drift to the n-region and the electrons will drift into the p-region. The holes and electrons are now spatially coincident and hole-electron recombination occurs (see Figure 12.33).

Notice that in the nonequilibrium situation, the quasi-Fermi levels for the electrons and holes have separated. The spatial distance between the quasi-Fermi levels is essentially the depth d of the active region. In III-V semiconductors (the most common semiconductors for commercial laser diodes), the electrons are much more mobile than the holes. Therefore, the depth of the active region is principally determined by the mobility of the electrons. This distance is approximately given by

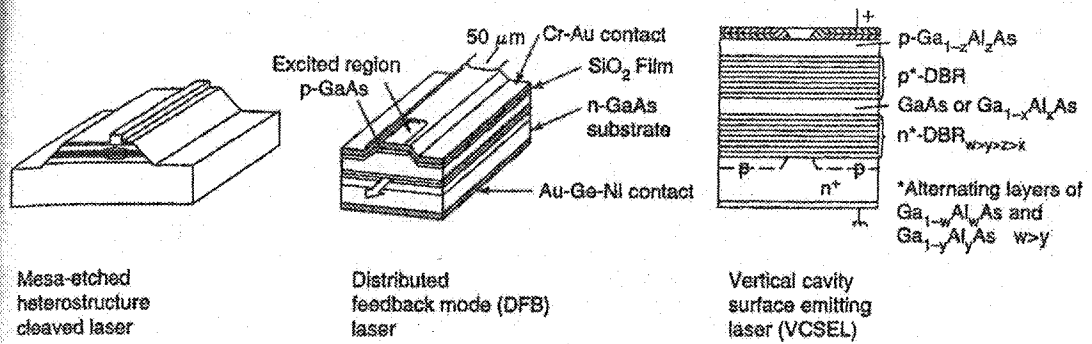$$d = \sqrt{D_n \tau_n} = \sqrt{\frac{D_n n_p}{dn_p/dt}}$$

Mesa-etched heterostructure cleaved laser

Distributed feedback mode (DFB) laser

Vertical cavity surface emitting laser (VCSEL)

Figure 12.34   A few of the possible semiconductor laser resonator structures: DFB is from K. Aiki, M. Nakamura, and J. Umeda, "Schematic Structure of a GaAlAs/GaAS Distributed Feedback Laser," *IEEE J. of Quantum Electron.* QE-12:597 (1976), ©1976 IEEE; VCSEL is from R. Burnham, D.R. Scifres, and W. Streifer, U.S. Patent #4,309,670 (1982).

where n_p is the electron concentration in the p-region and D_n is the diffusion constant for electrons. Typical numbers for d are on the order of 1 μm. (Again, notice that this is on the order of the same size as the wavelength of the electromagnetic mode being amplified.)

Creating the semiconductor diode laser resonator.   There are an astonishing number of possible forms for the semiconductor laser resonator (see Figure 12.34).

In the simplest form, a semiconductor laser consists of small rectangular slab of semiconductor material with two polished or cleaved facets to act as resonator mirrors. The other facets are destroyed in some way (etched, ground, sawn, ion implanted, etc.) in order to avoid spurious laser modes.

The typical horizontal cleaved laser construction can be modified in a number of ways. For example, the facets can be etched using wet or dry processing techniques. External mirrors, gratings, or combinations of mirrors and gratings can be used in place of cleaved facets. External elements can be incorporated off-chip or integrated into the chip.

Semiconductor lasers can be fabricated to lase vertically. With this type of construction, reflecting layers are fabricated on the substrate and the laser operates perpendicularly to the substrate. Reflecting layers can be made from metal, dielectric films, and semiconductor multilayers. Such lasers are called VCSEL.

It is also possible to incorporate gratings directly into the laser design. This results in a laser with a single longitudinal mode forced by distributed feedback from the internal grating. Such lasers are termed DFB lasers. In DBR lasers, a variation on DFB lasers, lasing occurs between the grating mirrors, or between one grating and a conventional facet.

Light propagation in the semiconductor diode laser.   In a laser diode, the photons must be modeled as collective entities traveling in a confined fashion down a waveguide. This gives a different character to the issue of modeling light output from a laser diode as compared to a conventional laser. In general, the far-field pattern from a laser diode is determined by the Fourier integral of the electromagnetic field propagating in the waveguide. The electromagnetic field within the waveguide can be calculated using

the eigenvalue equations for wave propagation in a slab waveguide (for example, see Casey and Panish[143]).

Homostructure semiconductor diode lasers, heterostructure semiconductor diode lasers, and the importance of lattice matching. Early semiconductor lasers were constructed from n- and p-type layers of the same semiconductor material. Such lasers are called homostructure lasers. Homostructure lasers have the advantage of structural simplicity.

However, semiconductor lasers can also be constructed from n- and p- type layers of different semiconductor materials. Such lasers are called heterostructure lasers. The energy band structure and index of refraction profiles of heterostructure lasers can be tailored to meet a given application.

The majority of commercial heterostructure semiconductor lasers are fabricated from semiconductor materials in columns III and V of the periodic table. [Column III is boron (B), aluminum (Al), gallium (Ga), indium (In), and thallium (Tl); column V is nitrogen (N), phosphorus (P), arsenic (As), antimony (Sb), and bismuth (Bi).] Common laser materials include virtually all combinations of Al, Ga, and In, with P and As. Some work has been done with B, Al, and Ga, with N; as well as Al, Ga, and In with Sb. Very little has been done with Tl and Bi.

Heterostructure lasers require layering these different materials. This is a very complex problem, as the materials have different physical properties. Perhaps the most important of these properties is the lattice spacing. If the materials do not have the same lattice spacing, then dislocations can appear in the semiconductor laser. In addition to the structural difficulties imposed by dislocations, dislocations can also be highly detrimental to semiconductor laser operation as they can serve as a nonradiative sink for carriers.

A very useful diagram for visualizing lattice match in heterostructure lasers is the energy versus lattice constant diagram. (An example of such a diagram for III-V materials is given in Figure 12.35). Notice that only the AlAs-GaAs system is lattice-matched across the entire compositional range. This is one major reason for the widespread use of AlGaAs/GaAs heterostructures on GaAs substrates for semiconductor laser diodes.

12.3.3 Confinement in the Semiconductor Diode Laser

Since the electromagnetic mode in semiconductor lasers is on the order of the size of the laser device, then horizontal and vertical confinement are important issues in semiconductor laser design. These issues usually do not arise in conventional laser design, as conventional lasers are typically operating in a propagation mode where the wavelength is much smaller than the resonator dimensions.

Vertical confinement. Typically vertical confinement is provided by creating material combinations with index of refraction profiles that confine the optical wave. Some of these combinations offer the additional advantage of confining the carriers as well.

[143]H. C. Casey, Jr., and M. B. Panish, *Heterostructure Lasers, Parts A and B* (New York: Academic Press, 1978), Chapter 2.
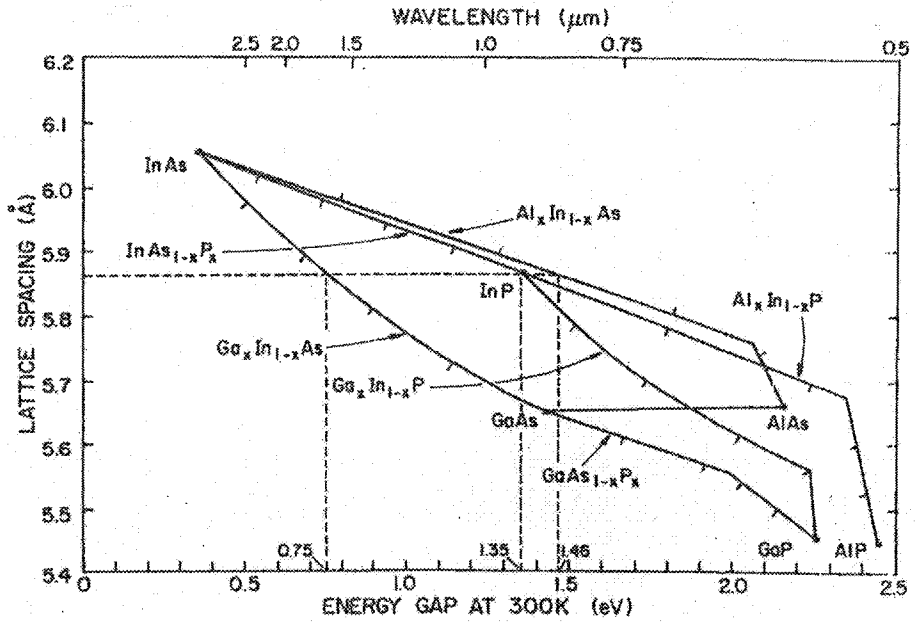
Figure 12.35 The energy versus lattice constant diagram is very useful for visualizing lattice match in heterostructure lasers. (From E. C. H. Parker, *Physics of Molecular Beam Epitaxy* (New York: Plenum Press, 1985), p. 277, Figure 2. Copyright Plenum Press.)
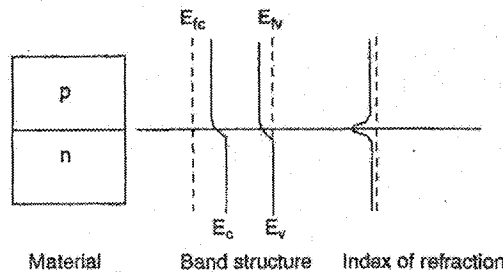

Figure 12.36 A typical homostructure laser consists of one material type with degenerately doped p and n regions. There is only a slight refractive index change at the n-junction to assist in vertical optical confinement of the laser beam.

Homostructure lasers were the very first type of semiconductor laser structure demonstrated. A typical homostructure laser (see Figure 12.36) consists of one material type (for example, GaAs) with degenerately doped p and n regions. There is only a slight refractive index change at the n-junction to assist in vertical optical confinement of the laser beam. Homostructure lasers offer the advantages of simplicity, but the disadvantages of poor confinement.

Single heterostructure lasers were the first type of semiconductor heterostructure laser developed. A typical single heterostructure GaAs laser (see Figure 12.37) is composed of a homojunction GaAs laser diode followed by a p-type AlGaAs layer (with a larger bandgap and lower index of refraction). This geometry creates an index of refraction bump

in the p-type GaAs layer. The index of refraction bump provides some vertical confinement for the laser action occurring in the p-type GaAs. Single heterostructure lasers provide significantly more vertical confinement than homostructure lasers, but require more complex heterostructure growth processes.
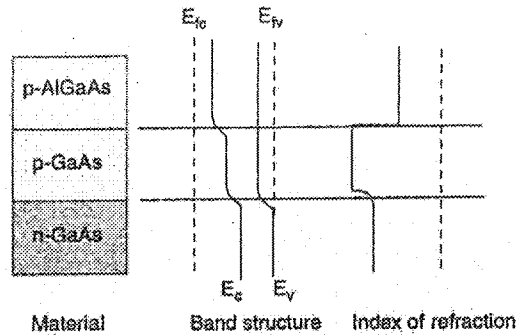

Figure 12.37   A typical single heterostructure laser is composed of a homojunction laser diode followed by a p-type layer with a larger bandgap and lower index of refraction. This geometry creates an index of refraction bump in the p-type GaAs layer. The index of refraction bump provides some vertical confinement for the laser action.

Double heterostructure (DH) lasers have become the standard heterostructure laser type. A typical DH GaAs laser (see Figure 12.38) is composed of a p-type GaAs layer sandwiched between n-type and p-type AlGaAs layers. This geometry creates a large index of refraction bump in the p-type GaAs layer. The index of refraction bump provides vertical confinement for the laser action occurring in the p-type GaAs. DH lasers offer a very nice compromise between the advantages of an index guiding vertical confinement layer, and the disadvantages of heterostructure laser growth.

GRINSCH (graded-index separate confinement heterostructure) lasers offer both optical and electrical confinement in an effort to achieve lower thresholds and narrower beam patterns. A GRINSCH laser is basically a DH laser, but one where the AlGaAs layer has been graded down to meet the GaAs layer (see Figure 12.39). This provides both electron confinement (from the energetic well created by the graded bandgap) and optical confinement (from the index of refraction bump between the AlGaAs and GaAs materials).

GRINSCH lasers frequently find application as quantum well lasers, because the graded bandgap provides a good "funnel" to confine the electrons to the the quantum well regions (see Figure 12.40). MQW-GRINSCH lasers are very popular geometries as they combine many of the best features of DH lasers and quantum wells.

Horizontal confinement.   For many semiconductor laser diode applications it is necessary to confine the carriers both in the horizontal and vertical directions. The most popular method for horizontal confinement is to restrict the size of the gain region, a method called *gain confinement*. There are a large number of gain confinement techniques, but the most popular tend to fall into the categories of contact stripe, mesa etch, ion-implantation methods, and regrowth techniques (such as buried heterostructures).

In the contact stripe method, the gain confinement is provided by restricting the spatial extent of the metal contact (see Figure 12.41). This method offers processing simplicity, but provides relatively poor confinement due to electron transport underneath the stripe.
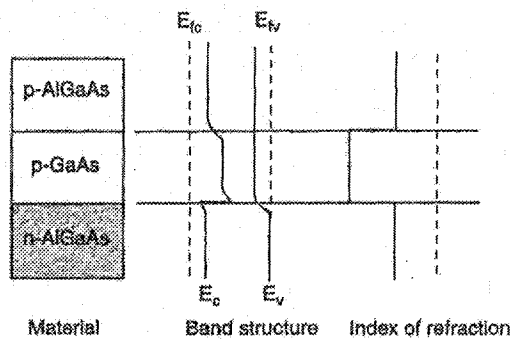
Figure 12.38   A typical double heterostructure laser is composed of a p-type lower bandgap layer sandwiched between n-type and p-type higher bandgap layers. This geometry creates a large index of refraction bump in the p-type layer. The index of refraction bump provides vertical confinement for the laser action occuring in the p-type layer.
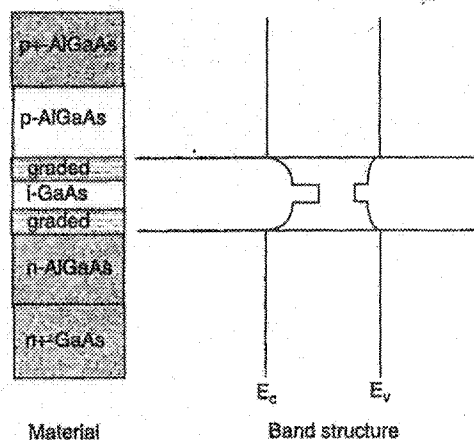

Figure 12.39   A GRINSCH laser is basically a DH laser, but one where the higher bandgap layer has been graded down to meet the lower bandgap layer. This provides both electron confinement (from the energetic well created by the graded bandgap) and optical confinement (from the index of refraction bump between the high and low index materials).

In the mesa etch method, the gain confinement is provided by etching one or several layers of the structure (see Figure 12.42). This method is more difficult to process (as it is both highly nonplanar and requires a sensitive etch stop), but it offers significantly better confinement than the contact stripe method.

In the ion-implantation method, ions are implanted in regions other than the region of interest (see Figure 12.43). This method offers process simplicity and provides a good quality output beam.

In the buried heterostructure method, the gain region is surrounded in both the vertical and horizontal directions by a waveguide of material (see Figure 12.44). Thus, the buried heterostructure process is a two-part method. First, an initial set of layers is grown in an epitaxial system. Then, the wafer is removed from the epitaxial growth system, processed, and returned to the system for new layers to be grown on the material. This process provides outstanding confinement, as the laser is essentially operating in a square waveguide. However, the two-part process cycle is exceptionally complex.
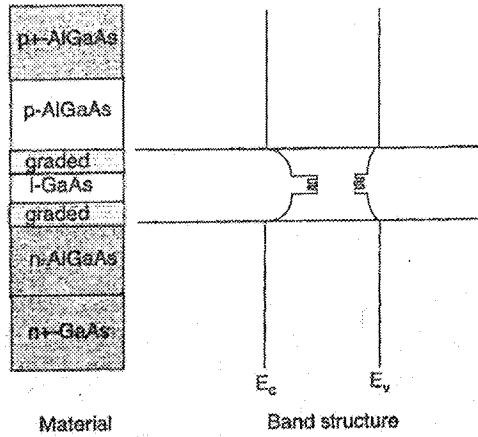
Material   Band structure

E_c E_v

Figure 12.40   GRINSCH lasers frequently find application as quantum well lasers, because the graded bandgap provides a good "funnel" to confine the electrons to the quantum well regions.
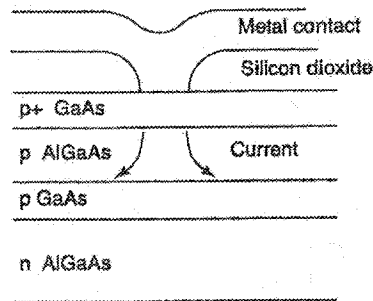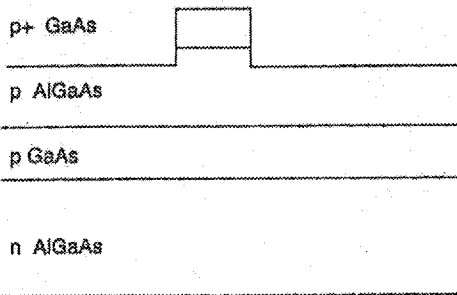

Metal contact

Silicon dioxide

p+ GaAs

p AlGaAs   Current

p GaAs

n AlGaAs

Figure 12.41   In the contact stripe method, the gain confinement is provided by restricting the spatial extent of the metal contact.

p+ GaAs

p AlGaAs

p GaAs

n AlGaAs

Figure 12.42   In the mesa etch method, the gain confinement is provided by etching one or several layers of the structure.

12.3.4 The Quantum Well Semiconductor Diode Laser

A quantum well is a heterostructure composed of two materials of differing bandgap. The two materials are fabricated in a sandwich with the higher bandgap material forming the outside (or barrier) and the lower bandgap material forming the inside (or well). Under these conditions, energy wells are created in both the conduction and valence bands of the heterostructure (see Figure 12.45).

Discrete quantum states (similar to states in a hydrogen atom) will form in the conduction and valence wells (see Figure 12.46). As with a hydrogen atom, electrons transitioning between these states will produce photons possessing the difference energy between the states.

However, unlike a hydrogen atom, the energy of these quantum well states is a function of the width of the quantum wells. The narrower the quantum well, the larger the resulting transitional energy (to the eventual limit that the transition energy between the first valence and first conduction band state matches the energy gap of the barrier material). The wider the quantum well, the smaller the resulting transitional energy (to the eventual limit that the transition energy between the first valence and first conduction band state matches the energy gap of the well material).

In engineering practice, quantum wells provide the means to manufacture semiconductor lasers at any wavelength between that of the barrier material and the well material. In addition, quantum well lasers provide lower lasing thresholds and higher differential quantum efficiencies than equivalent DH lasers.
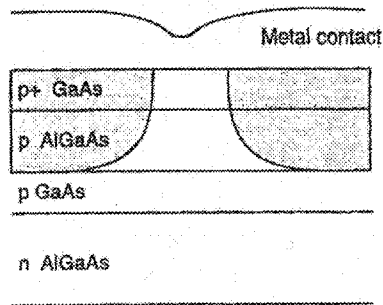

Figure 12.43   In the ion-implantation method, ions are implanted in regions other than the region of interest.
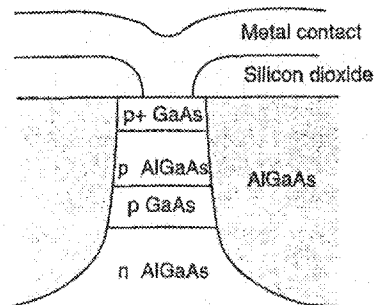

Figure 12.44   In the buried heterostructure method, the gain region is surrounded in both the vertical and horizontal directions by a waveguide of material.
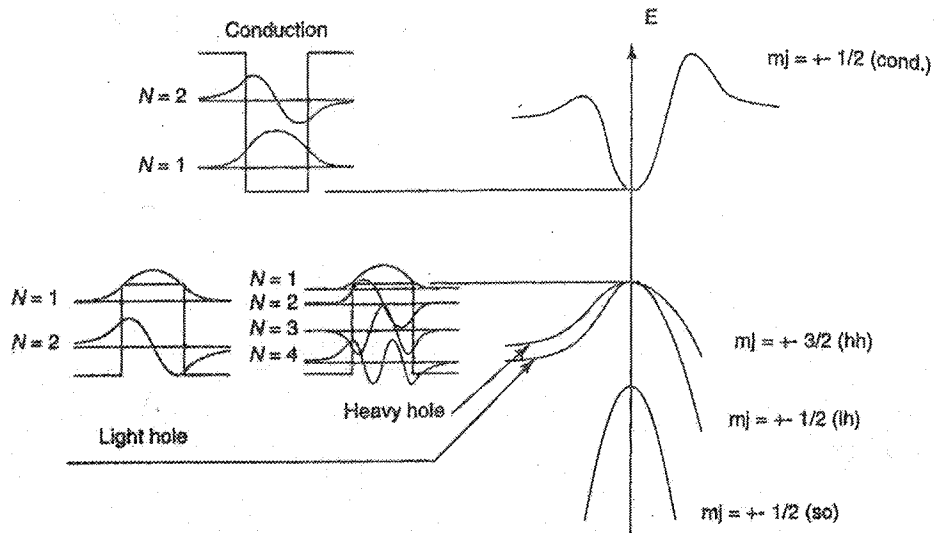
Conduction

E

$N = 2$

$N = 1$

$mj = +- 1/2$ (cond.)

$N = 1$
$N = 2$

$N = 1$
$N = 2$
$N = 3$
$N = 4$

$mj = +- 3/2$ (hh)

Heavy hole

$mj = +- 1/2$ (lh)

Light hole

$mj = +- 1/2$ (so)

Figure 12.45 A quantum well is a heterostructure composed of two materials of differing bandgap. Under these conditions, energy wells are created in both the conduction and valence bands of the heterostructure.
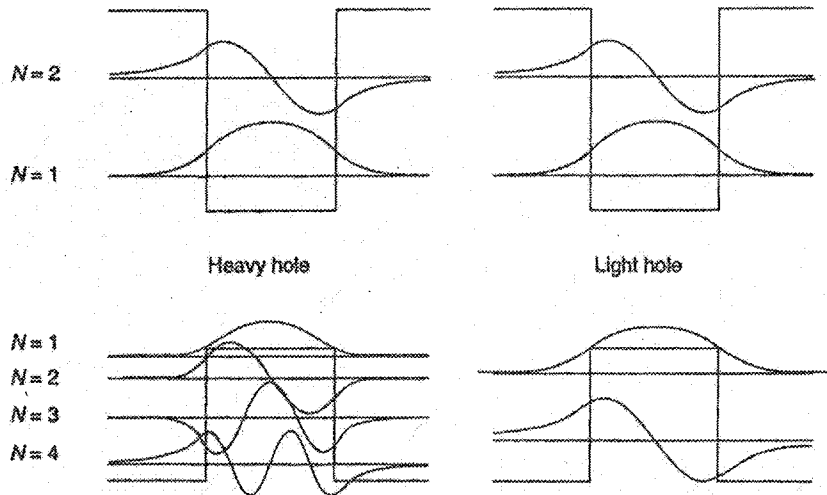
$N = 2$

$N = 1$

Heavy hole

Light hole

$N = 1$
$N = 2$
$N = 3$
$N = 4$

Figure 12.46 Discrete quantum states (similar to states in a hydrogen atom) will form in the conduction and valence wells of a quantum well material.
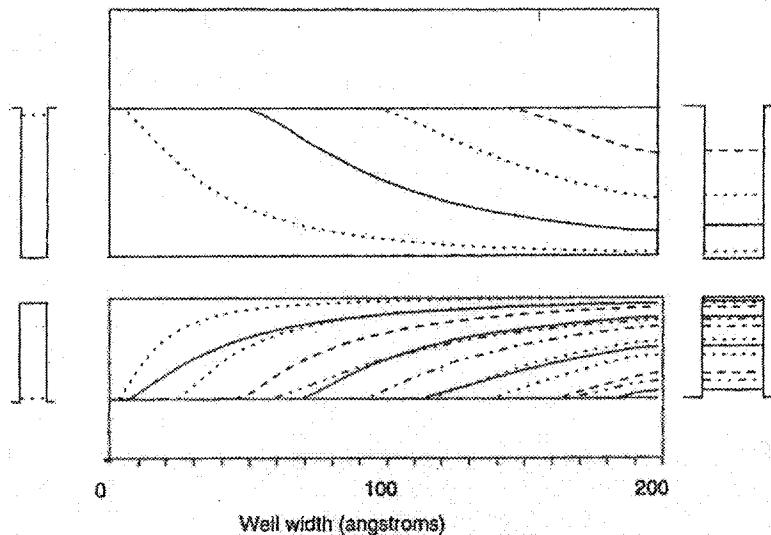
Figure 12.47 The narrower the quantum well, the larger the resulting transitional energy (to the eventual limit that the transition energy between the first valence and first conduction band state matches the energy gap of the barrier material). The wider the quantum well, the smaller the resulting transitional energy (to the eventual limit that the transition energy between the first valence and first conduction band state matches the energy gap of the well material).

12.3.5 Application Highlight: The CD Player

Introduction to the CD audio player. The CD audio player (and its close relative, the CD ROM) are probably the most widely known applications of laser diodes.

A CD disk contains a long string of pits written helically on tracks on the disk. Each pit is approximately 0.5 μm wide and 0.83 μm to 3.56 μm long. Each track is separated from the next track by 1.6 μm. The CD disk is actually read from the bottom. Thus, from the viewpoint of the laser beam reading the disk, the "pit" in the CD is actually a "bump." Interestingly enough, the *edges* of each pit (rather than the pit itself) correspond to binary ones. The signal has been encoded to ensure that there are no adjacent ones. (See Figure 12.48.)

The polycarbonate disk itself is part of the optical system for reading the pits (see Figure 12.49). The index of refraction of air is 1.0 while the index of refraction of the polycarbonate is 1.55. Laser light incident on the polycarbonate surface will be refracted at a greater angle into the surface. Thus, the original incident spot of around 800 μm (entering the polycarbonate) will be focused down to about 1.7 μm (at the metal surface). This helps to minimize the effect of dust and scratches on the surface.

The laser used for the CD player is typically an AlGaAs laser diode with a wavelength (in air) of 780 nm. The wavelength inside the polycarbonate is a factor of $n = 1.55$ smaller (about 500 nm). The pit/bump is carefully fabricated so that it is a quarter-wavelength high (notice a wavelength *inside* the polycarbonate). Light striking the land travels 1/4 + 1/4 =

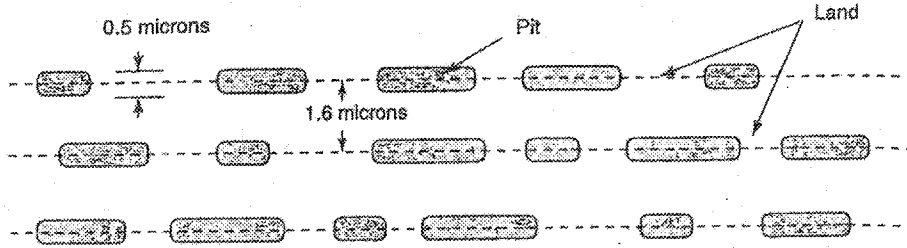0.5 microns

Pit

Land

1.6 microns

Figure 12.48   A CD disk contains a long string of pits written helically on tracks on the disk. Each pit is approximately 0.5 microns wide and 0.83 microns to 3.56 microns long.

Depth is 1/4 wavelength of incident laser light

1.7 μm

$n = 1.55$

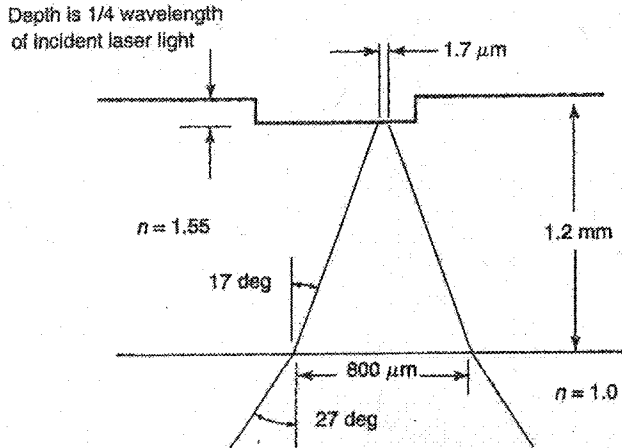1.2 mm

17 deg

800 μm

$n = 1.0$

27 deg

Figure 12.49   The polycarbonate disk is part of the optical system for reading the pits. The original incident spot of around 800 microns (entering the polycarbonate) will be focused down to about 1.7 microns (at the metal surface). This helps to minimize the effect of dust and scratches on the surface.

1/2 of a wavelength further than light striking the top of the pit. The light reflected from the land is then delayed by 1/2 wavelength, and so is exactly out-of-phase with the light reflected from the pit. Thus, these two waves will interfere destructively.

The spacing between pits is also carefully selected. Recall that the image of a beam passing through a round aperture will form a characteristic pattern called an Airy disk. The FWHM center of the Airy disk pattern is a spot about 1.7 μm wide and falls neatly on top of the pit track. The nulls in the Airy pattern are carefully situated to fall on the neighboring pit tracks. This minimizes crosstalk from neighboring pits.

The three-beam optical train.   The most common optical train in modern CD players is the three-beam optical train (see Figure 12.50).

The basic operation of the optical train relies on the polarization properties of light. Light is emitted by the laser diode and enters a diffraction grating. The grating converts the light into a central peak plus side peaks. (The main central peak and two side peaks are important in the tracking mechanism.) The three beams go through a polarizing beam splitter. This only transmits polarizations parallel to the page. The emerging light (now polarized parallel to the page) is collimated. The collimated light goes through a quarter-
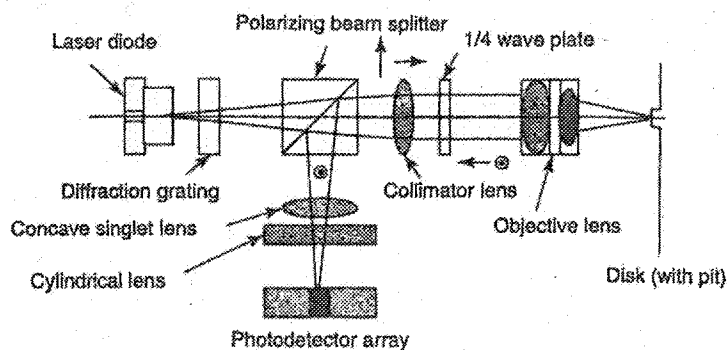
Figure 12.50 The most common optical train in modern CD players is the three-beam optical train.

wave plate and is converted into circularly polarized light. The circularly polarized light is then focused down onto the disk. If the light strikes land, it is reflected back into the objective lens; if the light strikes the pit, it is not reflected. The light then passes through the quarter wave plate again and emerges polarized perpendicular to the original beam (in other words, the light polarization is now vertical with respect to the paper). When the vertically polarized light hits the polarizing beam splitter this time, it will be reflected (not transmitted as before). Thus, it will reflect though the focusing lens and then the cylindrical lens and be imaged on the photodetector array.

Three-beam autofocus.   The separation between the laser and the compact disk is critical for the correct operation of the CD player. A clever astigmatic autofocus mechanism is used to maintain this distance. This autofocus mechanism incorporates a cylindrical lens immediately in front of the photodetector array (see Figure 12.51).

If the objective lens is closer to the compact disk than the focal length of the object lens, then the cylindrical lens creates an elliptical image on the photodetector array. If the objective lens is further away from the compact disk than the focal length of the object lens, then the cylindrical lens again creates an elliptical image on the photodetector array. However, this elliptical image is perpendicular to first image. (Of course, if the disk is right at the focal length of the objective lens, then the cylindrical lens does not affect the image and it is perfectly circular.)

So, if the disk is too far away, quadrants D and B will get more light quadrants A and C (see Figure 12.52). Similarly, if the disk is too close, quadrants A and C will get more light than D and B. If things are just right, then all quadrants will get the same amount of light. So, it is possible to build a simple circuit that will maintain the object lens at just the right distance from the disk.

Three-beam tracking.   Maintaining the laser beam on the track is also critical for the correct operation of the CD player. The three-beam optical train uses three separate beams to maintain the tracking. These beams are created by the diffraction grating (see Figure 12.53). When the laser beam goes through the diffraction grating, it is split up into a
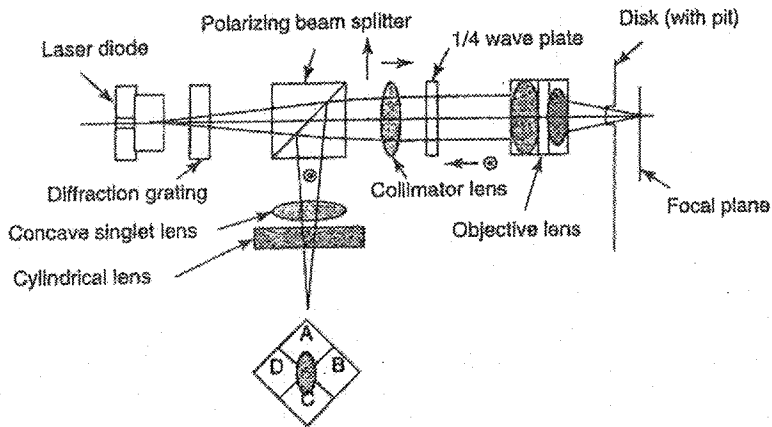
Figure 12.51 The separation between the laser and the compact disk is critical for the correct operation of the CD player. A clever astigmatic autofocus mechanism is used to maintain this distance.
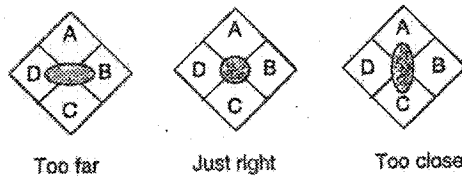

Too far   Just right   Too close

Figure 12.52 If the objective lens is closer to the compact disk than the focal length of the object lens, then the cylindrical lens creates an elliptical image on the photodetector array.
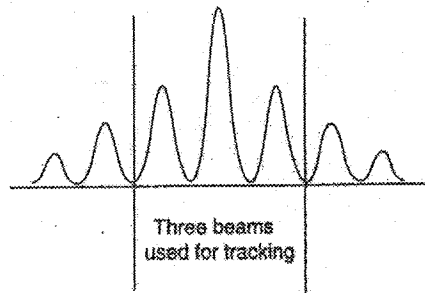

Three beams
used for tracking

Figure 12.53 The three-beam optical train uses three separate beams to keep the laser beam on the track. These beams are created by the diffraction grating.

central bright beam plus a number of side beams. The central beam and one beam on each side are used by the CD for the tracking system.

To appreciate the tracking mechanism, consider a segment of the CD player containing several tracks (see Figure 12.54). If the optical head is on track, then the primary beam will be centered on a track (with pits and bumps) and the two secondary beams will be centered on land. (The three spots are deliberately offset approximately 20 microns with respect to each other to avoid crosstalk.)

Two additional detectors are placed alongside the main quadrant detector in order to pick up these subsidiary beams. If the three beams are on track, then the two subsidiary photodetectors have equal amounts of light and will be quite bright because they are only
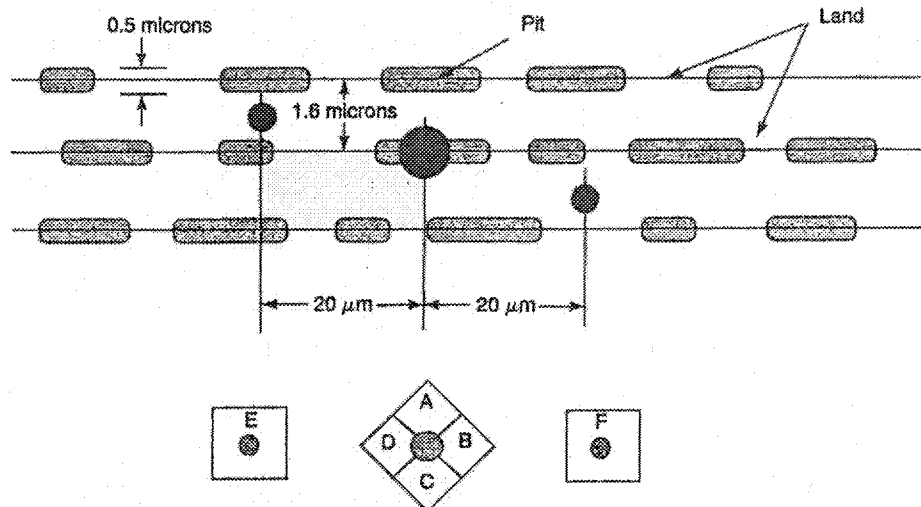
Figure 12.54 If the optical head is on track, then the primary beam will be centered on a track (with pits and bumps) and the two secondary beams will be centered on land.
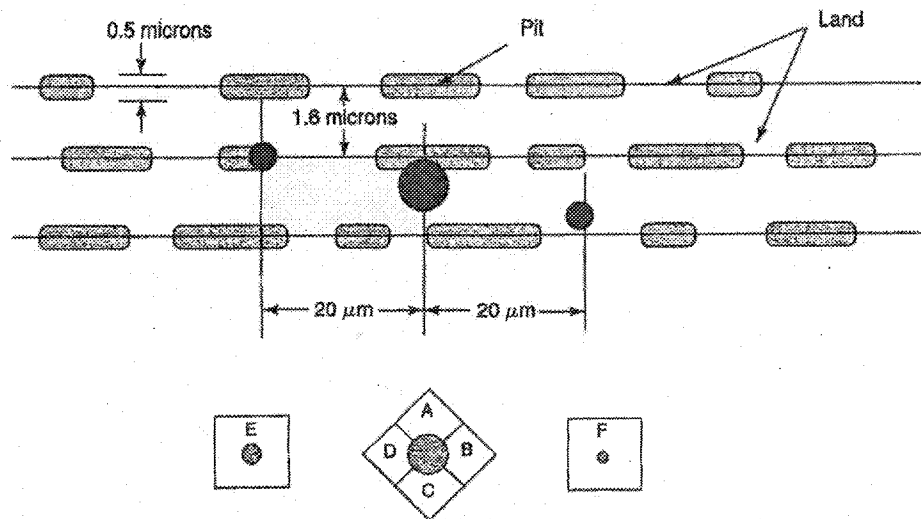

Figure 12.55 If the optical head is off track, then the center spot gets more light energy (because there are fewer pits off track) and the side detectors will be misbalanced.

tracking on land. The central beam will be reduced in brightness because it is tracking on both land and pits (see Figure 12.54). However, if the optical head is off track, then the center spot gets more light (because there are fewer pits off track) and the side detectors will be misbalanced (see Figure 12.55).

Additional optical storage applications using lasers.   The CD audio player is just one of many optical storage applications using lasers. The CD recordable (CD-R) is another technology advancement in the optical storage area. The CD-R uses a laser beam to interact with a nonlinear dye and "write" pits in the CD-R disk. CD-R disks are "write once" devices, but offer exceptional performance for archival applications. (This textbook was delivered to the publisher on a CD-R disk.)

Magneto-optical storage is another fascinating laser diode application. Magneto-optical systems use a laser beam to change the orientation of a magnetic material. The process requires heating the magnetic material to near its Curie temperature and using the focused field of the laser to localize the change. The resulting magnetic spots are read optically using either the Kerr or the Faraday effect.

Another optical storage application that is just achieving success in the commercial marketplace is the DVD or digital video disk player. A combination of CD laser technology and clever digital algorithms has resulted in a more robust alternative to the video tape machine.